UNIVERSITY OF OKLAHOMA

GRADUATE COLLEGE

# HLD-NAC BASED SOLUTIONS FOR SURFACTANT FLOODING

A DISSERTATION

SUBMITTED TO THE GRADUATE FACULTY

in partial fulfillment of the requirements for the

Degree of

DOCTOR OF PHILOSOPHY

By

LUCHAO JIN
Norman, Oklahoma
2016

HLD-NAC BASED SOLUTIONS FOR SURFACTANT FLOODING

A DISSERTATION APPROVED FOR THE
MEWBOURNE SCHOOL OF PETROLEUM AND GEOLOGICAL ENGINEERING

BY

_____
Dr. Ahmad Jamili, Chair

_____
Dr. Jeffrey H. Harwell

_____
Dr. Bor-Jier (Ben) Shiau

_____
Dr. Xingru Wu

_____
Dr. Maysam Pournik

# DEDICATION

This dissertation is dedicated to my wife Jiman, my parents Yuhui Jin & Guizhi Zhang, and my sister Lujing Jin.

Thank you for endless love, sacrifices and supports.

## Acknowledgements

I would like to express my gratitude to my advisor Dr. Ahmad Jamili for his advice and support on my research. His generous guidance and understanding made it possible for me to work on a topic that was of great interest to me. It was a pleasure working with him. I am hugely indebted to Dr. Jeffrey Harwell for instructing me to work on the new microemulsion phase behavior model. His encouragement and inspiration has allowed me to explore new areas and techniques in surfactant flooding theories. I am also grateful to Dr. Ben Shiau for his suggestions and help. I would like to thank Dr. Xingru Wu, who has become an example for my academic and personal life. And I want to thank Dr. Maysam Pournik for his comments on my work. My appreciation also to Dr. Edgar Acosta, who is the inventor of the HLD-NAC model, for his generous sharing of unpublished work and insightful discussions on my research work.

This dissertation cannot be accomplished without the help of scholars from The University of Texas at Austin. I want to express my appreciation to Dr. Mojdeh Delshad for her advice and teachings on chemical flooding simulation. The help I obtained from Dr. Mojdeh Delshad and her research group significantly facilitated my research work. I am indebted to Dr. Zhitao Li for teaching me UTCHEM and advancing our cooperated projects. It was a pleasure to work on the HLD-NAC model and writing publications together with him. I also want to thank Dr. Haishan Luo and Dr. Jun Lu for their help and contributions on our publications. I am grateful to Drs. Gary Pope and Upali P. Weerasooriya for providing me experiment data and surfactant samples.

I am also in debt to my mentors and colleagues during my internships, Dr. Harry L. Chang from Chemor Tech International LLC, Drs. Lu Hu, Michael Lin and Rong Xiao

from ExxonMobil Upstream Research Company. They helped me understand chemical EOR technologies from the industrial aspects.

I want to express my thanks to my colleagues in the Applied Surfactant Lab for helping me in these experimental work. And I am thankful to my friends at Norman for the joyful time we spend together.

I want to express my gratitude to the Mewbourne School of Petroleum and Geological Engineering and the Research Partnership to Secure Energy for America (RPSEA) for the funding support of this dissertation.

Finally, thanks to my wife Jiman for her accompany, support and understanding. And thanks to my family for their endless love.

# Table of Contents

# List of Tables

# List of Figures

# Abstract

Surfactant flooding is a well-established technology for enhanced oil recovery (EOR). In the process of surfactant flooding from lab study to field application, microemulsion phase behavior plays a critical role. During formulation design, microemulsion phase behavior tests are conducted to screen candidate surfactant and optimize the surfactant formulation, which is time consuming and highly dependent on the experiences of formulation researchers. And in coreflood process, microemulsion type leads to different displacement mechanisms. Moreover, it is Type III microemulsion that most efficient in reducing oil-water IFT and mobilized trapped oil. In compositional surfactant flooding simulators, microemulsion phase behavior model is an important package to calculate phase composition, phase saturation and interfacial tension, etc. Therefore, an incorrect phase behavior model or improper input will lead to an unreliable simulation results.

This dissertation aims to provide solutions to these problems of surfactant flooding by introducing a novel hydrophilic-lipophilic deviation (HLD) and net-average curvature (NAC) called thereafter HLD-NAC equation of state (EOS). This model uses experimentally characterized parameters to describe the effects of brine salinity, surfactant properties, oil EACN, alcohol, temperature and pressure on microemulsion phase behavior. Through the HLD-NAC flash calculation, microemulsion phase type, phase composition and saturation, and interfacial tension can be obtained. In this work, the HLD-NAC model is firstly validated by modeling phase behavior of surfactant/brine/crude oil systems. Solubilization ratios and phase fraction diagrams of various formulations are reproduced by using only one fitting parameter, the surfactant tail length L. And the predictability of the HLD-NAC equation of state is further

evaluated. Without using any matching parameter, four optimum formulations and corresponding microemulsion phase behavior are predicted with the HLD-NAC model using laboratory characterized parameters as input. Based on the HLD-NAC EOS, an flash calculation algorithm is developed and implemented into UTCHEM. The algorithm can describe composition distribution on a ternary phase diagram using surfactant, water and oil as the pseudo-component. As a replacement of Hand's rule phase behavior model in UTCHEM, the HLD-NAC EOS shows various advantages in both physical significance and computational efficiency. This work also attempts to analytically study three-component, two-phase surfactant flooding by coupling the HLD-NAC EOS and coherent theory. The analytical solution is compared with the results from the developed numerical simulator with HLD-NAC EOS, to prove that the algorithm is correctly implemented into UTCHEM. Using the analytical solution, the effects of phase behavior dependent parameters on surfactant flooding can by systemically studied.

Through the study of this dissertation, the HLD-NAC EOS is proved to be an effective and accurate microemulsion phase behavior model for surfactant flooding. It can shorten the surfactant screening process hence help chemical EOR formulation design and optimization. It is a predictive model that can not only predict optimum surfactant formulation but also microemulsion phase behavior based on the ambient conditions and surfactant structures. On the basis of the HLD-NAC EOS, the developed simulator and analytical solution can systemically study the effect of phase behavior dependent parameters on the effectiveness of surfactant flooding, hence can give more accurate simulation results and help chemical flooding design.

# Chapter 1 Overview

Established technologies like primary recovery methods using gas pressure and other natural forces in the reservoir, and secondary recovery by water flooding can only approximately recover one-third of the crude oil present in known reservoirs. The overall recovery of a reservoir is a product of microscopic displacement efficiency, $E_D$, and macroscopic displacement efficiency, $E_V$,. In equation form,

$$E = E_D E_V \quad (1)$$

$E_D$ measures the effective ness of the displacing fluid in mobilizing the oil at the pore scale. In water flooding reservoirs, $E_D$ is usually around 0.6-0.7, which means the residual oil saturation, $S_{or}$, in the regions contacted by the displacing water is 0.3-0.4. The primary reason for this high residual oil saturation is the capillary trapping at the pore throat, since in most sandstone reservoir water is the wetting phase. Researchers have recognized that a dimensionless capillary number $N_c = \mu v/\sigma$ controlled the residual oil saturation, where $v$ is the interstitial velocity, $\mu$ is the viscosity of aqueous solution and $\sigma$ is the oil-water interfacial tension (IFT) (Taber 1969; Stegemeier 1977; Melrose 1974; Foster 1973). Correlations between residual oil saturation and capillary number find as the capillary number increases to $10^{-2}$ magnitude, residual oil saturation can be reduced to lower than 0.05 (Abrams 1975). Surfactant is such a chemical that is added into aqueous solution to reduce oil-water IFT, hence increase the capillary number.

Surfactant flood processes have been well developed in the past decades. Various new surfactants and formulations were invented and tailored to fit the reservoir of interest. The general procedures of a surfactant flooding project is shown in Figure 1-1. A candidate reservoir suitable for surfactant flooding is firstly screened. And formulation is

designed according to the reservoir conditions at lab. Considered reservoir conditions include brine salinity, reservoir temperature and oil properties. Then coreflood is conducted to evaluate the displacement efficiency of the designed formulation. In next step, coreflood simulation is performed to explain the coreflood results and obtain parameters that can capture the multiphase displacement process. These parameters are then used as input in pilot test simulation to predict the oil recovery in field scale, hence the economics can be evaluated.

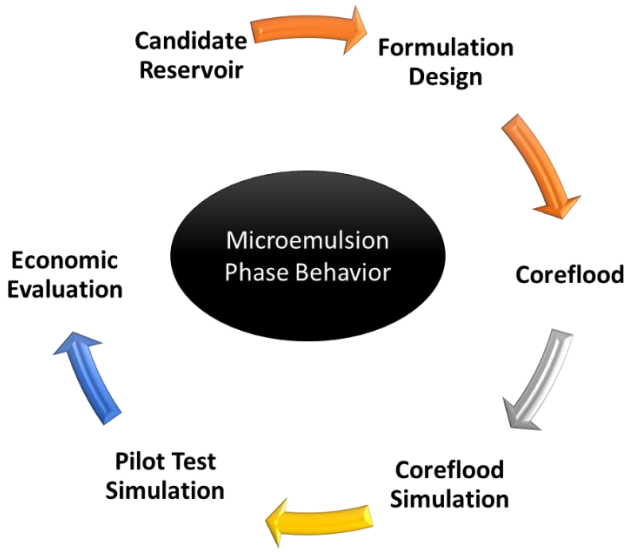


**Figure 1-1 Procedures of a surfactant flooding project**

In these procedures, microemulsion phase behavior plays a critical role. During formulation design, microemulsion phase behavior tests are conducted to screen candidate surfactant and optimize the surfactant formulation, which is time consuming and highly dependent on the experiences of formulation researchers. And in coreflood process, different microemulsion type corresponds to different displacement mechanism. Moreover, it is Type III microemulsion that most efficient in reducing oil-water IFT and mobilized trapped oil. In compositional surfactant flooding simulators, microemulsion

phase behavior model is an important package to calculate phase composition, phase saturation and interfacial tension, etc. Therefore, an incorrect phase behavior model or improper input will lead to an unreliable simulation results. This work aims to provide solutions to these problems in surfactant flooding technology, by using a novel hydrophilic-lipophilic deviation (HLD) and net-average curvature (NAC) called thereafter HLD-NAC equation of state.

In this dissertation, Chapters 2 and 3 focus on microemulsion modeling. Chapter 2 validated the HLD-NAC model for surfactant/brine/crude oil systems. Microemulsion phase behavior of various formulations were reproduced by using only one fitting parameter, the surfactant tail length L. The contribution has appeared in the Journal of Petroleum Science and Engineering. Chapter 3 further evaluated the predictability of the HLD-NAC equation of state. Without using any matching parameter, four optimum formulations and corresponding microemulsion phase behavior are predicted with the HLD-NAC model using laboratory characterized parameters as input. This contribution has been accepted in 2016 SPE Improved Oil Recovery Symposium and been submitted to SPE Journal for peer review.

Chapters 4 and 5 combine the HLD-NAC model with numerical and analytical methods to study its advantages in modeling surfactant flooding. In Chapter 4, a new chemical flooding simulator is developed by implementing the HLD-NAC EOS into UTCHEM. An algorithm is invented to describe composition distribution on a ternary phase diagram using surfactant, water and oil as the pseudo-component. As a replacement of Hand's rule phase behavior model in UTCHEM, the HLD-NAC EOS shows various advantages in both physical significance and computational efficiency. Chapter 5 attempts to

analytically study three-component, two-phase surfactant flooding by coupling the HLD-NAC EOS and coherent theory. The analytical solution is compared with the results from numerical simulator developed in Chapter 4, to prove that the algorithm is correctly implemented into UTCHEM. Using the analytical solution, the effects of phase behavior dependent parameters on surfactant flooding can by systemically studied.

Finally, Chapter 6 presents some concluding remarks of this work and recommendations for the future studies.

# Chapter 2 Physics based HLD-NAC Phase Behavior Model for Surfactant/Crude Oil/Brine Systems


## Abstract

Compositional simulation of surfactant flooding highly depends on accurate modeling of surfactant/oil/brine microemulsion phase behavior. This paper introduces a physics-based Hydrophilic-Lipophilic Difference (HLD) equation and the Net-Average Curvature (NAC) called thereafter HLD-NAC equation of state to model the phase behavior of surfactant/crude oil/brine systems. A non-iterative and physics-based algorithm is developed and validated by modeling the solubilization ratio curves and phase volume fraction of different microemulsion systems.

The HLD values are calculated by the natural logarithm of salinity over optimum salinity when lacking of oil hydrophobicity and surfactant Characteristic curvature information. Together with lab measured head area of per surfactant molecule, the HLD-NAC model reproduces the microemulsion phase behavior of various formulations for surfactant flooding with only one fitting parameter, the length constant L, which physically represents the surfactant tail length size. Modeling results show that the fitted parameter increases with the surfactant or surfactant mixture tail length in the formulation. Moreover, this paper proves that the length parameter determined from one system can be readily applied to other systems, indicating the physical significance of the HLD-NAC model, which can to some extent predict the performance of one surfactant in various systems. The fitted length parameter for formulations with alcohol is underestimated because of this paper assuming all alcohol partition on the interface

leading to overestimated interfacial area. The effect of cosolvent partitioning on the micelle structure and phase behavior modeling will be demonstrated in future studies.

In this paper, the HLD-NAC equation of state is proved to be a simple and robust tool for modeling phase behavior of surfactant/crude oil/brine systems. The HLD-NAC model can shorten the surfactant screening process hence help chemical EOR formulation design and optimization, and can be used in compositional chemical flooding reservoir simulation to improve the predictability of surfactant floods.

Keywords: HLD-NAC; Phase Behavior; Surfactant Flooding;

## 2.1 Introduction

Surfactant flooding is a well-established method in Enhanced Oil Recovery (EOR), and its primary mechanism is by lowering the oil/water interfacial tension (IFT) and, ultimately, reducing residual oil saturation (ROS). In order to obtain a system that can achieve ultralow IFT ($10^{-3}$ mN/m) between given brine and oil, phase behavior tests are widely used in the formulation design process.

The phase behavior of microemulsion is dependent on conditions like surfactant hydrophobicity, oil equivalent alkane carbon number (EACN), co-surfactants, salinity, and temperature (Green and Willhite, 1998). Accurate modeling of surfactant/oil/brine microemulsion phase behavior is critical to surfactant flooding simulation. The general method is to use a phase behavior model matching lab phase behavior data such as solubilization ratio curves or IFT, and then predict the microemulsion phase behavior in reservoir conditions with the tuned phase behavior model.

Various models have been developed for describing microemulsion phase behavior. Generally, these models fall into two categories: empirical and physical models. A widely used empirical model is the Hand's rule (Hand, 1939), which is used in compositional chemical flood simulators such as UTCHEM. However, Hand's rule does not consider physical properties like surfactant hydrophobicity and oil equivalent alkane carbon number (EACN). In order to model microemulsion phase behavior as a function of salinity, Hand's rule needs at least 5 empirical parameters, representing the height of binodal curve at zero, optimum and twice optimum salinity as well as the Type III salinity window, to match lab phase behavior experiments. Additional matching parameters are introduced to model other effects (Delshad et al., 1996). The solution to Hand's equation requires an initial guess for phase composition with iteration (Sheng, 2010). By using a thermodynamic model for alcohol partitioning and coupled with the Hand's equation, Prouvost (1984) developed a phase behavior model considering up to three amphiphilic species for compositional surfactant flooding simulation. However, the empirical feature of Hand's rule constraints the ability of these models in helping formulation design.

Typical physical models study microemulsion phase behavior from the geometry of interfacial surfactant layer (Mitchell and Nihanm, 1981). Chou and Bae (1988) developed a phase behavior model for high salinity surfactant formulations by extending the approach of Mitchell and Nihanmb (1981), considering the effects of salinity, surfactant structure, alcohol and EACN. This model can predict the microemulsion transition with increasing salinity by using three adjustable parameters which related to the characteristic of each component indicating its advantage in helping formulation design, since the determined parameters from one system can be applied to other systems. This is an

excellent model in trying to predict optimum formulation. However, many assumptions in the model are valid only in high salinity conditions, and it has not been used for phase behavior tests with crude oil. On the other hand, all methods mentioned previously have limited abilities in helping formulation design.

Acosta et al. (2003) developed an efficient and physics-based HLD-NAC equation of state which can not only model the microemulsion phase type under different conditions, but also the solubilization capacity and phase volume fractions. The HLD-NAC equation of state consists of two portions. First is the hydrophilic lipophilic difference (HLD) equation proposed by Salager et al. (Salager et al., 1979a, 1999), correlating variables affecting microemulsion chemical potential such as salinity, EACN, surfactant Characteristic curvature (Cc) reflecting the surfactant hydrophobicity,

$$HLD = ln(S) - K \times EACN - \alpha_T \Delta T + Cc + f(A) \quad (1)$$

where, $S$ = salinity (g/100 ml), the electrolyte concentration

$EACN$ = equivalent alkane carbon number of the oil

$K$ = slope of the logarithm of optimum salinity as a function of ACN

$f(A)$ = function of alcohol type and concentration

$Cc$ = characteristic parameter of surfactant

$a_T$ = temperature coefficient of optimum salinity expressed in units of ln S per °C

$T$ = temperature, °C

Ghosh and Johns (2014) added a pressure dependent term $\beta \Delta P$ to predict the microemulsion phase behavior for live oil.

HLD depicts the change in free energy associated with transferring a surfactant molecule from the oil phase to the aqueous phase normalized by the thermal energy (Salager et al., 2000). And the HLD value measures the departure from the optimum formulations. Negative, zero or positive HLD values suggest the formation of Winsor Type I, Type III or Type II microemulsion, respectively. The signs that these variables bear in the HLD equation indicate their effects on phase transition. A positive sign means that an increase in the value of that variable would produce a Type I → Type III → Type II transition, while a negative sign would correspond to the opposite transition (Salager and Antón, 1999).

The value of *K* ranges from 0.1 to 0.2, for numerous surfactants-oil combinations, but a value of 0.17 is typically used for most surfactants (Salager and Antón, 1999). The factor $\alpha_T \Delta T$ reflects the weakening of the hydrogen bonds between water molecules with the increase of temperature (Acosta, 2008a). A typical value of $\alpha_T$ is 0.01 $K^{-1}$ for anionic surfactants (Salager and Antón, 1999). Characteristic Curvature (*Cc*) corresponds to the normalized net curvature of the surfactant at reference condition (Acosta et al., 2008b, Hammond et al., 2012), representing the hydrophobicity of surfactant. A negative *Cc* value corresponds to a surfactant that forms normal micelles under the reference condition; and conversely, a positive *Cc* value corresponds to a hydrophobic surfactant that produces reverse micelles.

The HLD parameters, including *Cc*, *K*, and $\alpha_T$, are surfactant-dependent. And this feature has been used for helping chemical flooding formulation design (Trahan et al., 2015). It allows formulators to rapidly narrow the choices of suitable surfactant systems that fit for field conditions. With given oil EACN, reservoir temperature, salinity, and

HLD parameters for available surfactants, an optimized formulation can be obtained with manipulating the surfactant mixture $Cc$, $K$, and $a_T$ so that the HLD equals zero, when an ultralow IFT is achieved.

For a phase behavior test subject to a salinity scan, HLD can be obtained by Eq. 2 if these parameters are unknown.

$$HLD = \ln\left(\frac{S}{S^*}\right) \tag{2}$$

$S^*$ is the optimum salinity at which HLD equals to zero. So,

$$-ln(S^*) = -K \times EACN - \alpha_T \Delta T + Cc + f(A) \tag{3}$$

The HLD equation quantitatively describes the transition of phase types with the effects of factors such as salinity, EACN, surfactant hydrophobicity, etc. But it cannot tell the amount of oil or water dissolved in the microemulsion phase. Coupling the HLD equation, Acosta (Acosta et al., 2003) introduced a Net-Average Curvature (NAC) equation of state (EOS) for microemulsion system, which assumes any microemulsion could be represented as coexisting hypothetical spherical droplets of oil and water. The reciprocal of the water and oil droplet is the curvature of the microemulsion. In this way, the HLD-NAC EOS is able to calculate phase compositions, and has since been used to fit and predict the phase behavior, solubilization capacity, IFT, and viscosity of microemulsion produced by surfactants (Acosta et al., 2003, 2008a, 2012).

Surfactants are composed of a hydrophilic head and a hydrophobic hydrocarbon tail, and a fundamental characteristic of surfactants is their tendency to adsorb at interfaces. For surfactant concentration above its Critical Micelle Concentration (CMC), micelles will be formed as shown in Figure 2-1. By assuming that the concentration of the

surfactant in monomer form is negligible, the total surfactant interface area ($A_s$) can be calculated as (Acosta et al., 2003)

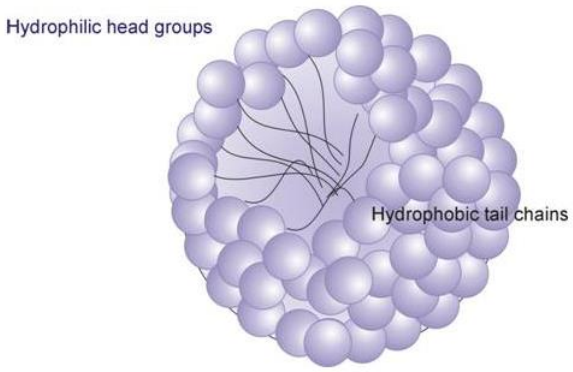


**Figure 2-1 Schematic of a spherical micelle**

$$A_s = \sum_i V_w \times C_{s_i} \times 6.023 \times 10^{23} \times a_s \quad (4)$$

where $V_w$ = the volume of water in the system;

$C_{s_i}$ = the concentration of the surfactant species *"i"* in water, mol/L;

$a_s$ = the surface area per molecule of the surfactant, Å.

The net curvature is expressed as

$$H_n = \left|\frac{1}{R_o}\right| - \left|\frac{1}{R_w}\right| = \frac{-HLD}{L} \quad (5)$$

where $R_o$ and $R_w$ are the radii of coexisting hypothetical spherical aggregates of oil and water. The $H_n$ determines the curvature of the surfactant film adsorbed at the oil/water interface. A net zero curvature ($H_n = 0\ or\ \text{HLD} = 0$) corresponds to a bicontinuous microemulsion containing equal amounts of oil and water ($R_o \approx R_w$). A positive net curvature ($H_n > 0\ or\ \text{HLD} < 0$) corresponds to Type I microemulsion ($R_w \gg R_o$), and negative values ($H_n < 0\ or\ \text{HLD} > 0$) to Type II microemulsion ($R_o \gg R_w$). The net

curvature scales to HLD by L, which is a length parameter that has found to be proportional to the extended length of the surfactant tail group (Acosta et al., 2003).

For Type I microemulsion, the hypothetical radius of the continuous aqueous phase ($R_w$) is calculated using the volume of water in the system and the total surfactant area as shown in Eq. 6, and finally the oil swollen micelle radius $R_o$ is calculated using Eq. 5.

$$R_w = \frac{3 \times V_w}{A_s} \tag{6}$$

The calculation procedure for Type II system is the same as for Type I, only the oil becomes the continuous phase and the hypothetical radius of oil $R_o$ is calculated based on the volume of oil. Therefore,

$$R_o = \frac{3 \times V_o}{A_s} \tag{7}$$

No radius of oil or water can be used to solve Eq. 5 for middle phase microemulsion since the volumes of oil and water are not the same as those initially added. In this case, the concept of characteristic length is introduced (De Gennes et al., 1982), which corresponds to $\xi^*$ and is the maximum length scale at which any oil or water can be correlated to the surfactant membrane. The value of $\xi^*$ indicates the maximum solubilization capacity of a microemulsion system, and is calculated from the phase volumes in middle phase microemulsions:

$$\xi^* = \frac{6 \varphi_o \varphi_w V_m}{A_s} \tag{8}$$

where $\varphi_o$ and $\varphi_w$ represent the water and oil volume fraction in the middle phase microemulsion, and $V_m$ is the volume of the middle phase.

The average curvature ($H_a$) corresponds the ratio of surface area to volume ratio:

$$H_a = \left|\frac{1}{R_o}\right| + \left|\frac{1}{R_w}\right| = \frac{1}{\xi^*} \tag{9}$$

$1/H_a$ is the characteristic size that equals to the characteristic length of the microemulsion in bicontinuous system.

The HLD-NAC EOS is a simple but robust model to fit and predict the phase behavior of microemulsions formulated with conventional ionic and non-ionic surfactants (Acosta et al., 2008a), as well as extended surfactants (Acosta et al., 2012). However, the HLD-NAC EOS has not been used for microemulsion systems with crude oil in previous studies. Bourrel et al. (1987) have observed that the relationship between the oil type to be solubilized and the surfactant lipophile is not affected by the ACN for alkane series, but is affected by crude oils. Because the packing of the surfactant molecules at the water/oil interface may be modified in relation with the oil molecule structures, and the cohesive energy between the lipophile and the oil may also be modified.

Therefore, the objective of this paper is to examine the applicability of the HLD-NAC model for surfactant/crude oil/brine system, and describing its physical significance as well as prediction capability in microemulsion phase behavior.

## 2.2 HLD-NAC Algorithm

For HLD-NAC model, there are three groups of input parameters:

1) surfactant and oil properties such as Cc, K, EACN, a_i and L, etc.;
2) experimental data including volume fraction of water oil and surfactants, salinity, temperature and pressure;
3) optimum salinity S* and the characteristic length ξ^* from phase behavior test results.

The general assumptions in the algorithm are listed as follows:

1) microemulsion could be represented as coexisting hypothetical spherical droplets of oil and water;
2) the concentration of the surfactant in the monomer form is negligible;
3) mole concentration of surfactant is calculated by assuming the surfactant density is 1 g/ml;
4) the surfactant head area is constant at different salinities.

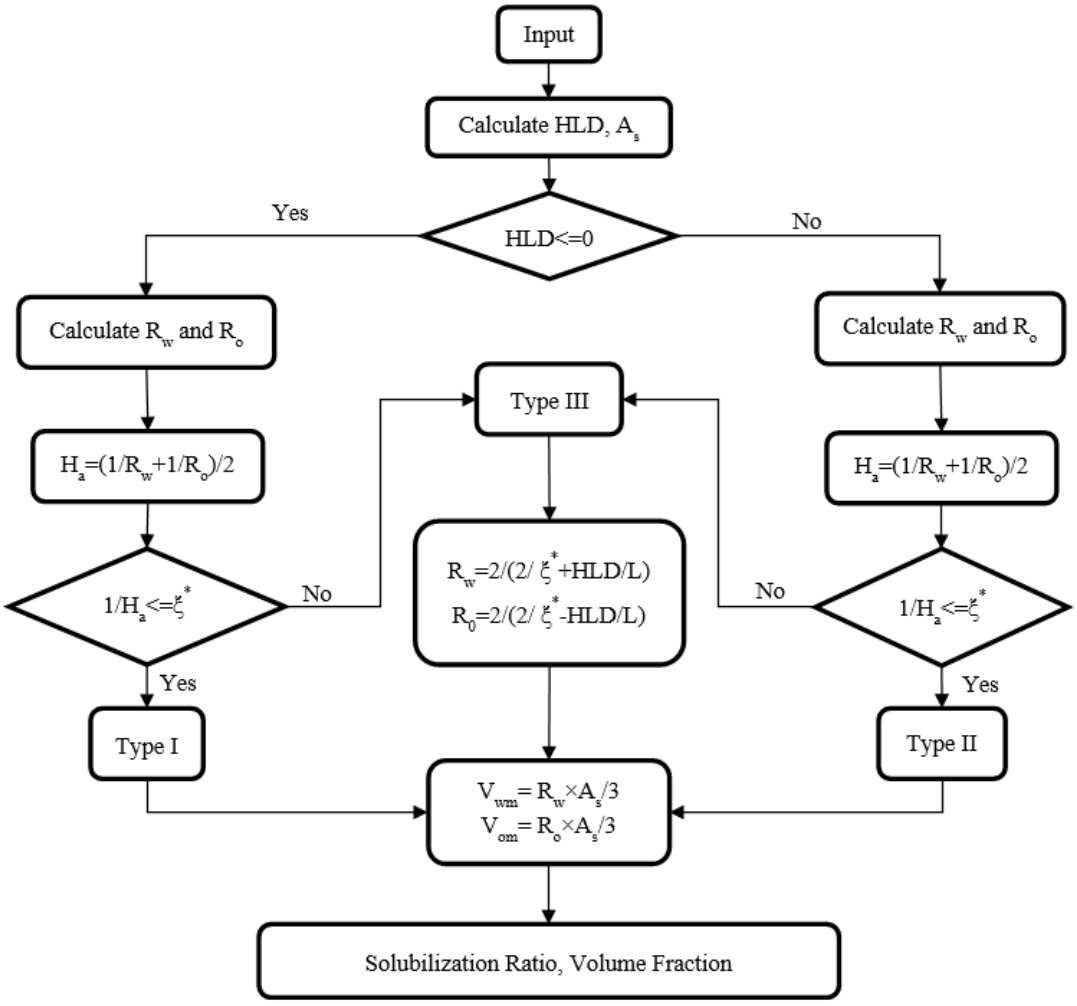


**Figure 2-2 Flowchart of HLD-NAC model for calculating solubilization ratio**

Figure 2-2 presents the flowchart for solubilization ratio and IFT estimation by HLD-NAC model. HLD is firstly calculated from given input parameters. In this work, HLD values are calculated using Eq. 2 for simplification, since the values of *K* and *Cc* for surfactants used in this paper have not been reported so far. The interfacial area provided by the surfactant ($A_s$) was estimated using Eq. 4, where the mole concentration of surfactant is calculated by assuming the surfactant density is 1 g/ml, and the molecular weight as summarized in Table 2-2. If HLD $\leq 0$, it is assumed that water is the continuous phase, otherwise oil is the continuous phase. The hypothetical radius of the continuous phase is calculated by Eq. 6 or Eq. 7 as described. And the droplet radius of internal phase is then obtained by the net curvature as Eq. 5.

The average curvature $H_a$ is further calculated by $R_w$ and $R_o$ obtained from previous steps. The average curvature $H_a$ describes the size of microemulsion aggregates which should not exceed the characteristic length, so $1/H_a < \xi^*$ is a criterion in differentiating microemulsion types. Phase transition has occurred when the characteristic size ($1/H_a$) is larger than the characteristic length ($\xi^*$), which means bicontinuous microemulsion system is formed coexisting with excess oil and water phases (Acosta et al., 2012). In this case, Eqs. 5 and 9 are solved simultaneously. Hence the hypothetical radii of water and oil droplets in middle phase microemulsion are obtained.

After previous condition check and calculations, microemulsion phase type and oil and water droplet radii are obtained. Hence the volume of oil and water in microemulsion phase ($V_{om}$ and $V_{wm}$) are calculated as $V_{w,o} = R_{w,o} \times A_s/3$. Solubilization ratios are further obtained to compare with experiment results. In the calculation process, optimum salinity, characteristic length and optimum solubilization ratio are obtained from phase

behavior experiments, and surfactant head area is calculated from measuring surfactant surface tension versus surfactant concentration, so only surfactant tail length ($L$) is the fitting parameter.

## 2.3 Experimental Measurements

### *2.3.1 Chemical Formulation*

Guerbet alkoxy carboxylates (GAC) were synthesized from Guerbet alkoxylates at the University of Texas at Austin (Adkins et al., 2012, Lu et al., 2014c). The internal olefin sulfonates (IOS), alcohol propoxy sulfates (APS) and alkyl benzene sulfonates (ABS) used in this study were obtained from Stepan Company, Huntsman Chemicals and Shell Chemical Company. Isobutyl alcohol (IBA) was received from Aldrich Chemicals. Sodium chloride, sodium carbonate, calcium chloride, magnesium chloride hexahydrate, and sodium sulfate were obtained from Fisher Chemical.

Several dead crude oils and surrogate oils (a mixture of dead crude and a pure hydrocarbon) were used in this study (Table 2-1). The surrogate oil is made based in part on the equivalent alkane carbon number (EACN) of the dead oil (Cayias et al., 1976; Salager et al., 1979b; Puerto and Reed, 1983; Roshanfekr et al., 2012; Jang et al., 2014).

**Table 2-2 Oil properties**

| Oil Number | Temperature (℃) | °API | Total acid number (mg KOH/g oil) | Viscosity (cp) |
|---|---|---|---|---|
| 1 | 85 | -- | -- | 3 |
| 2 | 104 | -- | -- | 15 |
| 3 | 100 | 22 | 0.15 | 2.1 |
| 4 | 100 | 34 | 0.05 | 0.5 |
| 5 | 38 | 45.4 | 0.15 | 5.4 |

**Table 2-3 Properties of surfactants and co-solvents**

| Descriptive Name | Abbreviated Chemical Formula | MW (g/mole) | Head Area $a_s$, (Å) |
|---|---|---|---|
| $C_{15-18}$ Internal Olefin Sulfonate (IOS) | R-CH(OH)-$CH_2$-CH($SO_3^-$)-R', R'-CH=CH-CH($SO_3^-$)-R', Where R+R'=$C_{12}$-$C_{15}$ | 326 | 56[a] |
| $C_{14-26}$ Internal Olefin Sulfonate (IOS) | R-CH(OH)-$CH_2$-CH($SO_3^-$)-R', R'-CH=CH-CH($SO_3^-$)-R', Where R+R'=$C_{11}$-$C_{23}$ | 386 | 56 [a] |
| $C_{19-23}$ Internal Olefin Sulfonate (IOS) | R-CH(OH)-$CH_2$-CH($SO_3^-$)-R', R'-CH=CH-CH($SO_3^-$)-R', Where R+R'=$C_{16}$-$C_{20}$ | 398 | 50 [a] |
| $C_{20-24}$ Internal Olefin Sulfonate (IOS) | R-CH(OH)-$CH_2$-CH($SO_3^-$)-R', R'-CH=CH-CH($SO_3^-$)-R', Where R+R'=$C_{17}$-$C_{21}$ | 410 | 51 [a] |
| $C_{28}$-25PO-25EO-carboxylate | R,R'-O-($CH_2$-CH($CH_3$)-O)$_{25}$-($CH_2$-$CH_2$-O)$_{25}$-$CH_2$-$CO_2^-$ where R+R'=$C_{28}$ | 3011 | 170 [a] |
| $C_{32}$-7PO-32EO-carboxylate | R,R'-O-($CH_2$-CH($CH_3$)-O)$_7$-($CH_2$-$CH_2$-O)$_{32}$-$CH_2$-$CO_2^-$ where R+R'=$C_{32}$ | 2331 | 194 [a] |
| $C_{28}$-25PO-55EO-carboxylate | R,R'-O-($CH_2$-CH($CH_3$)-O)$_{25}$-($CH_2$-$CH_2$-O)$_{55}$-$CH_2$-$CO_2^-$ where R+R'=$C_{28}$ | 4331 | 262 [a] |
| $C_{11}$ Alkyl Benzene Sulfonate (ABS) | $C_{11}$-($C_6H_5$)-$SO_3^-$ | 334 | 50 [b] |
| $C_{13}$-13PO-Sulfate | $C_{13}$-O-($CH_2$($CH_3$)CH-O)$_{13}$-$SO_3^-$ | 1041 | 60 [b] |
| $C_{16-17}$-7PO-Sulfate | $C_{16-17}$-O-($CH_2$($CH_3$)CH-O)$_7$-$SO_3^-$ | 741 | 60 [b] |
| $C_{20-24}$ Alpha Olefin Sulfonate (AOS) | $C_{17-21}$-CH(OH)-$CH_2$-$CH_2$- $SO_3^-$ (~75%) $C_{17-21}$-CH=CH-$CH_2$- $SO_3^-$ (~25%) | 387 | 60 [b] |
| *sec*-butanol (SBA) | $CH_3CH_2CH(OH)CH_3$ | 74 | 30 [b] |
| *iso*-butanol (IBA) | $(CH_3)_2CHCH_2OH$ | 74 | 30 [b] |

a: lab measured at 2 wt% NaCl, room temperature

b: obtained from reference (Rosen, 1989)

The microemulsion phase behavior methodology was used in this study to develop and test chemical formulations and can be found from many references (Jackson et al., 2006; Zhao et al., 2008; Flaaten et al., 2008; Levitt et al., 2009; Adkins et al., 2010; Adkins et al., 2012; Lu et al., 2014b,c; Liyanage et al., 2015). The phase behavior of formulations 4, 5 and 8 in Table 2-3 was carefully observed over an extended period of time. After reaching equilibrium, the phase volumes can be read and used to calculate solubilization ratio. Aqueous stability experiments were performed at reservoir temperature to ensure

that a clear aqueous surfactant solution was obtained up to the desired injection salinity, which is usually the optimum salinity.

**Table 2-4 Simulated formulation summary**

| No. | Type | Surfactant Formulations | Oil | Optimum Salinity $S^*$, ppm NaCl | Optimum Sol. Ratio, $\sigma$, cc/cc | Characteristic Length, $\xi^*$, Å | Length Parameter, L, Å |
|---|---|---|---|---|---|---|---|
| 1 [a] | Single Surfactant | $C_{14-26}$ IOS | 1 | 91,000 | 5 | 127.6 | 30 |
| 2 [a] | Single Surfactant | $C_{20-24}$ IOS | 1 | 19,000 | 14.8 | 377.8 | 50 |
| 3 [a] | Single Surfactant | $C_{20-24}$ IOS | 2 | 52,000 | 20 | 510.5 | 50 |
| 4 [b] | Surfactant Mixture | 0.5 wt% of $C_{28}$-25PO-25EO-carboxylate 0.5 wt% of $C_{15-18}$ IOS | 3 | 62,500 | 12 | 524 | 80 |
| 5 [b] | Surfactant Mixture | 0.7 wt% of $C_{28}$-25PO-55EO-carboxylate 0.3 wt% of $C_{11}$ ABS | 4 | 30,000 | 11 | 628 | 100 |
| 6 [c] | Surfactant Mixture with Alcohol | 0.5 wt% of $C_{13}$-13PO-sulfate, 0.5 wt% of $C_{20-24}$-IOS, and 2.0 wt% IBA | 5 | 21,000 | 20 | 100 | 8 |
| 7 [c] | Surfactant Mixture with Alcohol | 1.5 wt% of $C_{16-17}$-7PO-sulfate, 0.5 wt% of $C_{20-24}$-AOS, and 4.0 wt% SBA | 5 | 17,000 | 11 | 50 | 8 |
| 8 [b] | Surfactant Mixture | 1.0 wt% of $C_{32}$-7PO-32EO-carboxylate and 1.0 wt% of $C_{19-23}$-IOS | 4 | 36,500 | 11 | 347 | 65 |
| 9 [c] | Surfactant Mixture with Alcohol | 0.75 wt% of $C_{16-17}$-7PO-sulfate, 0.25 wt% of $C_{15-18}$-IOS, and 2.0 wt% SBA | 5 | 41,000 | 12 | 57 | 5 |

a: from reference (Zhao et al., 2008)

b: lab measured

c: from reference (Levitt et al., 2006)

### *2.3.2 Surfactant Head Area*

Head areas of conventional surfactants with various structures have been summarized in the book by Rosen (Rosen, 1989). Except the GAC and IOS surfactants, the rest in Table 2-2 are approximate to surfactant or alcohol with similar structure (Rosen, 1989). The surface area per surfactant molecule at the interface is calculated by the slope of linear trend line between surface tension and logarithm of surfactant concentration before CMC (Rosen, 1989). Surface tension at different surfactant concentration is measured by Cahn DCA 322 Analyzer. GAC and IOS surfactants listed in Table 2-2 are measured with the presence of 2 wt% NaCl addition at room temperature.

From the results as listed in Table 2-2, it is noticed that for the GAC surfactant the area occupied by EO group increases as the length of the EO group is increased. The IOS surfactant has similar surfactant head area regardless of the carbon chain length.

On the other hand, for ionic surfactant, the surface area of each surfactant molecule would be reduced as the electrolyte concentration in surfactant solution increasing, due to the electrostatic repulsion. It is assumed here the surfactant area is constant.

## 2.4 Results and Discussion

### *2.4.1 Modeling solubilization ratio*

In order to validate the HLD-NAC model for microemulsion systems with crude oil, solubilization ratio curves of formulations with various single surfactant, surfactant mixture with and without alcohol, and different oils are simulated.

**Single Surfactant:** Zhao et al. (2008) presented phase behavior results of IOS surfactants with various crude oils, showing excellent performance of IOS in formulation design for difficult oils. Three formulations were selected, as shown in Table 2-3 from

formulation 1 to 3, to illustrate the capability of HLD-NAC model. Solubilization ratio of formulation 1 and 2 were modeled and compared to the experimental. The optimum salinity and solubilization ratio at optimum of each formulation is obtained from reading the experimental data in the literature. The characteristic length is supposed to be calculated as Eq. 8. But the phase volume was not reported, the characteristic lengths were calculated from the optimum solubilization ratio ($SP^*$),

$$\xi^* = \frac{3 \times SP^* \times MW \times 10^{24}}{a_s \times N_a} \tag{10}$$

With given required HLD variables like *EACN* and *Cc* of each surfactant, etc., the optimum salinity is predictable as the calculated HLD equals zero by Eq. 1 (Acosta et al., 2012). But for cases in this paper, the HLD is calculated by Eq. 4 at various salinities.

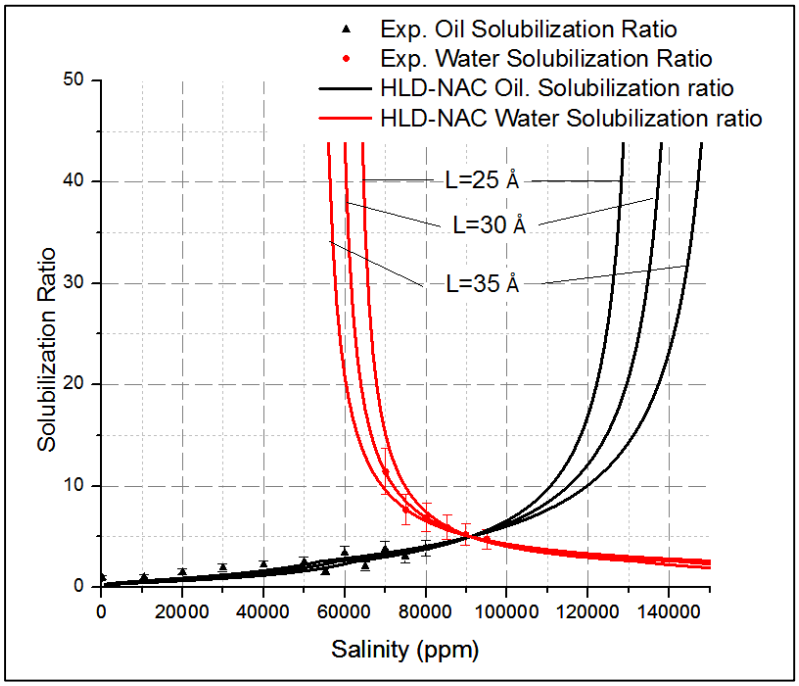


**Figure 2-3 HLD-NAC model fitted solubilization ratio curves of C14-26 IOS for Oil #1**

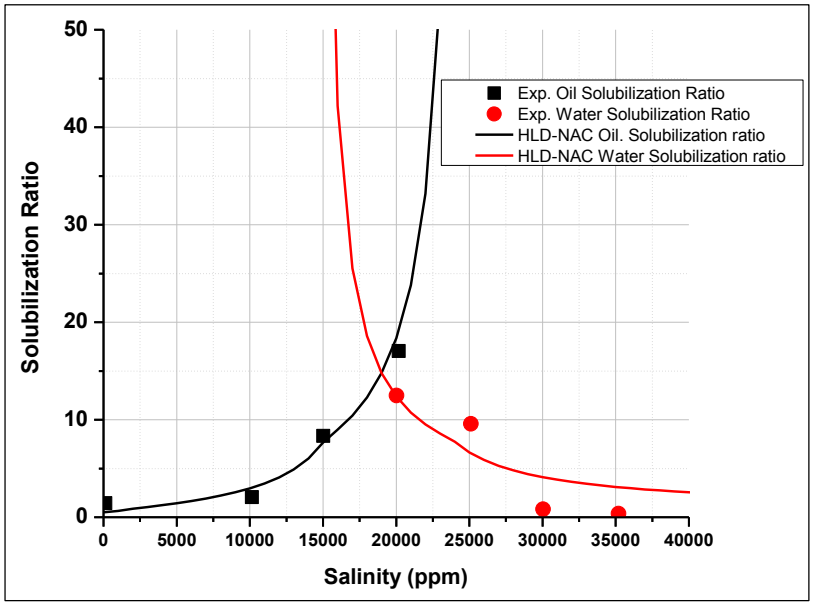


**Figure 2-4 HLD-NAC model fitted solubilization ratio curves of C20-24 IOS for Oil #1**

The only adjusting parameter is the length constant in Eq. 5 to fit the salinity window, with the resulting value being $L = 30$ Å for $C_{14\text{-}26}$ IOS, and $L = 50$ Å for $C_{20\text{-}24}$ IOS. Figures 2-3 and 2-4 present the experimental data from literature (Zhao et al., 2008) and the solubilization ratio curves calculated by the HLD-NAC model. By using only one matching parameter, the experimental data are well matched, considering the complexity of crude oil.

Even as a matching parameter, the fitted $L$ physically representing the fully extended tail length of the surfactant. There have been correlations reported to estimate the surfactant length constant. Acosta found $L = 1.2 \times \delta \times N_c$ for anionic surfactants and $L = 1.4 \times \delta \times N_c$ for nonionic surfactants (Acosta et al., 2003, 2008a), where $\delta$ is the length C-C of 1.5 Å and $N_c$ is the linear carbon number. This is how $L$ parameters of

branched $C_{12-13}$-4PO-1EO-sulfates are estimated ranging from 16.6 to 20.6 Å, without taking into account the PO groups(Acosta et al., 2012). Another correlation is from Tanford (1980), $L = 1.5 + 1.265N_c + 3.64N_{EO}$. These correlations are for single surfactant with a single carbon chain tail. But the IOS used in this study are all mixtures with a range of surfactant tail carbon number. So this paper will only use the length constant as a matching parameter without any estimation from the correlations. However, the matched length parameter is still corresponding to the physical surfactant size. For this case, the average size of $C_{20-24}$ IOS is larger than $C_{14-26}$ IOS with fitted value of 50 Å and 30 Å, respectively. The differences of fitted values are consistent with the surfactant structure, providing an important basis when guessing the value.

This paper takes the system of $C_{14-26}$ IOS for Oil #1 as an example to discuss the uncertainties in using the HLD-NAC model to simulate the microemulsion phase behavior. In Figure 2-3, the measured solubilization ratio is best fitted by surfactant tail length of 30 Å, but also fairly fitted by L ranging from 25 to 35 Å, considering 20% of experimental error. Meanwhile, it can be noticed that varying the surfactant tail length from 25 to 35 Å influences much on the type III window, but less on the type I and type II region. In order to reduce the uncertainty in the fitted length parameter L, more data are required at the phase transit boundaries.

The concept of equivalent carbon number or effective chain lengths of surfactants with complex hydrophobes has been reported in Rosen (2004). The rules of how carbon atoms on the branch, ethoxylates or propoxylates of extended surfactants, and benzene ring contribute to the equivalent carbon number of a surfactant were described in Rosen (2004), and have been used in Ghosh and Johns (2014) for tail length calculation. However, to

the best knowledge of the authors, there is no rule has been used to calculate the equivalent carbon numbers of surfactants with two tails like IOS. In this paper, we assume the carbon atoms in both tails of IOS have the same contribution and treat IOS as single tail surfactants. For $C_{14\text{-}26}$ IOS, we assume the average carbon number is 20, so the tail length is 26.8 Å according to Tanford (1980), $L = 1.5 + 1.265N_c + 3.64N_{EO}$. The surfactant tail length of 26.8 Å calculated from empirical correlation lies in the region from 25 to 35 Å. This reinforces the physical significance of the HLD-NAC model, indicating its prediction ability for microemulsion phase behavior simulation.

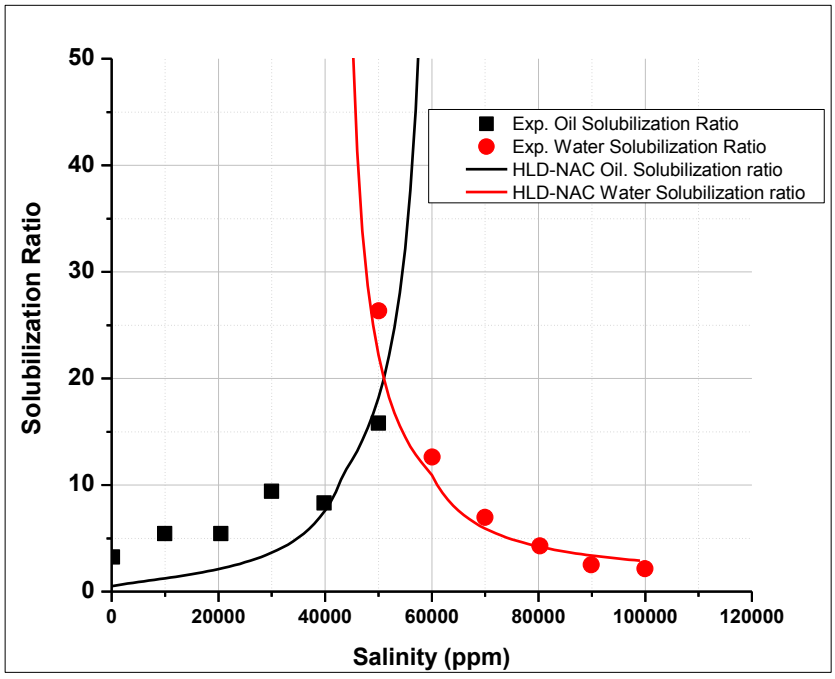


**Figure 2-5 HLD-NAC model predicted solubilization ratio curves of C20-24 IOS for Oil #2**

To further demonstrate the physical significance of the HLD-NAC model, this paper tried to predict the microemulsion phase behavior of a surfactant/crude oil/brine system, since the length parameter in the HLD-NAC model is independent of the temperature and

oil type (Acosta et al., 2003). Figure 2-5 presents the predicted solubilization ratio curves of $C_{20\text{-}24}$ IOS for oil #2 at a higher temperature, comparing to the experimental results from literature (Zhao et al., 2008). The values of input and matching parameters are summarized as formulation 3 in Table 2-3. The optimum salinity, optimum solubilization ratio and characteristic length were dealt the same as previous formulations, and the length constant $L = 50$ Å for $C_{20\text{-}24}$ IOS was obtained from formulation 2. Results in Figure 2-5 indicate the phase behavior of $C_{20\text{-}24}$ IOS and oil #2 are well predicted without tuning any parameter. The HLD-NAC model perfectly predicted the phase transition from Type I through Type II, salinity window, and water solubilization ratio, but only underpredicted the oil solubilization ratio in Type I. This underprediction is possibly due to the assumption of constant surfactant head area at various salinities in HLD-NAC model, which is not very solid when electrolyte concentration is low. Nevertheless, this case proved the physical significance and predicting ability of HLD-NAC model, indicating great advantage in helping formulation design.

**Surfactant Mixtures:** Most formulations for surfactant flooding are mixtures due to the synergistic enhancement effects. In this section, solubilization ratio curves of surfactant mixture and crude oil are reproduced by HLD-NAC model. GAC surfactants used in this section were synthesized at the University of Texas at Austin, and have shown excellent performance under harsh reservoir conditions like high salinity, high hardness and high temperature (Lu et al., 2014). Phase behavior experimental data in this section are lab measured.

The solubilization ratio of a 0.5 wt% of $C_{28}$-25PO-25EO-carboxylate and a 0.5 wt% of $C_{15\text{-}18}$ IOS for Oil #3 at 100 ℃ are matched by the HLD-NAC model and compare against

the experimental data. Parameters are summarized as formulation 4 in Table 2-3. The optimum salinity is 62,500 ppm, and the characteristic length 524 Å is calculated from Eq. 8. The area per molecule of the surfactant ($a_s$) and the length parameter ($L$) determine predicted solubilization for Type I and Type II, as well as the Type III window. $a_s$ of each surfactant has been measured as shown in Table 2-2, therefore, only the length parameter $L$ is the fitting parameter. None of the correlations for estimating the surfactant tail length (Acosta et al., 2012; Tanford, 1980) is suitable for this case. Because this formulation uses a surfactant mixture, and the effect of PO/EO group on the length parameter cannot be ignored. The GAC surfactant used in this formulation has a large amount of PO/EO groups, and the POs and EOs connecting the alkyl chain and hydrophilic head, adsorb on the interface between the oil and water phase. On the other hand, not all the PO/EO groups can be accounted when calculating the surfactant tail length, since when the PO/EO group numbers over than 10, they are in the form of a coil rather than a stretched line.

The experimental data are well reproduced as shown in Figure 2-6 with best fitted length of 80 Å, which is much larger than the obtained length parameter of IOS surfactant (30 Å for $C_{14-26}$ IOS, and 50 Å for $C_{20-24}$ IOS). Obviously, the increase in the length parameter of formulation 4 over formulations 1 to 3 is the contribution of $C_{28}$-25PO-25EO-carboxylate. Literature results shows the linear average mixing rule is not suitable for calculating surfactant mixture length constant (Acosta et al., 2008b). It is also worth to notice that the Type III salinity window of formulation 4 as shown in Figure 2-6, ranging from 50,000 to 80,000 ppm, is much larger than that of formulations 1 to 3. From the modeling results of HLD-NAC model, the enlarging of Type III salinity window is

caused by the increasing of surfactant tail length. In other words, a surfactant or surfactant mixture with longer tail size is favorable for a larger Type III salinity window.

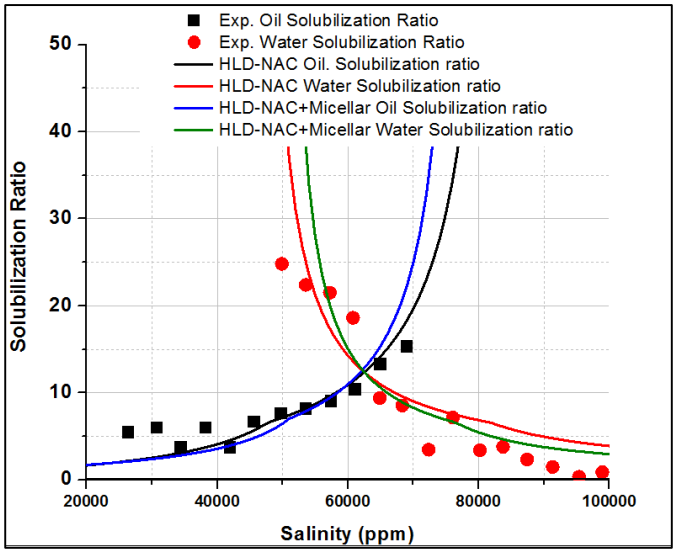


**Figure 2-6 HLD-NAC fitted solubilization ratio curves of 0.5 wt% of C28-25PO-25EO-carboxylate and 0.5 wt% of C15-18 IOS for Oil #3**

In Figure 2-6, the system of 0.5 wt% of $C_{28}$-25PO-25EO-carboxylate and 0.5 wt% of $C_{15-18}$ IOS for Oil #3 was also reproduced by considering palisade solubilization, which has described in Acosta et al., (2003). The total micellar solubilization equals to the core plus the palisade solubilizaiton, as shown in Eq. 10,

$$R_m = R_o + R_p \quad (10)$$

where $R_o$ is the radius of oil droplet calculated from the HLD-NAC model, and $R_p$ is the equivalent radius of the oil solubilized in the palisade layer and $R_m$ is the adjusted radius.

The value of $R_p$ in the case of Figure 2-6 is 10 Å, and the fitted surfactant tail length is 60 Å, which is more in line with the conventional surfactant. This provides an alternative explanation for the fitted long tail length in systems with the GAC surfactants.

The HLD-NAC model is also used to simulate the phase behavior of a 0.7 wt% of $C_{28}$-25PO-55EO-carboxylate and a 0.3 wt% of $C_{11}$-ABS for Oil #2, as shown in Figure 2-7. The optimum salinity and characteristic length for this formulation are 30,000 ppm and 628 Å from the experimental results. The fitted length parameter is 100 Å, and the larger value comparing with the 80 Å for the surfactant mixture of Figure 2-6 corresponds to the 30 more EO groups in the carboxylate surfactants.

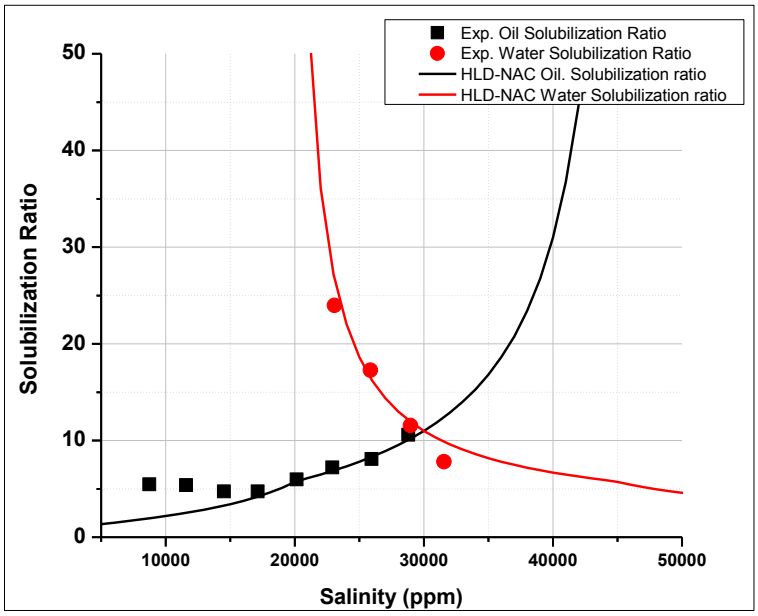


**Figure 2-7 HLD-NAC fitted solubilization ratio curves of 0.7 wt% of C28-25PO-55EO-carboxylate and 0.3 wt% of C11-ABS for Oil #4**

**Surfactant Mixture with Cosolvents:** Cosolvents such as alcohol are widely used in the surfactant formulation design to reduce the microemulsion viscosity, increase the aqueous solubility of the surfactants, and minimize the occurrence of gels/liquid crystals/emulsions for stabilizing the microemulsion. Unlike the surfactant primarily adsorbed on the interface, alcohol partitions between the microemulsion and excess phases. Also, partial alcohol partitioned into the interface increases the interfacial area.

In order to accurately estimate the amount of alcohol at the interface, it is needed to know not only the partitioning coefficient, but also the ratio of alcohol and surfactant in the micelle (Chou and Bae, 1988). To simplify the calculation procedure, this paper assumes the alcohol is completely adsorbed at the interface throughout the salinity scan (Acosta et al., 2003), which will lead to overestimated interfacial area. A rigorous examination of this assumption is currently not in the scope of our study.

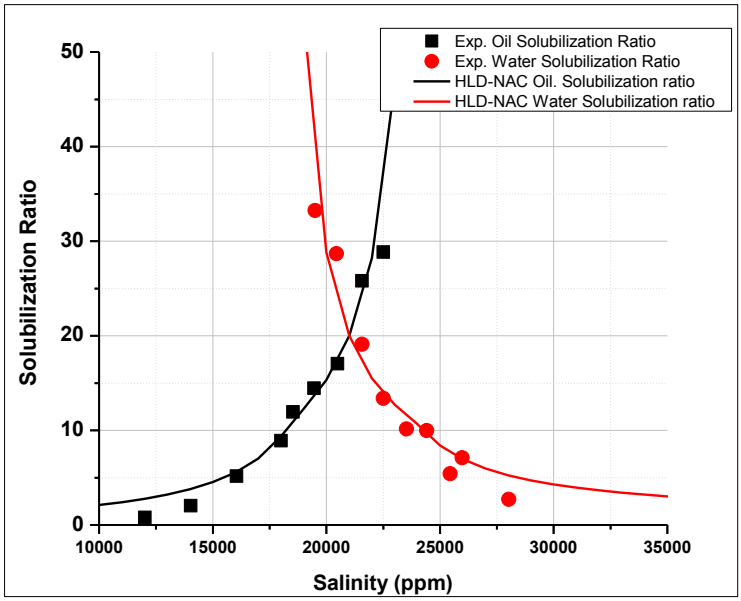


**Figure 2-8 HLD-NAC modeled phase behavior of a 0.5 wt% of C13-13PO-sulfate and a 0.5 wt% of C20-24-IOS, and 2.0 wt% IBA for Oil #5**

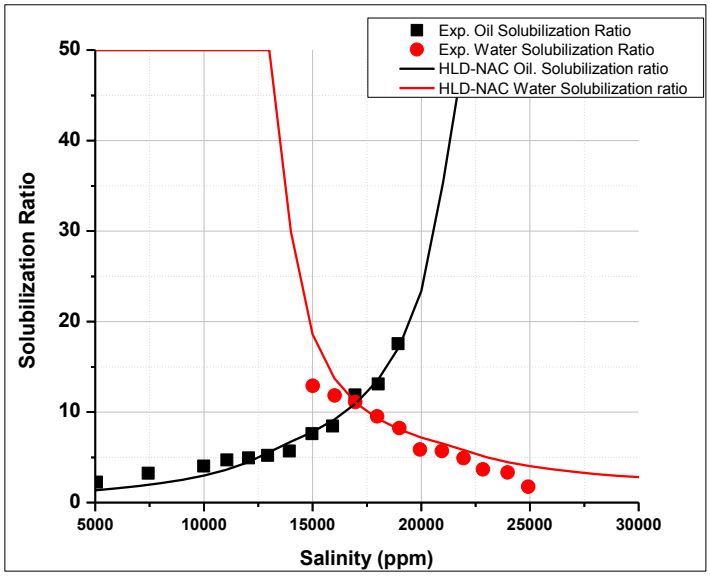


**Figure 2-9 HLD-NAC modeled phase behavior of a 1.5 wt% of C16-17-7PO-sulfate, a 0.5 wt% of C20-24-AOS, and 4.0 wt% SBA for Oil #5**

Figure 2-8 presents phase behavior results of a 0.5 wt% of $C_{13}$-13PO-sulfate and a 0.5 wt% of $C_{20\text{-}24}$-IOS, and 2.0 wt% IBA for Oil #5. The optimum salinity is observed at 21,000 ppm and characteristic length $\xi^*$ is 100 Å from the experimental results. The solubilization ratio curves are matched very well with length parameter of 8 Å and all parameters are shown as formulation 6. Calculated interfacial area is large in this case because all alcohol is assumed to partition on the interface. Therefore, the estimated characteristic length is relatively low from Eq. 8. The relatively low fitted length parameter of 8 Å is due to the same reason, since fitting the solubilization ratio of Type I and Type II systems is dependent on both of the $A_s$ and length parameter $L$. A higher assumed percentage of alcohol in the interface needs a lower length parameter as compensate. Another formulation of a 1.5 wt% of $C_{16\text{-}17}$-7PO-sulfate, a 0.5 wt% of $C_{20\text{-}24}$-AOS, and 4.0 wt% SBA was also matched as presented in Figure 2-9. The fitted length

parameter is also 8 Å same as formulation 6, showing the flexibility of HLD-NAC equation of state in modeling microemulsion phase behavior of various formulations with only one fitting parameter.

### *2.4.2 Modelling phase volumes*

The HLD-NAC model is also capable of predicting the volumes of the different phases (Acosta, 2003). After obtaining the volume of oil and water in microemulsion ($V_{om}$ and $V_{wm}$) as described in Figure 2-2, the volume of microemulsion phase can be calculated as the sum of the volumes of the internal and continuous phase ($V_{om} + V_{wm}$), and the volume of excess phases can be obtained by subtracting the $V_{om}$ or $V_{wm}$ from initial oleic or aqueous phases before equilibrium.

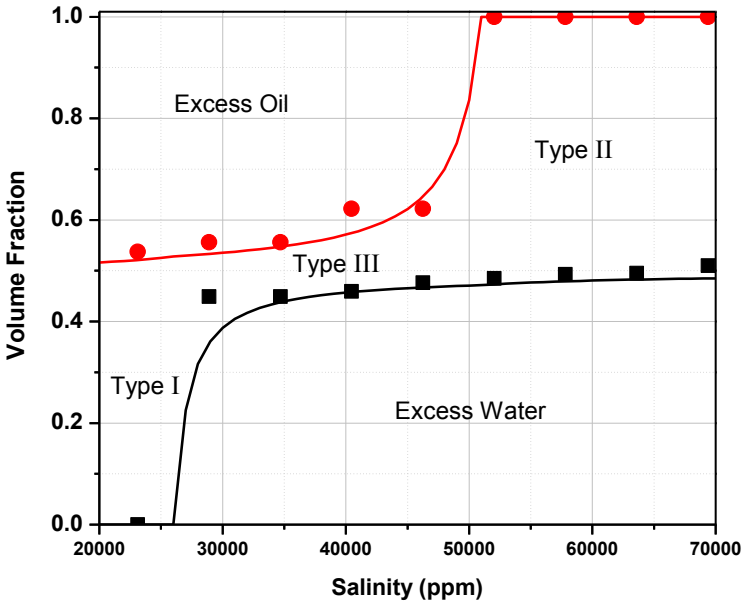


**Figure 2-20 HLD-NAC modeled phase volume fraction of a 1.0 wt% of C32-7PO-32EO-carboxylate and a 1.0 wt% of C19-23-IOS for Oil #4**

Phase volume fraction of 1.0 wt% of $C_{32}$-7PO-32EO-carboxylate and 1.0 wt% of $C_{19\text{-}23}$-IOS for Oil #4 (formulation 8) and 0.75 wt% of $C_{16\text{-}17}$-7PO-sulfate, a 0.25 wt% of $C_{15\text{-}}$

$_{18}$-IOS, and 2.0 wt% SBA for Oil #5 (formulation 9) were reproduced by the HLD-NAC model, and related parameters are summarized in Table 2-3. These two phase volume diagrams are well matched, only a minor differences on the phase transition boundary. Relative errors between the matched results and experimental data are less than 5%, proving the HLD-NAC model can be used for modeling phase behavior in compositional surfactant flooding simulations.

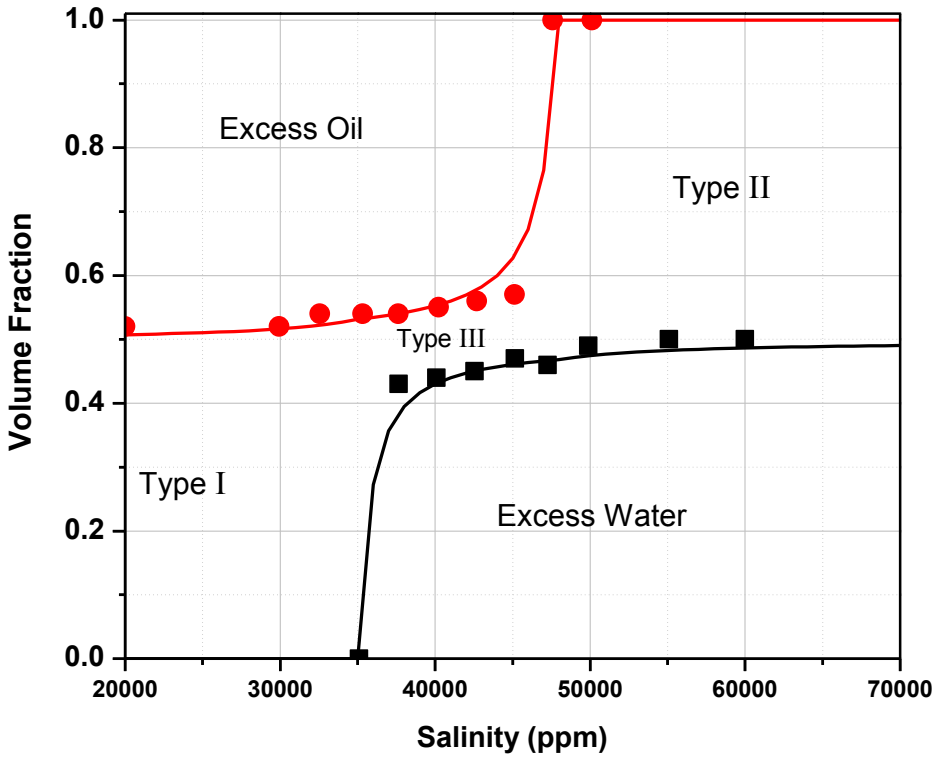


**Figure 2-11 HLD-NAC modeled phase volume fraction of a 0.75 wt% of C16-17-7PO-sulfate, a 0.25 wt% of C15-18-IOS, and a 2.0 wt% SBA for Oil #5**

In this section, solubilization ratio and phase volumes of various formulations are modeled by the HLD-NAC model. The only matching parameter is L, where other model parameters are obtained from microemulsion phase behavior and surface tension measurements. These experiments are traditional formulation and surfactant

characterization tests. Therefore, the HLD-NAC model is practical and can be widely used for various formulations.

## 2.5 Conclusions

This paper employs physics-based HLD-NAC equation of state to model the phase behavior of surfactant/crude oil/brine systems. Algorithm of modeling the solubilization ratio and phase volume fractions were described. Solubilization ratio curves and phase volume fraction diagrams of single surfactant, surfactant mixture with and without alcohol for various crude oil are modeled. The following conclusions are made in this study:

1. With only one fitting parameter, length constant $L$, the HLD-NAC model is capable of reproducing microemulsion phase behavior of various surfactant formulations.
2. Even as a fitting parameter, the length constant is physically representing the surfactant tail length size. The fitted parameter increases with the surfactant or surfactant mixture tail length in the formulation. Moreover, this paper proved that the length parameter determined from one system can be readily applied to other oil, indicating the physical significance of the HLD-NAC model.
3. The fitted length parameter for formulations with alcohol is underestimated because this paper assumes all alcohol partition on the interface leading to overestimated interfacial area. The effect of alcohol partitioning is subject to future studies.
4. In this paper, the HLD-NAC equation of state is proved to be a simple but robust tool for modeling phase behavior of surfactant/crude oil/brine systems. The HLD-NAC model can shorten the surfactant screening process hence help chemical EOR

formulation design and optimization, and can be used in compositional chemical flooding reservoir simulation to improve the predictability of surfactant floods.

# Chapter 3 Predicting Microemulsion Phase Behavior for Surfactant Flooding


## Abstract

The surfactant screening process to develop an optimum formulation under reservoir conditions is typically time consuming and expensive. Theories and correlations like HLB, R-ratio and packing parameters have been developed. But none of them can quantitatively consider both the effect of oil type, salinity, hardness and temperature, and model microemulsion phase behavior.

This paper uses the physics based Hydrophilic Lipophilic Difference (HLD) Net Average Curvature (NAC) model, and comprehensively demonstrated its capabilities in predicting the optimum formulation and microemulsion phase behavior based on the ambient conditions and surfactant structures. By using HLD equation and quantitatively characterized parameters, four optimum surfactant formulations are designed for target reservoir with high accuracy compared to experimental results. The microemulsion phase behavior is further predicted, and well matched the measured equilibrium interfacial tension. Its predictability is then reinforced by comparing to the empirical Hand's rule phase behavior model. Surfactant flooding sandpack laboratory tests are also interpreted by UTCHEM chemical flooding simulator coupled with the HLD-NAC phase behavior model.

The results indicate the significance of HLD-NAC equation of state in not only shorten the surfactant screening processes for formulators, but also predicting microemulsion phase behavior based on surfactant structure. A compositional reservoir simulator with

such an equation of state will increase its predictability and hence help with the design of surfactant formulation.

## 3.1 Introduction

Surfactant formulation for chemical flooding is designed individually for each target reservoir with different oil properties, temperature, and salinity, etc. However, the surfactant screening process is usually time consuming and expensive (Trahan et al., 2015). Typical experimental works like microemulsion phase behavior test and oil water interfacial tension (IFT) measurement are required to ensure the designed formulation can lower the crude oil-brine IFT reaches to ultra-low ($10^{-3}$ mN/m) to reduce the capillary forced and mobilize the trapped oil in rock pores.

Researchers have been working on exploring the predictability in formulation design for decades. Theories like hydrophilic-lipophilic balance (HLB) concept (Griffin, 1949), R-ratio (Winsor, 1948 and 1968) and packing parameters concept (Israelachvili et al., 1976 and 1977; Mitchell and Ninham, 1981) have been developed to describe the surfactant relative affinity on the oil water interfaces, relative energies of interaction between the surfactant on the interface and surrounding aqueous and oleic phases, and the effect of surfactant molecular structure on the interfacial properties, respectively. However, none of these theories can quantitatively consider effects that influencing microemulsion phase behavior such as oil properties, salinity, hardness and temperature, etc. By extending the approach of Mitchell and Nihanmb (1981), Chou and Bae (1988) developed a model for high salinity surfactant formulations, considering the effects of salinity, surfactant structure, alcohol and equivalent alkane carbon number (EACN) of oil. This model predicts the microemulsion transition with increasing salinity by using

three adjustable parameters, which related to the characteristic of each component. This is the first microemulsion phase behavior model ever in literature predicted optimum formulation based on quantitative parameters. However, many assumptions in the model are valid only in high salinity conditions, and it has not been used for phase behavior tests with crude oil.

Acosta et al. (2003) built a physics based hydrophilic lipophilic difference (HLD) Net-Average Curvature (NAC) called thereafter HLD-NAC microemulsion phase behavior model. The HLD equation in this model was proposed by Salager et al. (1979a, 1999) correlates variables affecting microemulsion phase behavior, and these variables can be quantitatively characterized (Witthayapanyanon, 2008; Acosta et al., 2003, 2008a, 2012;). And the NAC concept was introduced to calculate the size and number of micelle, by assuming any microemulsion could be represented as coexisting hypothetical spherical droplets of oil and water. In the HLD-NAC EOS, the HLD value determines the microemulsion type and is used as a scaling parameter to calculate the net and average curvature of the surfactant at the water/oil interface. These curvatures determine the phase compositions, phase volumes, phase transition and solubilization capacity in microemulsion (Acosta and Bhakta, 2009). Recent research shows the HLD-NAC EOS can be used for predicting extended surfactant micromulsion phase behavior (Acosta et al., 2012), and has been used to model microemulsion phase behavior with crude oil (Jin et al., 2015a). Ghosh and Johns (2014 and 2015) modified and extended the HLD-NAC EOS to predict surfactant-oil-brine phase behavior for live oil and alkali-surfactant-oil-brine phase behavior, which advances the physical significance of the HLD-NAC EOS in modeling microemulsion for surfactant flooding. However, none of these work have

ever evaluated the capability of the HLD-NAC EOS in predicting optimum formulation, or ever predicted the micromulsion phase behavior with the least matching parameter, which is the characteristic length that is the only parameter that cannot be predicted in HLD-NAC model so far (Acosta et al., 2003). Moreover, there is no publication reporting modeling surfactant flooding using HLD-NAC EOS yet.

Therefore, this work is firstly going to describe a predictive HLD-NAC algorithm for predicting optimum formulation, microemulsion phase behavior, and as a phase behavior model for compositional surfactant flooding simulator. Then uses four surfactant binary mixtures to evaluate the predictability of the HLD-NAC EOS, by comparing the predicted and experimental measured optimum formulation as well as equilibrium IFT for a target reservoir with high salinity of above 300,000 mg/l, and comparing to Hand's rule that is an empirical microemulsion phase behavior model. Finally, sandpack test results with designed optimal formulations are simulated by UTCHEM (a compositional chemical flooding simulator developed at the University of Texas at Austin) implemented with HLD-NAC EOS. The predictability of the HLD-NAC EOS will be comprehensively demonstrated.

### 3.2 Predictive HLD-NAC Algorithm

The general assumptions in the algorithm are listed as follows:

1) Microemulsion could be represented as coexisting hypothetical spherical droplets of oil and water;

2) The concentration of the surfactant in monomer form is negligible;

3) Mole concentration of surfactant is calculated by assuming the surfactant density is 1 g/ml;

4) The surfactant head area is constant at various salinities;

5) Pseudocomponents are surfactant, brine, and oil;

6) Plait points are estimated as the intersection of solubilization capacity line and the catastrophic phase inversion line.

### *3.2.1 HLD equation for predicting optimum formulation*

The first section of the algorithm is the HLD equation (Salager et al., 1979a, 1999, 2000) as:

$$HLD = ln(S) - K \times EACN - \alpha_T(T - 273.15) + Cc + f(A) \quad (1)$$

where,

$S$ = salinity (the electrolyte concentration, g/100 ml)

$EACN$ = equivalent alkane carbon number of the oil

$K$ = slope of the logarithm of optimum salinity as a function of ACN

$f(A)$ = function of alcohol type and concentration

$Cc$ = characteristic parameter of surfactant

$\alpha_T$ = temperature coefficient of optimum salinity expressed in units of ln S per °C

$T$ = temperature, K

Ghosh and Johns (2014) added a pressure dependent term $\beta\Delta P$ to incorporate the effects of pressure, to predict the microemulsion phase behavior for live oil.

Convention of the HLD value is defined as a negative or positive corresponds to Winsor Type I or Type II microemulsion respectively, and HLD value of zero suggests the optimum state. Therefore, for a target reservoir and given oil property ($EACN$), salinity ($S$) and temperature ($T$), formulators are able to quickly screen candidate surfactant based

on their *K*, *Cc* and $\alpha_T$ values, and even predict optimum formulation. In recent years, the HLD equation has been applied to surfactant formulation design for cEOR. Solairaj et al. (2012) used the HLD concept but developed correlations to predict the optimum carbon number of the surfactant hydrophobe by taking into account the effect of propylene oxide number and ethylene oxide number. Trahan et al. (2015) found comparable phase behavior and coreflood results are obtained if the surfactants have similar Cc values.

Most formulations for surfactant flooding are mixtures due to the synergistic enhancement effects. Therefore, it is desirable to obtain an optimum surfactant ratio in the mixture to reduce the trial and error experiments. At optimum status, HLD equals to zero and if the formulation is alcohol free, $f(A) = 0$. Hence the HLD equation can be rewritten as:

$$0 = \ ln(S) - K_{mix} \times EACN - \alpha_{T_{mix}}(T - 25) + Cc_{mix} \quad (2)$$

Based on the linear mixing assumption (Salager et al., 1979b),

$$K_{mix} = \sum x_i K_i \quad (3)$$

$$\alpha_{T_{mix}} = \sum x_i \alpha_{T_i} \quad (4)$$

$$Cc_{mix} = \sum x_i Cc_i \quad (5)$$

$$1 = \sum x_i \quad (6)$$

Mole fraction of each surfactant in the binary mixture, $x_i$, can be directly calculated.

### *3.2.2 NAC concept for predicting microemulsion phase behavior*

The NAC concept is that the net curvature is scaled to the HLD value by the surfactant length L:

$$H_n = \left|\frac{1}{R_o}\right| - \left|\frac{1}{R_w}\right| = \frac{-HLD}{L} \quad (7)$$

where $R_o$ and $R_w$ are the radii of coexisting hypothetical spherical aggregates of oil and water. $H_n$ is the curvature of surfactant film packed at the oil/water interface. A positive net curvature ($H_n > 0\ or$ HLD $< 0$) corresponds to Type I microemulsion ($R_w \gg R_o$), and negative values ($H_n < 0\ or$ HLD $> 0$) to Type II microemulsion ($R_o \gg R_w$).

L is the fully extended length of surfactant tail group (Acosta et al., 2003). In Jin et al. (2015), it was treated as matching parameter for large surfactant molecule. And there have been correlations developed for estimating its value. Acosta found $L = 1.2 \times \delta \times N_c$ for anionic surfactants and $L = 1.4 \times \delta \times N_c$ for nonionic surfactants (Acosta et al., 2003, 2008a), where $\delta$ is the length C-C of 1.5 Å and $N_c$ is the linear carbon number. Using this method, Acosta et al. (2012) estimated the $L$ parameters of branched $C_{12\text{-}13}$-4PO-1EO-sulfates ranges from 16.6 to 20.6 Å, without taking into account the PO groups. Another correlation is $L = 1.5 + 1.265N_c + 3.64N_{EO}$ developed by Tanford (1980), where $N_c$ is equivalent carbon number in the surfactant tail chain that can take account of the branched carbon and benzene ring. Ghosh and Johns (2014 and 2015) used this method in their work to estimate lengths of related surfactants. For surfactant mixtures, it is assumed here that the mole fraction weighted linear mixing rule still applies (Acosta et al., 2008b; Ghosh and Johns, 2015) as Eq. 8. And in Acosta et al. (2008b), he also found there are some surfactant mixtures produces an L parameter larger than that predicted by the linear mixing rule because of synergistic effect, indicating uncertainties in this rule that needs further investigation.

$$L_{mix} = \sum x_i L_i \tag{8}$$

In Type I microemulsion, water is the external phase and solubilized oil in the micelles. The hypothetical radius of the continuous aqueous phase ($R_w$) is calculated using the volume of water in the system and the total surfactant area:

$$R_w = \frac{3 \times V_w}{A_s} \tag{9}$$

And finally the oil swollen micelle radius $R_o$ is calculated using Eq. 9. Same procedures are applied for Type II microemulsion, in which oil is the continuous phase and the hypothetical radius of oil $R_o$ is calculated based on the volume of oil.

$$R_o = \frac{3 \times V_o}{A_s} \tag{10}$$

The total surfactant interfacial area ($A_s$) can be calculated as (Acosta et al., 2003)

$$A_s = \sum_i V_w \times C_{s_i} \times 6.023 \times 10^{23} \times a_{si} \tag{11}$$

where

$V_w$ = the volume of water in the system;

$C_{s_i}$ = the concentration of the surfactant species *"i"* in water, mol/L;

$a_{si}$ = the surface area per molecule of the surfactant, $Å^2$.

For middle phase microemulsion (Winsor Type III), an average curvature concept needs to be involved since the volumes of oil and water are not the same as those initially added.

$$H_a = \left|\frac{1}{R_o}\right| + \left|\frac{1}{R_w}\right| = \frac{1}{\xi^*} \tag{12}$$

$\xi^*$ is the characteristic length and is the maximum length scale at which any oil or water can be correlated to the surfactant membrane (De Gennes et al., 1982). This is the only parameter in the HLD-NAC model cannot be predicted, but can be calculated from the phase volumes in middle phase microemulsions:

$$\xi^* = \frac{6\varphi_o\varphi_w V_m}{A_s} \quad (13)$$

where $\varphi_o$ and $\varphi_w$ represent the water and oil volume fraction in the middle phase microemulsion, and $V_m$ is the volume of the middle phase.

The $1/H_a < \xi^*$ is a criterion in differentiating microemulsion types. Phase transition occures when the characteristic size ($1/H_a$) is larger than the characteristic length ($\xi^*$), which means bicontinuous microemulsion system is formed coexisting with excess oil and water phases (Acosta et al., 2012). In this case, solving the net curvature (Eq. 7) and average curvature (Eq.11) simultaneously produces the hypothetical radii of water and oil droplets.

With obtained oil and water droplet radii from previous steps, the volume of oil and water in microemulsion phase ($V_{om}$ and $V_{wm}$) are calculated as $V_{w,o} = R_{w,o} \times A_s/3$. For a spherical droplet, the surface excess energy is $4\pi R^2\gamma$, where $\gamma$ is the interfacial tension. To predict the IFT between phases, the HLD-NAC model includes the concept of interfacial rigidity $E_r$, which is defined as the energy provided by the self-assembly of surfactant to counterbalance the surface excess free energy of the core of the micelle or reverse micelle (Acosta,2003). Therefore, the IFT can be calculated as:

$$\gamma_{om,wm} = \frac{E_r}{4\pi R_{o,w}^2} \quad (14)$$

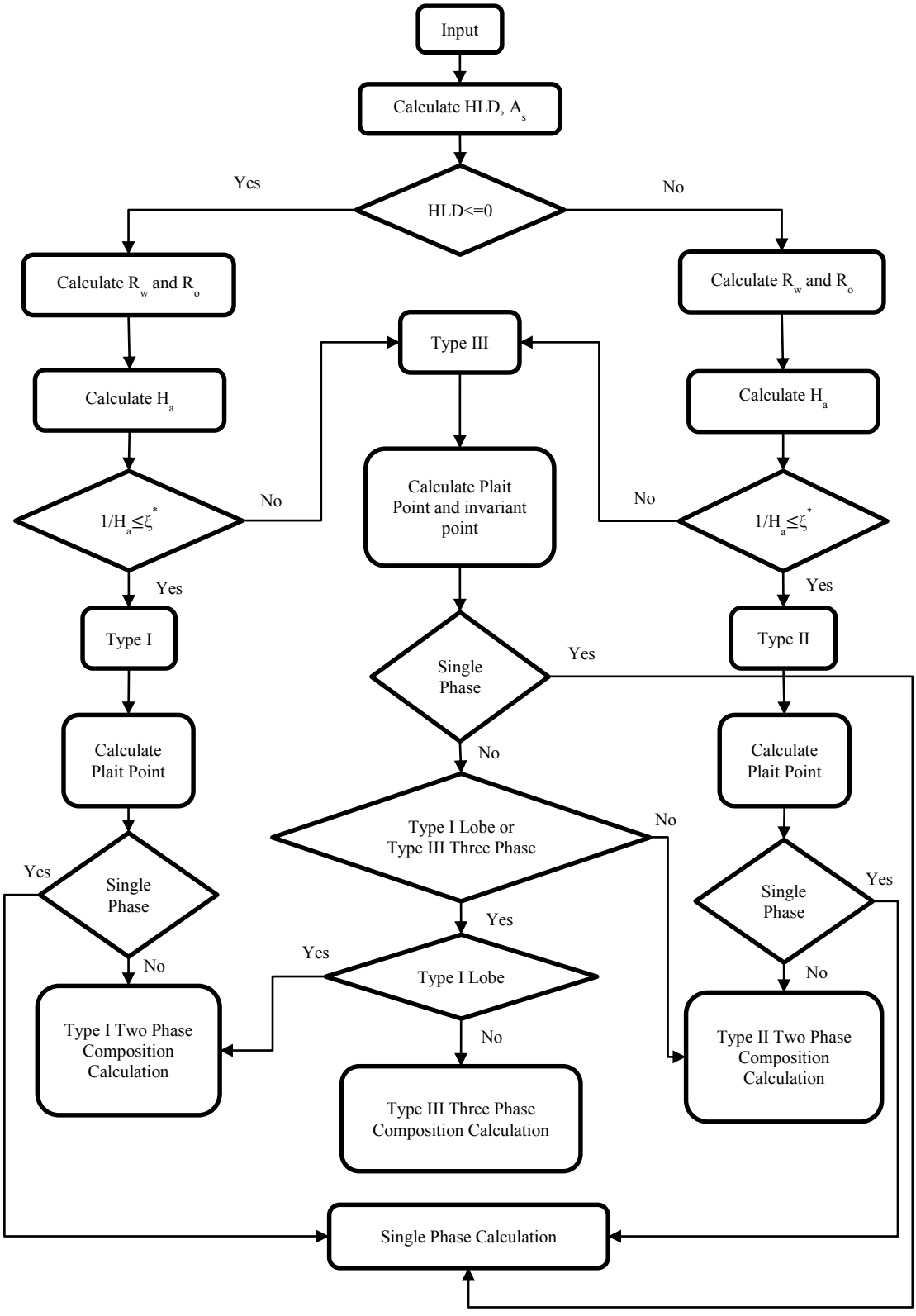


**Figure 3-1 Flowchart of HLD-NAC microemulsion phase behavior model**

### *3.2.3 Phase behavior algorithm for compositional simulator*

Previous described HLD-NAC equations is good for modeling solubilization ratio, phase volume fraction as well as IFT (Ghosh and Johns, 2014 and 2015; Jin et al., 2015a; Acosta et al., 2003). However, it was constrained to water oil ratio of 1:1 and low surfactant concentration. To model surfactant flooding, the phase behavior model should be applicable to various water oil ratio and surfactant concentration. In other words, the algorithm should be able to plot ternary phase diagrams with water, oil and surfactant as pseudo component at arbitrary condition. To do so, this paper improves the algorithm in Jin et al. (2015) that estimates the plait point coordinates on ternary phase diagram by applying the catastrophic theory (personal communication with Acosta, 2015). As the internal phase volume fraction in the microemulsion increases to some point, the internal phase inverse to the external phase naming catastrophic phase inversion. Although the catastrophic phase inversion is system dependent, a good assumption is that it occurs when internal phase volume fraction is over than 75% (personal communication with Acosta, 2015). In this paper, the microemulsion composition where phase inversion happens is the plait point, and the line connecting the plait point and the excess phase composition is the last tie-line.

Figure 3-1 presents the flow chart of the algorithm. For Type I and Type II systems, the microemulsion composition from phase behavior test is located on the binodal curve or solubilization capacity line, and the connections of the microemulsion composition at various surfactant concentration and excess phases are a series of tie lines. For Type III system, the coordinate of the microemulsion composition is the invariant point for a Type III system, and the connections of the microemulsion composition and excess phases are

the boundary of three phase region and two phase lobes. In this way, the solubilization capacity line together with the last tie-line divide the ternary phase diagram into multiphase region and single phase region. And microemulsion composition, solubilization ratio, saturation etc. are calculated in each of these regions.

## 3.3 Microemulsion Phase Behavior Prediction

### *3.3.1 HLD-NAC parameters*

Parameters required in HLD-NAC EOS for prediction fall into four groups,

1) Reservoir condition includes crude oil EACN, brine salinity and reservoir temperature.

In this work, an alcohol free surfactant formulation is designed for a target reservoir with brine total dissolved solids (TDS) over 300,000 mg/L. The detailed reservoir conditions are summarized in Table 3-1.

**Table 3-1 Reservoir brine and oil properties**

| Reservoir Temperature, °C | Brine | | Oil | | | |
|---|---|---|---|---|---|---|
| | TDS, mg/L | Total Hardness, mg/L | EACN | Density, g/mL | Viscosity, cP | Acid Number |
| 52 | 301,710 | 12,973 | 9.8 | 0.82 | 4.5 | 0.44 |

2) Characterized HLD parameters of surfactant candidates such as $Cc$, $K$, and $\alpha_T$.

To satisfy the high TDS, this work selected 4 sodium alkyl alkoxy surfate surfactants, also known as extended surfactants, separately mixed with sodium alkyl ethoxy surfactant (sodium laureth sulfate) with three EOs, because of their excellent performance for high salinity brines (Puerto et al., 2012 and 2014, Jin et al., 2015b). Properties of these surfactants are presented in Table 3-2. And the characterized HLD parameters of each

surfactant candidate are summarized in Table 3-3. The methods and results of measuring these parameters can be found elsewhere (Budhathoki et al., 2016).

**Table 3-2 Surfactant properties**

| Surfactants | Trade Name | # of EOs | # of POs | Alkyl C # | MW (g/mol) | Active (wt%) |
|---|---|---|---|---|---|---|
| C8–(PO)4–(EO)1–SO4Na | Alfoterra 8-4S | 1 | 4 | 8 | 507 | 32.3 |
| C8–(PO)4–SO4Na | Alfoterra 8-41S | -- | 4 | 8 | 466 | 33 |
| C10–(PO)4–(EO)1–SO4Na | Alfoterra 10-4S | 1 | 4 | 10 | 538 | 32.2 |
| C10–(PO)4–SO4Na | Alfoterra 10-41S | -- | 4 | 10 | 493 | 32.5 |
| C12–(EO)3–SO4Na | Steol CS-460 | 3 | -- | 12 | 441 | 60 |

3) Surfactant structure parameters include head area $a_{si}$ and tail length $L$.

The surface area per surfactant molecule at the interface is calculated by the slope of linear trend line between surface tension and logarithm of surfactant concentration before CMC (Rosen, 2004). Surface tension at different surfactant concentration is measured by Cahn DCA 322 Analyzer. Head area of surfactants listed in Table 3-4 is measured with 2 wt% NaCl at room temperature. For the surfactant tail length $L = 1.2 \times \delta \times N_c$ after Acosta (2008a) is applied by neglecting the contributions of EO and PO groups (Acosta et al., 2012). Results are shown in Table 3-3.

**Table 3-3 HLD-NAC values of candidate surfactants**

| Surfactants | K | Cc | $\alpha_T$, °C$^{-1}$ | $a$, Å$^2$ | L, Å |
|---|---|---|---|---|---|
| C8–(PO)4–(EO)1–SO4Na | 0.053 | -2.47 | -0.0059[b] | 71 | 14.4 |
| C8–(PO)4–SO4Na | 0.054 | -2.48 | -0.0059[b] | 66 | 14.4 |
| C10–(PO)4–(EO)1–SO4Na | 0.065 | -2.22 | -0.0059[b] | 68 | 18 |
| C10–(PO)4–SO4Na | 0.069 | -2.15 | -0.0059[b] | 55 | 18 |
| C12–(EO)3–SO4Na | 0.06[a] | -2.89 | 0.01[b] | 40 | 21.6 |

a: Ref. (Trahan et al., 2015)
b: Ref. (Hammond and Acosta, 2012)

4) Characteristic length $\xi^*$ and interfacial rigidity $E_r$ of the microemulsion system.

Characteristic length $\xi^*$ is directly related to the optimum solubilization ratio (Jin et al., 2015a), and hence optimum IFT according to Chun Huh equation (Huh, 1979). Interfacial rigidity $E_r$ was used as a matching parameter to calculate IFT and fit measured IFT data (Acosta et al., 2003). These two parameters are adjusted to fit the magnitude of optimum IFT. In this work, characteristic length $\xi^*$ is used as a fitting parameter, since the phase behavior tests were done in uncalibrated vials, as a consequence $\xi^*$ is hard to be calculated by Eq. 13. Witthayapanyanon (2010) found the interfacial rigidity of extended surfactant is estimated close to 7 $K_BT$, where $K_B$ is Boltzmann constant, and $T$ is absolute temperature in $K$. This work uses 7 $K_BT$ as the interfacial rigidity of the microemulsion systems because of the similar surfactant molecules.

Among all of these required parameters, only the characteristic length $\xi^*$is an adjusting parameter in this work for the whole prediction process.

### *3.3.2 Predict optimum formulation*

To develop optimum surfactant formulations for this high salinity reservoir, this work mixes each of these extended surfactants (Alfoterra) with Steol CS-460 forming binary mixture. With the parameters listed in Tables 3-1 and 3-3, optimal surfactant ratios of each binary mixture can be predicted according to Eqs. 2 to 6. The predicted optimal surfactant ratios are shown in Table 3-4. To validate the accuracy of the predicted optimal surfactant ratios, this paper did surfactant scan phase behavior tests and measured the equilibrium IFT.

Similar to traditional phase behavior test under salinity scan, surfactant scan phase behavior test is to identify an optimum surfactant ratio at the target reservoir salinity, by varying the ratio of surfactants with different hydrophilic-lipophilic properties. In this work, the Alfoterra surfactant concentration is kept constant as 0.25 wt%, and gradually increases the concentration of Steol 460 from 0.2 wt% to 0.7 wt%. Since Steol 460 is the most hydrophilic with the lowest Cc, with the increase of its concentration, HLD value transits from positive to negative, and at the same time the microemulsion type transits from Type II to Type I.

The detailed phase behavior test and equilibrium IFT measurement procedures can be found in Budhathoki et al. (2016). Figures 3-2 to 3-5 plot the IFT curves of each binary mixture, where the formulation of each binary mixture with the lowest IFT is identified as the optimum. Hence the optimum surfactant ratio for each extended surfactant is obtained and summarized in Table 3-4. Good agreement is got between the predicted and measured optimum surfactant ratios, indicating high accuracy of the HLD equation, considering experimental errors.

**Table 3-4 Prediction accuracy of the HLD equation**

| Formulation No. | Extended Surfactants (Alfoterra) | Optimal Ratio [Alfoterra:Steol (mol:mol)] | | Characteristic Length ($\xi^*$, Å) |
|---|---|---|---|---|
| | | Predicted | Measured | |
| 1 | C8-(PO)4-(EO)1-SO4Na | 0.496 | 0.593 | 208 |
| 2 | C8-(PO)4-SO4Na | 0.631 | 0.613 | 185 |
| 3 | C10-(PO)4-(EO)1-SO4Na | 0.410 | 0.450 | 230 |
| 4 | C10-(PO)4-SO4Na | 0.407 | 0.461 | 250 |

### *3.3.3 Predict equilibrium IFT*

Equilibrium IFT of each surfactant mixture is calculated according to the algorithm described above, showing as solid curves in Figures 3-2 to 3-5. Comparing to experimental measured data, the predicted IFT curves well reproduce the optimum IFT and IFT behavior transition caused by the increasing concentration of Steol 460.

To the best of our knowledge, this is the first time that the IFT behavior of surfactant-brine-crude oil system is predicted based on the quantitatively characterized surfactant hydrophobicity as well as surfactant structure properties. Although in Figures 3-4 and 3-5, the predicted IFT deviated from the measured IFT, the differences in the concentration of Steol 460 are less than 0.1 wt %. This error is relatively tolerable considering the uncertainties in experiments. On the other hand, the accuracy of the HLD equation highly relies on how precious of the related parameters. Nevertheless, these results prove the HLD-NAC EOS can shorten the surfactant screening processes and be used to guide formulation design, with a developed database of surfactant parameters as shown in Table 3-2 and Table 3-3.

To better reproduce the measured equilibrium IFT, one can slightly adjust the HLD value, and therefore the optimum surfactant mixture. Dashed lines in Figures 3-2 to 3-5 are fitted IFT curves by adjusting HLD value. Figures 3-4 and 3-5 show the adjusted surfactant tail length L. It has been mentioned in previous section that mole fraction weighted linear mixing rule may not be applicable because of the synergetic effects in surfactant mixture. In previous studies, the surfactant tail lengths were usually treated as a matching parameter to scale the Type III microemulsion window. For formulations 1

and 2, estimated tail length from correlation shows pretty high accuracy. The adjusted HLD-NAC parameters are summarized in Table 3-5.

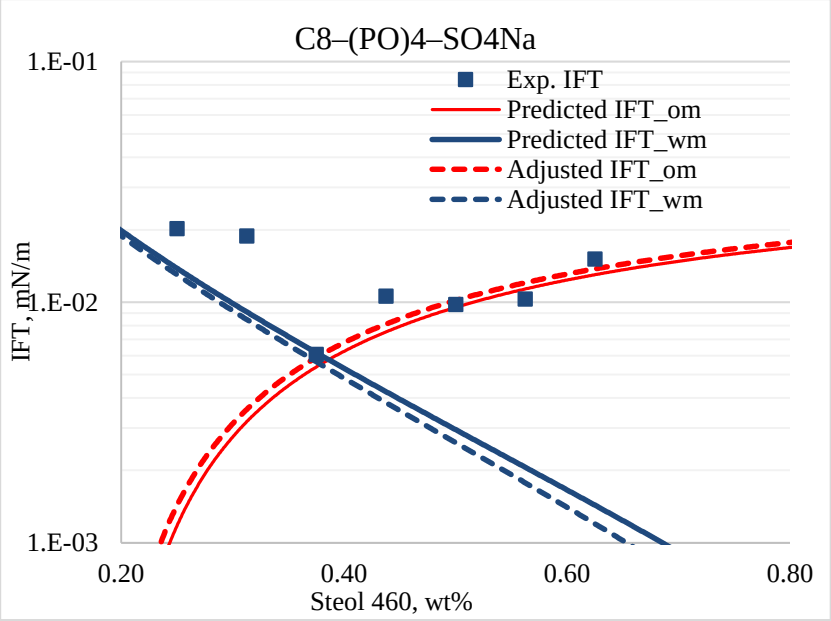


**Figure 3-2 Comparing HLD-NAC predicted and measured equilibrium IFT 0.25 wt % C8–(PO)4–SO4Na + C12–(EO)3–SO4Na binary mixtures with the reservoir crude oil at 52°C**

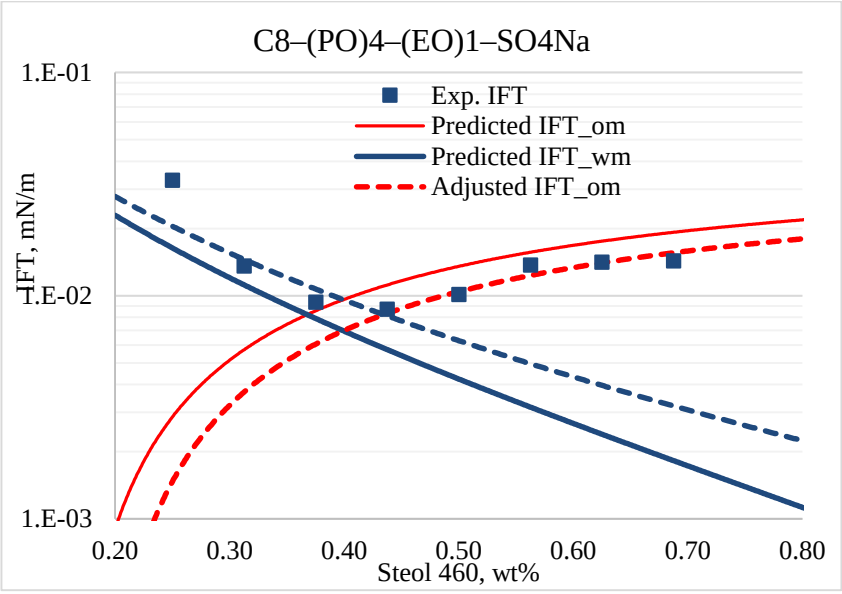


**Figure 3-3 Comparing HLD-NAC predicted and measured equilibrium IFT 0.25 wt % C8–(PO)4–(EO)1–SO4Na + C12–(EO)3–SO4Na binary mixtures with the reservoir crude oil at 52°C**

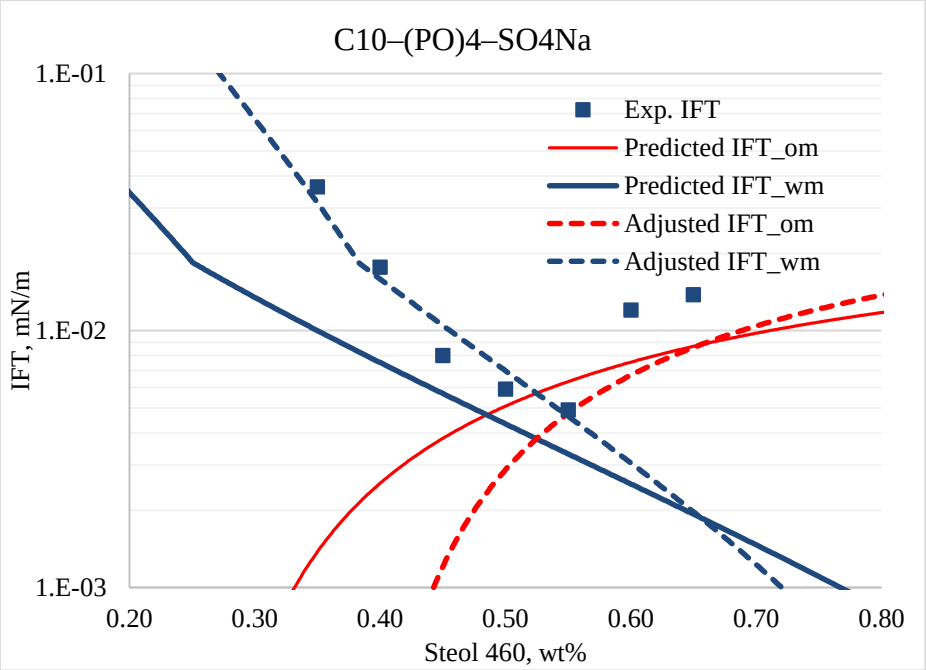


**Figure 3-4 Comparing HLD-NAC predicted and measured equilibrium IFT 0.25 wt % C10–(PO)4–SO4Na + C12–(EO)3–SO4Na binary mixtures with the reservoir crude oil at 52°C**

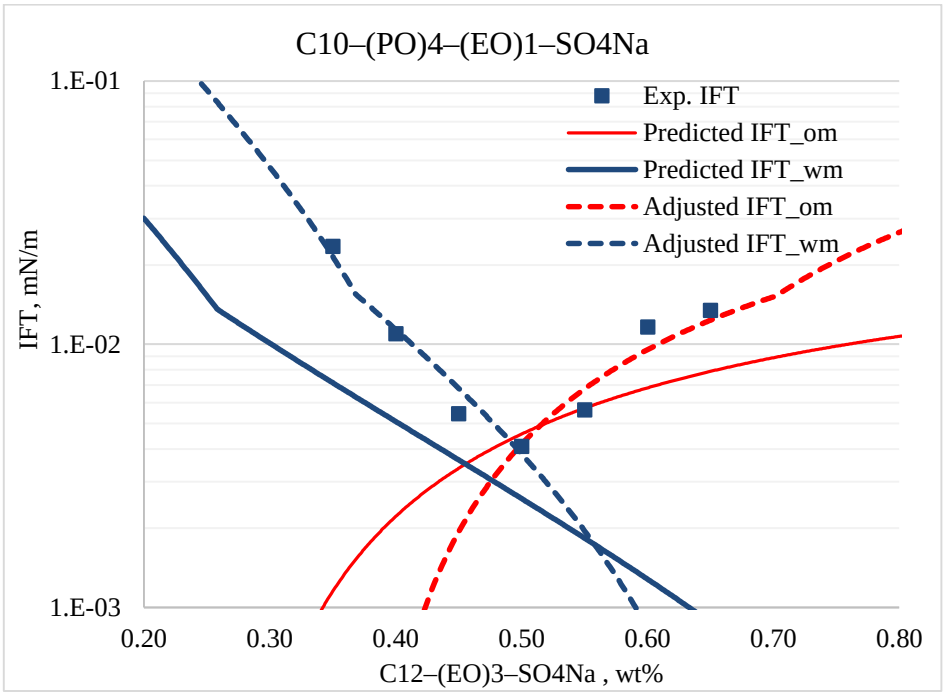


**Figure 3-5 Comparing HLD-NAC predicted and measured equilibrium IFT 0.25 wt % C10–(PO)4–(EO)1–SO4Na + C12–(EO)3–SO4Na binary mixtures with the reservoir crude oil at 52°C**

**Table 3-5 Adjusted HLD-NAC values**

| Formulation No. | Adjusted HLD | Length of Alfoterra surfactant, Å | | Length of Steol 460, Å | |
|---|---|---|---|---|---|
| | | Predicted | Adjusted | Predicted | Adjusted |
| 1 | -0.008 | 14.4 | 14.4 | 21.6 | 21.6 |
| 2 | 0.035 | 14.4 | 14.4 | 21.6 | 21.6 |
| 3 | 0.028 | 18 | 8 | 21.6 | 10 |
| 4 | 0.020 | 18 | 8 | 21.6 | 10 |

## 3.4 Comparison with Hand's rule

### *3.4.1 Hand's rule model*

Hand's rule is a generalized empirical model that can describe phase equilibrium for various systems, like chemical distribution in immiscible solvents (Hand, 1939), and gas-liquid equilibrium (Van-Quy et al., 1972). It is also used as the microemulsion phase behavior model in UTCHEM, a chemical flooding reservoir simulator developed at the University of Texas at Austin. It assumes water, oil, and surfactant as the pseudocomponents, and uses two empirical equations to represent tie-line and binodal curve of a microemulsion ternary phase diagram (Delshad et al., 1996; Camilleri et al., 1987).

In order to model microemulsion phase behavior as a function of salinity, Hand's rule needs at least 5 empirical parameters, representing the height of binodal curve at zero, optimum, and twice optimum salinity as well as the Type III salinity window, to match lab phase behavior experiments. Additional matching model parameters are introduced to model other effects. The solution to Hand's equation requires an initial guess for phase composition with iteration (UTCHEM Manual).

### *3.4.2 Pseudo salinity scan*

Since Hand's rule in UTCHEM assumes microemulsion phase behavior is subject to a salinity scan, and that IFT will vary with salinity. In order to use Hand's rule model IFT behavior under surfactant scan, this paper proposes a pseudo salinity concept, and varies the surfactant scan to a pseudo salinity scan by using the HLD equation. For each optimum formulation, HLD equals to zero, and the HLD parameters are defined as optimum $Cc$ ($Cc^*$), optimum $K$ ($K^*$), and optimum $\alpha_T$($\alpha_T^*$). Hence a pseudo-salinity can be obtained by keeping the HLD unchanging:

$$\ln(S^p) = HLD + K^* \times EACN - \alpha_T^* \Delta T + Cc^* \quad (15)$$

where the superscript p means pseudo.

### *3.4.3 Model equilibrium IFT*

Equilibrium IFT of formulation No. 2 and 4 with Alfoterra 8-41S and Alfoterra 10-41S as the main surfactants were selected to be modeled by Hand's rule. Solubilization ratio is calculated from matched Hand's rule parameters and then is used to calculate IFT by Chun Huh equation,

$$\gamma_{wm} = \frac{C}{SP_w^2} \quad (16)$$

$$\gamma_{om} = \frac{C}{SP_o^2} \quad (17)$$

where c is assumed to be a typical value of 0.3.

The converted IFT vs. Pseudo salinity curves and Hand's rule matched results are shown in Figure 3-6 and Figure 3-7. And matched Hand's rule parameters are summarized in Table 3-6. The IFT curves are well reproduced by Hand's rule model. However, the matched parameters from one system cannot be used others because of its

empirical nature. But for the HLD-NAC EOS, characterized surfactant properties can be used for various systems.

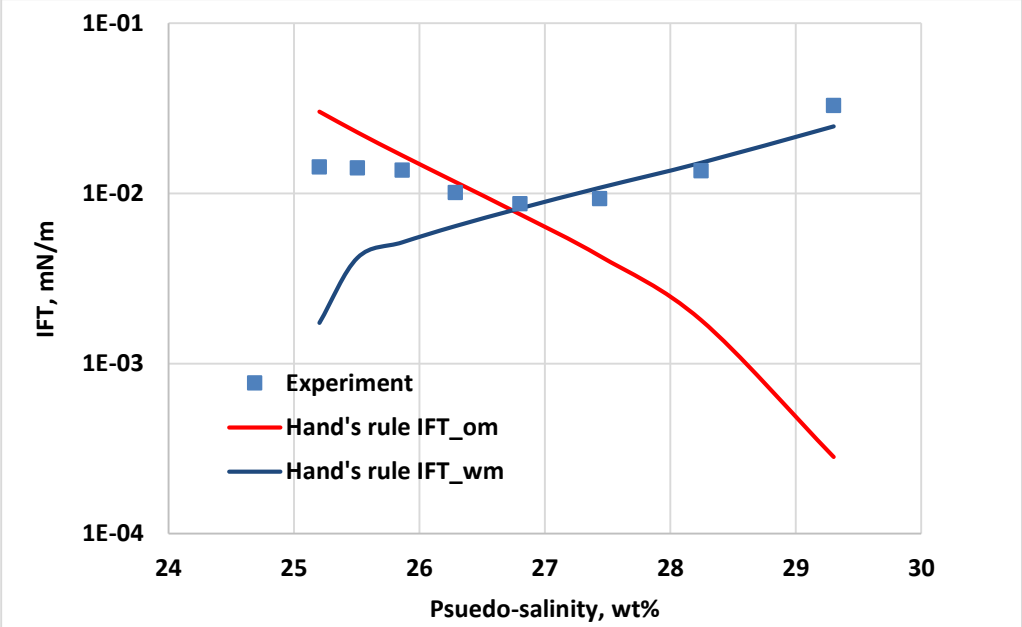


**Figure 3-6 IFT matching results of formulation 2 by Hand's rule**

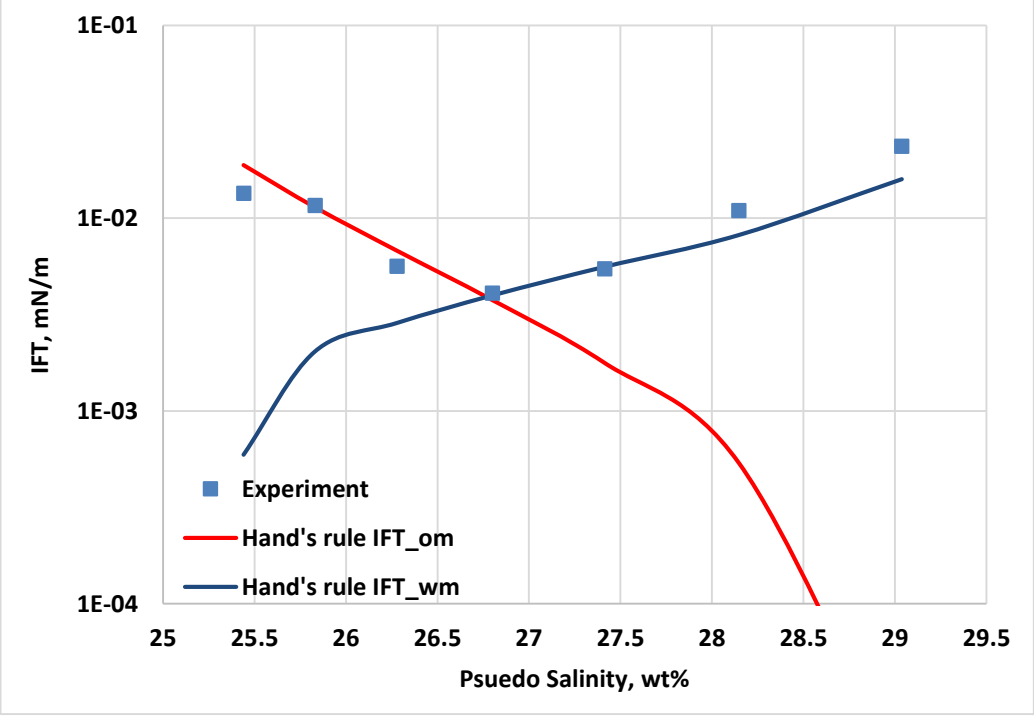


**Figure 3-7 IFT matching results of formulation 4 by Hand's rule**

**Table 3-6 Hand's rule parameters for two formulations**

| Parameter | Formulation 2 | Formulation 4 | Note[a] |
|---|---|---|---|
| HBNC70 | 0.10 | 0.07 | Maximum height of binodal curve of added surfactant at zero salinity |
| HBNC71 | 0.09 | 0.065 | Maximum height of binodal curve of added surfactant at optimal salinity |
| HBNC72 | 0.10 | 0.10 | Maximum height of binodal curve of added surfactant at twice optimal salinity |
| CSEL7, meq/ml | 4.00 | 4.3 | Lower effective salinity limit for type III phase region for added surfactant |
| CSEU7, meq/ml | 5.15 | 4.79 | Upper effective salinity limit for type III phase region for added surfactant |

a: Ref. (UTCHEM Manual)

## 3.5 Sandpack simulation

Sandpack studies were conducted to evaluate the performance of optimized surfactant only formulation in displacing waterflood residual oil saturation. Formulations 2 and 4 at optimal surfactant ratio (lowest measured IFT point in Figs. 3 and 5) were selected for sandpack experiment. The experimental procedure is detailed in Budhathoki et al. (2016).

The HLD-NAC algorithm was implemented into UTCHEM. More comprehensive study on the development of such a new simulator will be demonstrated in a companion paper. Parameters in the HLD-NAC EOS are used as model input parameters. Sandpack lab tests are then simulated by using relative permeability and surfactant adsorption as matching parameters. Figure 3-8 shows the history matched cumulative oil recovery from simulation against experimental data. The oil breakthrough and final cumulative oil recoveries are both well matched. 60% of waterflooding residual oil saturation was displaced. The matched relative permeability curves are shown in Fig. 9 and Fig. 10, respectively. Simulation results show surfactant adsorption is 2.49 mg/g rock for

formulation 2 with Alfoterra 8-41S, and 2.17 mg/g for formulation 4 with Alfoterra 10-41S, indicating high surfactant retention for these two systems.

The fitted relative permeability curves are not the only solution for this sandpack test history match. There are still other uncertainties involved in this process. For example, the capillary desaturation curve is unknown for the sandpack test, which requires much more experiments to be observed. On the other hand, since the objective of this sandpack experiment was to evaluate the displacing efficiency of these surfactant formulations at extreme high salinity of 301,710 mg/L, the effluent history of water flooding was not recorded, with which a more solid relative permeability curve at low capillary number can be obtained. Nevertheless, these uncertainties do not impair the significance of the HLD-NAC equation of state, which predicted the microemulsion phase behavior based on the ambient conditions and surfactant structures.

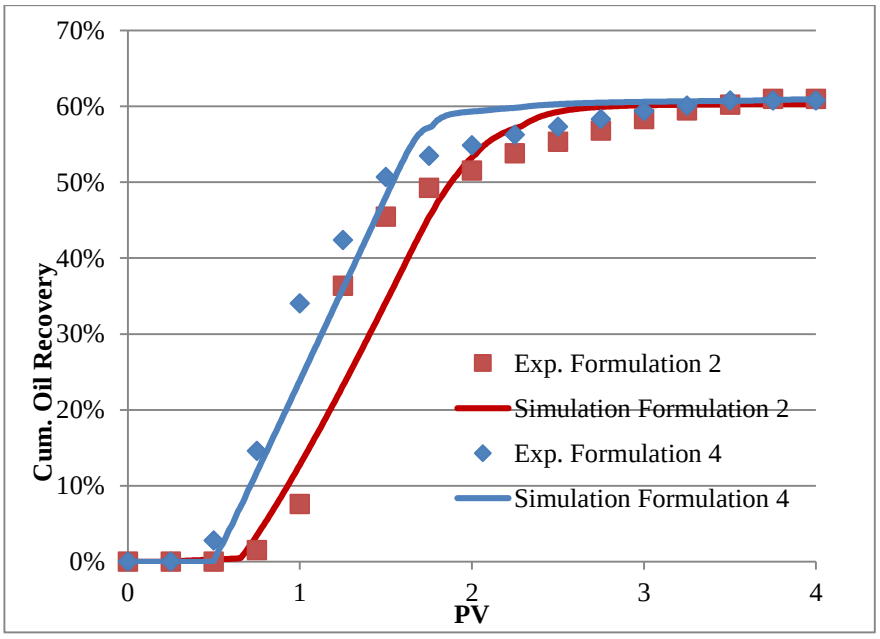


**Figure 3-8 Matching results of cumulative oil recovery**

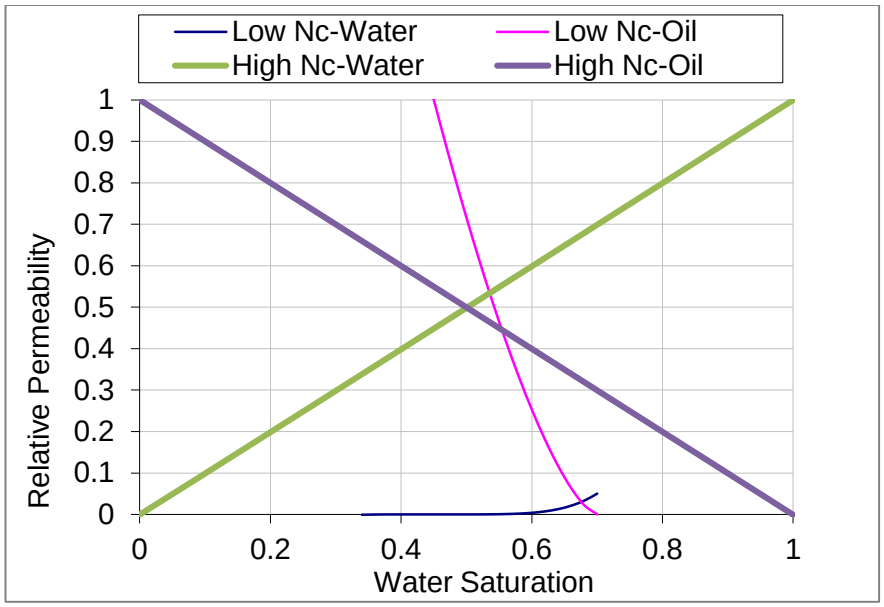


**Figure 3-9 Matched relative permeability curves for formulation 2**

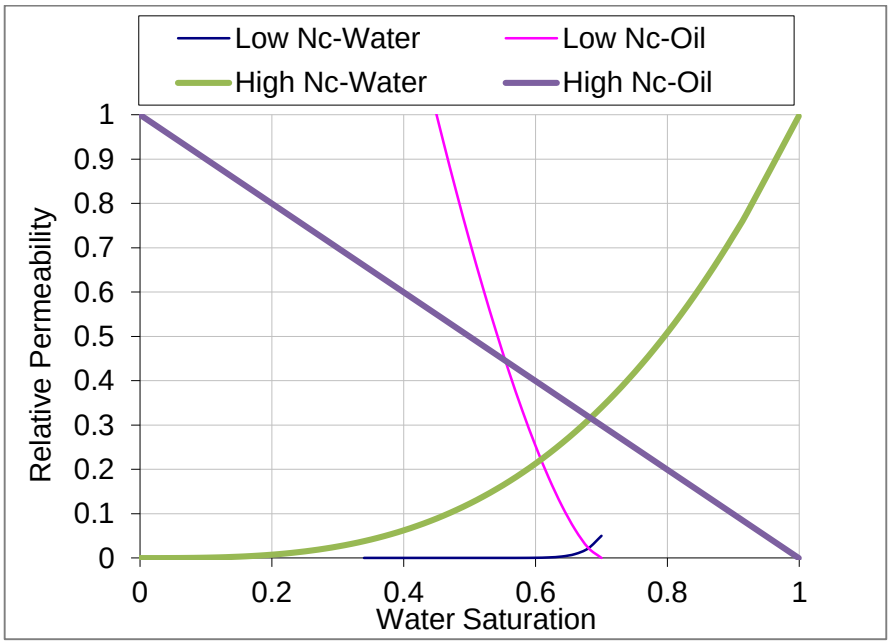


**Figure 3-10 Matched relative permeability curves for formulation 4**

### 3.6 Conclusions

This work firstly predicts the optimum surfactant formulation for a target reservoir, by using HLD equation and measured parameters i.e. EACN, salinity, K value as well as surfactant Characteristic curvature (Cc). Comparing to experiment results, the HLD

equation shows high accuracy in predicting optimum surfactant formulation for surfactant flooding, indicating its significance in shortening the surfactant screening process.

In addition, this work predicts the microemulsion phase behavior of four surfactant binary mixtures by using the HLD-NAC equation of state. The predicted results are in good agreement with the measured equilibrium IFTs. This is the first time that the IFT behavior of surfactant-brine-crude oil system is predicted based on the quantitatively characterized surfactant hydrophobicity as well as surfactant structure properties, showing the physical significance of HLD-NAC equation of state in predicting microemulsion phase behavior.

This paper then introduced a pseudo salinity concept that converts the IFT curves under surfactant scan into a salinity scan. Hence, empirical microemulsion phase behavior Hand's rule is able to model the IFT behavior. Five matching model parameters are required for each case. Comparing to Hand's rule, the HLD-NAC EOS is physics based and the characterized surfactant parameters can be used for different microemulsion system, indicating excellent predictability.

Finally, two surfactant flooding sandpack tests are simulated using UTCHEM with the novel HLD-NAC equation of state. This work comprehensively demonstrated the capabilities of HLD-NAC equation of state in not only predicting optimum surfactant formulation but also microemulsion phase behavior based on the ambient conditions and surfactant structures, and its significance for surfactant flooding simulation as a predictive phase behavior model.

## Nomenclature

*Roman*

$a_{si}$ = *Surface area per molecule of the surfactant i ($Å^2$)*

*As* = *Total interfacial area in microemulsion ($Å^2$)*

$C_{si}$ = *The concentration of the surfactant species i in water (mol/L)*

*Cc* = *Characteristic curvature of surfactant (dimensionless)*

*EACN* = *Equivalent alkane carbon number of the oil (EACN unit)*

*Er* = *Interfacial rigidity ($m^2 \cdot kg \cdot s^{-2}$)*

*f(A)* = *Function of alcohol type and concentration (dimensionless)*

$H_a$ = *Average curvature ($Å^{-1}$)*

$H_n$ = *Net curvature ($Å^{-1}$)*

*HLB* = *Hydrophilic lipophilic balance (dimensionless)*

*HLD* = *Hydrophilic lipophilic difference (dimensionless)*

*IFT* = *Interfacial tension (dynes/cm)*

*K* = *Slope of the logarithm of optimum salinity as a function of EACN (per EACN unit)*

$K_B$ = *Boltzmann constant*

*L* = *Surfactant length parameter (Å)*

$R_o$ = *Radius of hypothetical oil droplet in microemulsion (Å)*

$R_w$ = *Radius of hypothetical water droplet in microemulsion (Å)*

*S* = *Salinity (g/100mL)*

$SP_i$ = *Solubilization parameter of component i in microemulsion (dimensionless)*

*T* = *Temperature (K)*

$V_i$ = *volume of component i in a phase (mL)*

$x$ = *Mole fraction (dimensionless)*

*Greek*

$\alpha_T$ = *Temperature coefficient of optimum salinity expressed in units of ln S (°C$^{-1}$ or K$^{-1}$)*

$\delta$ = *Length of carbon carbon bond in surfactant tail (Å)*

$\varphi_i$ = *Fraction of component i in the microemulsion (dimensionless)*

$\xi^*$ = *Characteristic length of a microemulsion system (Å)*

*Subscripts*

$i$ = *Component in a phase*

$mix$ = *Mixture*

$o$ = *Oil*

$w$ = *Water*

$m$ = *Microemulsion*

$om$ = *Oil and microemulsion*

$wm$ = *Water and microemulsion*

*Superscripts*

$p$ = *Pseudo*

$*$ = *Optimum status unless mentioned otherwise*

# Chapter 4 Development of a Chemical Flood Simulator Based on Predictive HLD-NAC Equation of State for Surfactant


## Abstract

Accurately model microemulsion phase behavior is critical for compositional simulation of surfactant flood. The HLD-NAC equation of state has been proved to be an excellent model for shorten the surfactant screening process and help improve the predictability of surfactant floods. This paper developed an algorithm to generate ternary phase diagrams with water, oil and surfactant as the pseudo components, by utilizing the only fitted parameter L from modeling phase behavior test. The algorithm is then coupled with UTCHEM, a chemical flooding simulator developed at the University of Texas at Austin.

Comparing with the widely used empirical microemulsion phase behavior model Hand's rule which is currently built in UTCHEM, the HLD-NAC model is a physics-based model with predictability and has only one fitting parameter, L, which is proportional to the surfactant carbon chain length. Synthetic corefloods are simulated by UTCHEM with the HLD-NAC model and compared Hand's rule. These two models produce the same results at constant optimum salinity, and the HLD-NAC model predicts higher oil recovery than Hand's rule for the case with under salinity gradient. The differences are explained by comparing the solubilization profile along the core, and the shape of ternary phase diagrams produced by both models at Type I microemulsion.


## 4.1 Introduction

Microemulsion phase behavior of surfactant/brine/oil systems is critical to both surfactant flood formulation design and simulation. Winsor (1954) classified the

microemulsion to Type I, Type II and Type III phase behavior, corresponding to lower-, upper- and middle- phase microemulsion. Microemulsion phase transits from Type I through Type III to Type II, with increases in electrolyte concentration (Healy et al., 1976), surfactant hydrophobicity (Healy et al., 1976; Bourrel et al., 1980), the addition of heavy alcohol (Healy et al., 1976), and with decreases in equivalent alkane carbon number of the oil (EACN) as well as temperature for most ionic surfactants (Healy et al., 1976;). Achieving Type III is usually the target in surfactant flood formulation design, because ultralow interfacial tension (IFT) is generally found in the Type III region and an optimal state may be obtained as the equal amount of water and oil are solubilized in the microemulsion phase (Reed and Healy, 1977).

Phase transitions caused by these variables reflect the chemical potential differences of the surfactant between phases. Salager et al. (1979a, 1999, 2000) introduced a hydrophilic lipophilic difference (HLD) concept, which depicts the change in free energy associated with transferring a surfactant molecule from the oil phase to the aqueous phase normalized by the thermal energy, as shown in the following HLD equation:

$$HLD = \frac{\mu_w^s - \mu_o^s}{RT} = ln(S) - K \times EACN - \alpha_T \Delta T + Cc + f(A) \quad (1)$$

where, $\mu_w^s$, $\mu_o^s$ = standard chemical potentials of the surfactant in the water and oil phases \

R = universal gas constant

T = absolute temperature

S = salinity (g/100 ml), the electrolyte concentration

EACN = equivalent alkane carbon number of the oil

K = slope of the logarithm of optimum salinity as a function of ACN

f(A) = function of alcohol type and concentration

$Cc$ = characteristic parameter of surfactant

$a_T$ = temperature coefficient of optimum salinity expressed in units of ln S per °C

$\Delta$T = temperature, °C

To predict the microemulsion phase behavior for live oil, Ghosh and Johns (2014) added a term $\beta\Delta P$ to consider the effects of pressure.

The HLD value measures the departure from the optimum formulations. Negative or positive HLD values correspond to Winsor Type I or Type II microemulsion, respectively. HLD value of zero suggests optimum state. The signs that these variables bear in the HLD equation indicate their effects on phase transition. A positive sign means that an increase in the value of that variable would produce a Type I → Type III → Type II transition, while a negative sign would correspond to the opposite transition (Salager and Antón, 1999).

Quantitatively characterizing surfactant properties using HLD concept has been attracting attentions, since it provide formulators with guideline to quickly and effectively screen surfactants (Trahan and Jakobs-Sauter, 2015). K value of ionic surfactants in the HLD equation is depending on the structure of surfactant head group. Literatures have reported K ranges from 0.004 to 0.2 for numerous surfactant-oil combinations (Salager et al., 1979; Acosta et al., 2008a; Witthayapanyanon et al., 2008; Hammond and Acosta, 2012). Characteristic Curvature (Cc) corresponds to the normalized net curvature of the surfactant at reference condition (Acosta et al., 2008a, Hammond and Acosta, 2012), representing the hydrophobicity of surfactant. A negative Cc value corresponds to a surfactant that tends to form a Type I microemulsion; and conversely, a positive Cc value corresponds to a hydrophobic surfactant that has the tendency to form a Type II

microemulsion (Acosta et al., 2008a). Cc values of both conventional surfactants (Acosta et al., 2008a) and extended sulfate surfactants with EO/PO groups (Hammond and Acosta, 2012; Budhathoki et al., 2015) have been studied. With accurately characterized HLD parameters, the optimum formulation have been predicted by manipulating the surfactant ratio so that the calculated HLD equals to zero (Manish et al., 2015). This indicates that the HLD-NAC model can shorten the surfactant screening process hence help chemical EOR formulation design and optimization.

Surfactant flood simulation is also heavily rely on the phase behavior model, because physical properties such as microemulsion viscosities, interfacial tensions, surfactant adsorption as well as phase relative permeabilities are all functions of phase compositions and saturations (Prouvost et al., 1984; Delshad et al., 1996). In surfactant flood formulations, chemical species like water, electrolytes, oil, surfactants and cosolvents are included in the mixture. But it is challenging to consider all independent components in the phase behavior model. The most widely used method is to use pseudocomponents representing the mixture.

Modeling microemulsion phase behavior has been challenging because it is difficult to be mathematically described (Camilleri et al., 1987), especially for the Type III microemulsion (Huh, 1983). These published microemulsion phase behavior models generally fall into two categories: empirical and physical models. A widely used empirical model is the Hand's rule (Hand, 1939), which was invented to describe component distributions in two immiscible phases. An algorithm based on Hand's rule has been used in compositional chemical flood simulators such as UTCHEM (Pope, 1979; Camilleri et al., 1987; Delshad et al., 1996). However, in order to simplify the calculation,

Hand's rule in UTCHEM assumes symmetric binodal curve in all conditions (Camilleri et al., 1987; Delshad et al., 1996). On the other hand, in order to model microemulsion phase behavior as a function of salinity and comparing to experiment data, Hand's rule needs at least 5 empirical parameters, representing the height of binodal curve at zero, optimum and twice optimum salinity as well as the Type III salinity window (Delshad et al., 1996). Additional matching parameters are introduced to model other effects such as the effect of cosolvent and temperature (Delshad et al., 1996). The solution to Hand's equation requires an initial guess for phase composition with iteration (Sheng, 2010). Prouvost (1984) developed a phase behavior model based on Hand's equation considering up to three amphiphilic species for compositional surfactant flood simulation. However, the empirical nature of Hand's equation weakened the physical significance of the model.

Physics based microemulsion phase behavior models have been focused on the geometry of the micelle (Mitchell and Nihanm, 1981) and the bended curvature of interfacial layer (Huh, 1983). Chou and Bae (1988) developed a phase behavior model for high salinity surfactant formulations by extending the approach of Mitchell and Nihanmb (1981), which can predict the microemulsion transition with increasing salinity by using three adjustable parameters. These parameters related to the characteristic of each component. The advantage of this physical model is it can help formulation design, since the determined parameters from one system can be applied to other systems. However, many assumptions in the model are valid only in high salinity conditions, and it has not been used for phase behavior tests with crude oil. Huh (1983) investigated the affecting factors on the microemulson droplet size, but the model was not able to describe the Type III microemulsion.

Acosta (Acosta et al., 2003) introduced a Net-Average Curvature (NAC) equation of state (EOS) for microemulsion system, which assumes any microemulsion could be represented as coexisting hypothetical spherical droplets of oil and water. The reciprocal of the water and oil droplet is the curvature of the microemulsion. And it was found the net curvatures for Type I and Type II system are scaled to the HLD by the fully extended surfactant tail length, L. Coupling the HLD equation, the HLD-NAC EOS is able to calculate phase compositions, and has since been used to fit and predict the phase behavior, solubilization capacity, IFT, and viscosity of microemulsion produced by surfactants (Acosta et al., 2003, 2008a, 2012). Recently, the HLD-NAC model has been utilized into chemical EOR area. Jin et al., (2015) modeled solubilization ratio curves and phase volume fraction diagrams of different surfactant/brine/crude oil systems using the HLD-NAC model with the length constant, L, as the only fitting parameter. It proved that the HLD-NAC model can be used as the basis for surfactant flood simulation. However, to do surfactant flood simulation, the microemulsion phase behavior model should be able to determine the positions of the system on ternary phase diagram, in order to consider more complex conditions like single microemulsion phase and phase inversion due to the saturation and water oil ratio variations.

Therefore, this paper develops an algorithm that can plot the microemulsion ternary phase diagrams, which is then coupled into a compositional surfactant flood simulator UTCHEM. Surfactant flood is modeled by the UTCHEM simulator with HLD-NAC model and compared against Hand's rule.

## 4.2 Algorithm

The flowchart for modeling microemulsion phase behavior using HLD-NAC model is same as Figure 3-1. Generally, there are three groups of input parameters:

1) surfactant and oil properties such as Cc, K, EACN, $a_i$ and L, etc. The experimental methods to obtain Cc, K, EACN and $a_i$ can be found from Acosta et al. (2008 Cc), Salager et al. (1979a), Manish et al. (2015) and Rosen (2004). The length parameter L is the only matching parameter, which is obtained from fitting the solubilization ratio curves as described at Acosta et al. (2003) and Jin et al. (2015).
2) component composition include volume fraction of water oil and surfactants, salinity, temperature and pressure. These parameters are collected from experiment conditions in phase behavior test, or properties of each grid block in numerical simulation.
3) optimum salinity S* and the characteristic length $\xi^*$. These two parameters are gained from phase behavior test for formulation design as described at Acosta et al. (2003) and Jin et al. (2015).

The general assumptions in the algorithm are listed as follows:

1) microemulsion could be represented as coexisting hypothetical spherical droplets of oil and water;
2) the concentration of the surfactant in the monomer form is negligible;
3) the surfactant head area is constant at different salinities;
4) the surfactant density is 1 g/ml in calculating surfactant mole concentration;
5) pseudo components are surfactant, brine and oil;
6) plait points are estimated as the intersection of solubilization capacity line and the catastrophic phase inversion line.

HLD is firstly calculated from given input parameters. When the HLD parameters are measured, the HLD values can be calculated from Eq. 1. For new surfactants have not

been characterized by HLD concept, HLD values are determined by simplified method as shown in Eq. 2, since $S^*$ is the optimum salinity at which HLD equals to zero.

$$HLD = \ln\left(\frac{S}{S^*}\right) \quad (2)$$

The interfacial area provided by the surfactant ($A_s$) was estimated using Eq. 3, where the mole concentration of surfactant is calculated by assuming the surfactant density is 1 g/ml.

$$A_s = \sum_i V_w \times C_{s_i} \times 6.023 \times 10^{23} \times a_i \quad (3)$$

where $V_w$ = the volume of water in the system;

$C_{s_i}$ = the concentration of the surfactant species *"i"* in water, mol/L;

$a_i$ = the surface area per molecule of the surfactant, Å$^2$.

If HLD $\leq 0$, it means the microemulsion system is either Type I or Type III. It is then assumed that water is the continuous phase, so the hypothetical radius of the continuous aqueous phase ($R_w$) is calculated as shown in Eq. 4, the oil swollen micelle radius $R_o$ is furtherly calculated using the net curvature as shown in Eq. 5.

$$R_w = \frac{3 \times V_w}{A_s} \quad (4)$$

$$H_n = \left|\frac{1}{R_o}\right| - \left|\frac{1}{R_w}\right| = \frac{-HLD}{L} \quad (5)$$

$H_n$ is the net curvature determining the curvature of the surfactant film adsorbed at the oil/water interface. The sign of the net curvature indicates the microemulsion type. A positive net curvature ($H_n > 0$ *or* HLD $< 0$) corresponds to Type I microemulsion ($R_w \gg R_o$), and negative values ($H_n < 0$ *or* HLD $> 0$) to Type II microemulsion ($R_o \gg R_w$). As the net curvature approaching zero ($H_n = 0$ *or* HLD $= 0$), the microemulsion is reaching optimum status that a bicontinuous microemulsion containing equal amounts of oil and water ($R_o \approx R_w$). For Type I and Type II microemulsion, the net curvature scales to HLD

by L, which is a length parameter that has found to be proportional to the extended length of the surfactant tail group (Acosta et al., 2003).

If else the HLD>0, the microemulsion is either Type II or Type III. Oil is then assumed to be the continuous phase for calculating the hypothetical radius of the external phase by Eq. 6. And the droplet radius of internal aqueous phase is then obtained by the net curvature as Eq. 5.

$$R_o = \frac{3 \times V_o}{A_s} \tag{6}$$

The average curvature $H_a$ is further determined by $R_w$ and $R_o$ obtained from previous steps. The reciprocal of $H_a$ is the characteristic size that equals to the characteristic length of the microemulsion in bicontinuous system. Therefore, $1/H_a < \xi^*$ is a criterion in differentiating middle phase microemulsion, since the average curvature $H_a$ describes the size of microemulsion aggregates which should not exceed the characteristic length. For Type III microemulsion, Eqs. 5 and 7 are solved simultaneously. Hence the hypothetical radii of water and oil droplets in middle phase microemulsion are obtained.

$$H_a = \left|\frac{1}{R_o}\right| + \left|\frac{1}{R_w}\right| = \frac{1}{\xi^*} \tag{7}$$

To this step, the microemulsion composition and the solubilization ratio are ready to be calculated and model phase behavior test as shown in Jin et al. (2015). Nouraei and Acosta (2015) developed a method to plot ternary phase diagram based on the HLD-NAC theory. In phase behavior test, the water oil ratio is usually 1:1, so the overall compositions lie in the multiphase region on a ternary phase diagram. For Type I and Type II systems, the microemulsion composition from phase behavior test is located on the binodal curve or solubilization capacity line, and the connections of the microemulsion composition at various surfactant concentration and excess phases are a

series of tie lines. For Type III system, the coordinate of the microemulsion composition is the invariant point for a Type III system, and the connections of the microemulsion composition and excess phases are the boundary of three phase region and two phase lobes.

In Nouraei and Acosta (2015), it describes a method applying catastrophic theory to determine the plait point. As the internal phase volume fraction in the microemulsion increases to some point, the internal phase inverse to the external phase naming catastrophic phase inversion. Although the catastrophic phase inversion is system dependent, a good assumption is that it occurs when internal phase volume fraction is over than 75% (Nouraei and Acosta, 2015). In this paper, the microemulsion composition where phase inversion happens is the plait point, and the line connecting the plait point and the excess phase composition is the last tie-line. The ternary phase diagram plotted by this method shows a sharp triangle multiphase region, which is not like the real systems that the transition is more gradual at the places near plait point. However, how gradual the transition is at the plait point varies from one system to another and there is no good method to predict it yet. On the other hand, measuring more accurate plait point requires intensive lab experiments. Therefore, this procedure produces a more generic prediction of the phase diagram that can be applied to a wide range of systems without additional experimental work. And in surfactant flood, the surfactant concentration is usually lower than 2 wt%, which is much smaller than surfactant concentration at the plait point. So this assumption meets the objective of this paper for modeling microemulsion phase behavior in surfactant flood.

The plait point and invariant point divide the ternary phase diagram to several regions. And microemulsion composition, solubilization ratio, saturation etc. are calculated in each of these regions. To validate this algorithm, simulation results are compared with Hand's rule, which has been detailed in many other references (Camilleri et al., 1987; Delshad et al., 1994; Sheng, 2010).

## 4.3 Results and discussion

### *4.3.1. Modeling Solubilization Ratio*

The objective of modeling solubilization ratio from phase behavior test is to obtain L, which is the only matching parameter. Jin et al. (2015) described the procedures and results of modeling solubilization ratio curves of formulations with various single surfactant, surfactant mixture with and without alcohol. This paper chooses a formulation with 1.0 wt% of $C_{32}$-7PO-32EO-carboxylate and a 1.0 wt% of $C_{19-23}$ IOS for crude oil as an example. The matching results of solubilization ratio curves from HLD-NAC model are compared with Hand's Rule model, as shown in Figure 4-1.

The experiment results are well reproduced by both HLD-NAC model and Hand's rule. Table 4-1 and Table 4-2 summarize the parameters used in each model. It is obvious that the HLD-NAC model has its physical significance since all the parameters have their own features that can be characterized by experiment. It has been proved that the fitted L can be readily applied to other oil indicating the predictability of the HLD-NAC model. The 7 parameters used in Hand's rule are all matching parameters for curve fitting. HNBC0, HBNC1 and HBNC2 are the height of binodal curves at zero, optimum and twice optimum salinity. CSEL7 and CSEU7 are lower and upper salinity boundary for Type III

window, respectively. C2PLC and C2PRC are the total concentration of oil at left and right plait point, which are purely assumed in this case.

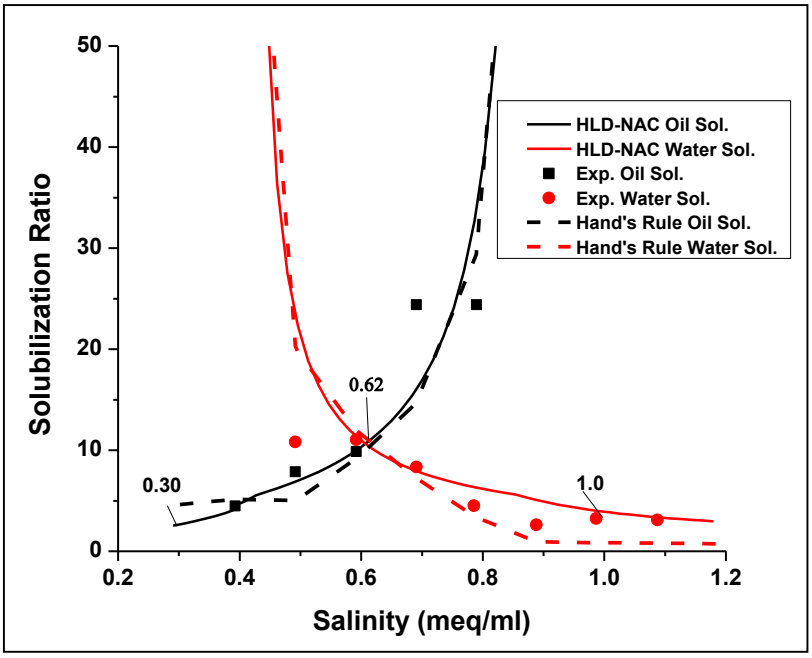


**Figure 4-1 HLD-NAC and Hand's rule fitted solubilization ratio curves of 1.0 wt% of C32-7PO-32EO-carboxylate and 1.0 wt% of C19-23-IOS for crude oil**

**Table 4-1 Parameters for modeling solubilization ratio by HLD-NAC model**

| Parameter | Surfactant MW, (g/mole) | Surfactant Head Area $a_s$, ($Å^2$) | Optimum Salinity $S^*$, meq/ml | Characteristic Length, $\xi^*$, Å | Length Parameter, L, Å |
|---|---|---|---|---|---|
| Value | $C_{32}$-7PO-32EO-carboxylate: 2331<br>$C_{19\text{-}23}$ IOS: 398 | $C_{32}$-7PO-32EO-carboxylate:: 194<br>$C_{19\text{-}23}$ IOS: 50 | 0.62 | 347 | 65 |

**Table 4-2 Parameters for modeling solubilization ratio by Hand's Rule model**

| Parameter | HBNC0 | HBNC1 | HBNC2 | CSEL7, meq/ml | CSEU7, meq/ml | C2PLC | C2PRC |
|---|---|---|---|---|---|---|---|
| Value | 0.055 | 0.045 | 0.055 | 0.4 | 0.84 | 0.1 | 0.9 |

As shown in Figure 4-1, in Type III region, the solubilization ratio curves from HLD-NAC overlap the curves from Hand's rule model, indicating excellent compatibility

between these two models. For Type I system, the oil solubilization ratio curve from the HLD-NAC model well matched the experiment data, but that from the Hand's rule is more flat and deviated from the experiment results. Similarly, in Type II region the solubilization of water is fairly modeled by the HLD-NAC model but under predicted by the Hand's rule model. The reasons for the deviation of HLD-NAC fitted results from experiment data have been analyzed in Jin et al. (2015), that the surfactant head area was measured at 2% NaCl and assumed to be constant at various salinities. As a matter of fact, the surfactant head area is a function of salinity which is worth to be further investigated to improve the physical significance of the HLD-NAC model. The transition of solubilization ratio curves between different phase types from Hand's equation is not as smooth as the HLD-NAC model. The reason is the assumption of symmetric binodal curve in Hand's equation is no longer valid when the microemulsion status approaching Type III.

### *4.3.2 Ternary Phase Diagram*

With the only fitting parameter L obtained from modeling solubilization ratio of the formulation with 1.0 wt% of $C_{32}$-7PO-32EO-carboxylate and a 1.0 wt% of $C_{19\text{-}23}$ IOS for crude oil, the HLD-NAC model is able to plot the ternary phase diagram at various HLD value. In this paper, the HLD value is represented by the salinity since the phase behavior test was done under salinity scan. Ternary phase diagrams are plotted at salinities of 0.3, 0.62 and 1.0 meq/ml as marked on Figure 4-1, corresponding to Type I, optimum Type III and Type II systems.

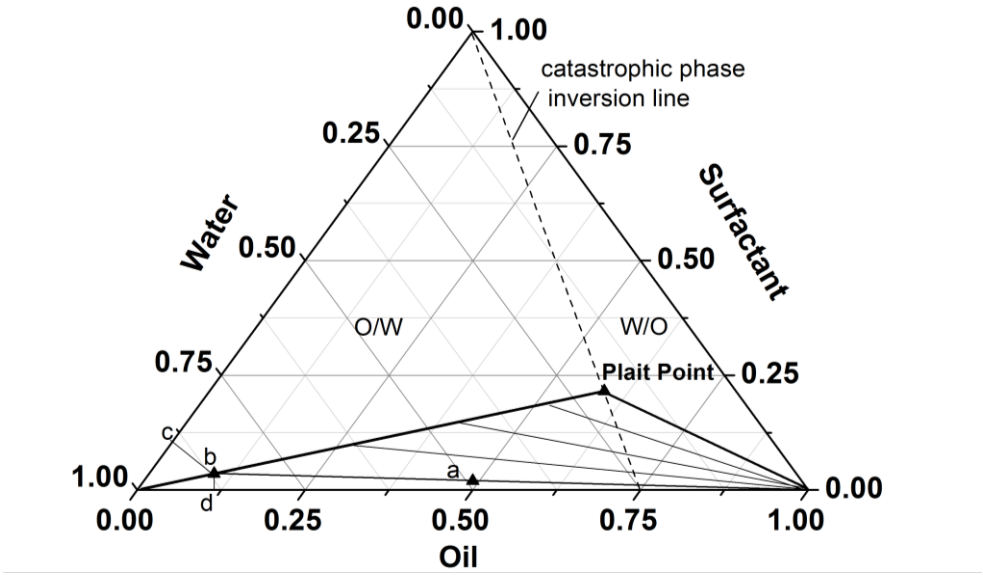


**Figure 4-2 Ternary phase diagram plotted by HLD-NAC model of 1.0 wt% of C32-7PO-32EO-carboxylate and 1.0 wt% of C19-23-IOS for crude oil at 0.3 meq/ml (Type I)**

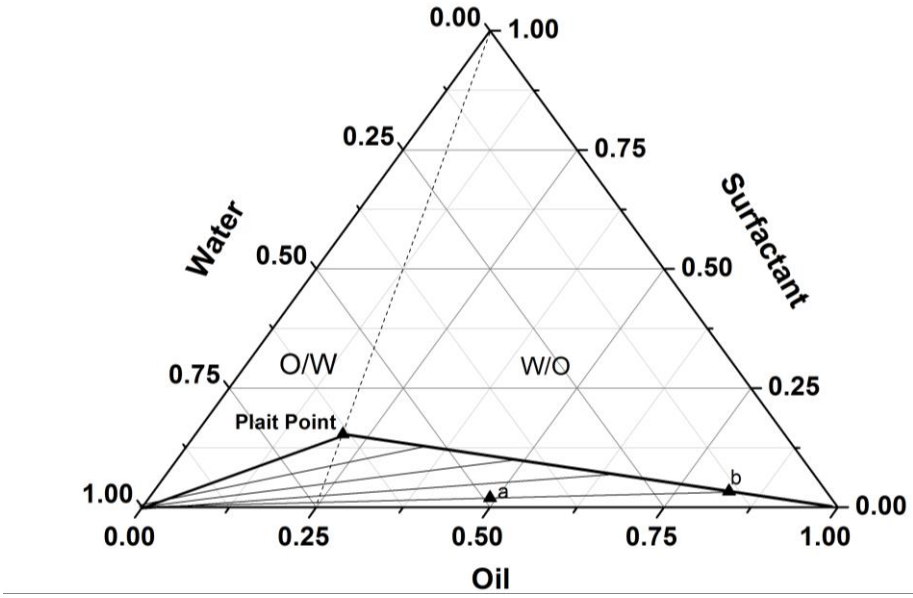


**Figure 4-3 Ternary phase diagram plotted by HLD-NAC model of 1.0 wt% of C32-7PO-32EO-carboxylate and 1.0 wt% of C19-23-IOS for crude oil at 1.0 meq/ml (Type II)**

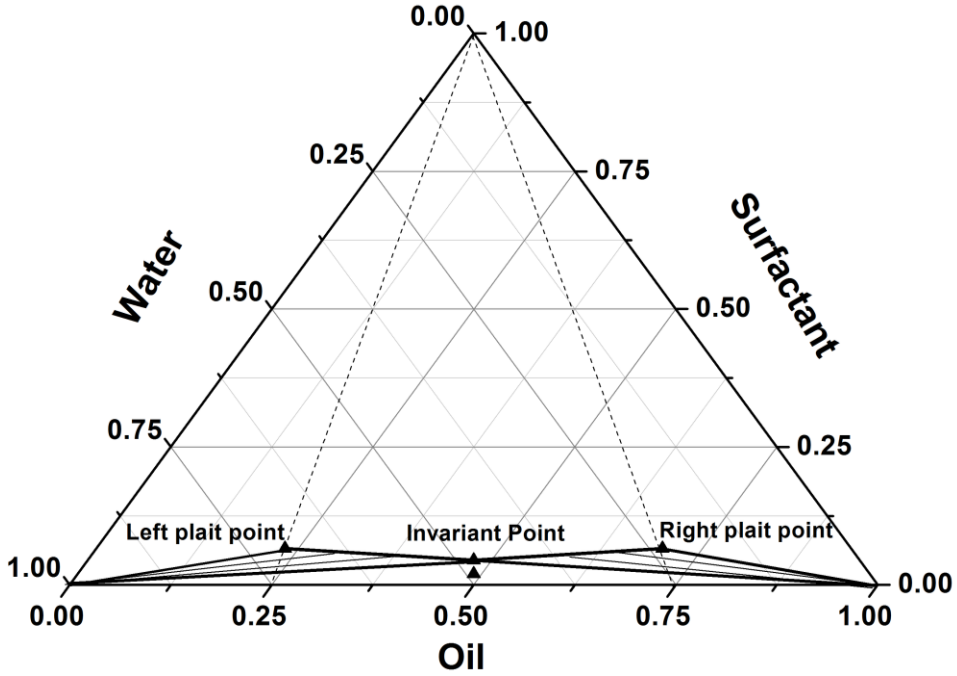


**Figure 4-4 Ternary phase diagram plotted by HLD-NAC model of 1.0 wt% of C32-7PO-32EO-carboxylate and 1.0 wt% of C19-23-IOS for crude oil at 0.62 meq/ml (Type III)**

Figure 4-2 presents the Type I ternary phase diagram at 0.3 meq/ml. Point a is the overall composition at phase behavior test with equal volume of oil and water, as well as 2 wt% of surfactant mixture. After the system reached equilibrium, it formed a lower phase microemulsion represented by point b and excess oil phase. The length ratio of b-c to b-d is the solubilization ratio, which is 2.7 for this system at 0.3 meq/ml. The algorithm assumes the micromeulsion at certain salinity has constant solubilization ratio as long as the overall composition lies in the multiphase region. Therefore, the points on the phase diagram with solubilization ratio of 2.7 compose the solubilization capacity curve which is a fraction of the binodal curve representing the microemulsion compositions. By assuming the internal phase volume fraction causing catastrophic phase inversion is 75%, which shown as dash line on Figure 4-2, the coordinates of plait point are then determined. The line connecting the plait point and the 100% oil point is the last

tie-line. In this way, the ternary phase diagram is divided into a multiphase region, a single phase O/W microemulsion and a single phase W/O microemulsion regions. The height of the plait point reflecting the solubilization capability of the system, which is consistent with the concept of the height of binodal curve in the Hand's rule model. As the salinity increases approaching the lower salinity for phase inversion from Type I to Type III, the oil solubilization ratio increases, hence the height of the plait point decreases and the two phase region is suppressed.

Figure 4-3 plots the ternary phase diagram at 1.0 meq/ml, where the microemulsion is Type II. Similarly as Figure 4-2, it is assumed that the W/O microemulsion inverse to O/W microemulsion as the internal water volume fraction is higher than 75%. Therefore, the plait point is on the left side with high water concentration. The water solubilization ratio for the formulation at 1.0 meq/ml is 3.8, so the height of the plait point is lower comparing to Figure 4-2.

The Type III ternary phase diagram at optimum salinity which is 0.62 meq/ml for this formulation is shown in Figure 4-4. Overall composition is point a, and it splits to a microemulsion with equal volume of water and oil and two excess phases as the system is equilibrated. The coordinate of the middle phase microemulsion is the invariant point. As long as the overall composition is in the three phase region, the microemulsion composition is constant as the invariant point, although the microemulsion volume fraction varies. When the initial water or oil volume is smaller than the solubilization capacity of the formulation, the overall composition lies in the Type II or Type I lobe. So the middle phase microemulsion composition moves from the invariant point along the

binodal curve toward the plait points. Positions of the left and right plait points are determined under the same assumption as Type II and Type I microemulsion.

### *4.3.3 Surfactant Flood Simulation*

The HLD-NAC model is implemented into the chemical flood simulator UTCHEM, which is developed at the University of Texas at Austin. The simulator keeps all the rest features of UTCHEM except the Hand's rule microemulsion phase behavior model is replaced by the HLD-NAC model.

Synthetic surfactant core floods with the same formulation of 1.0 wt% of $C_{32}$-7PO-32EO-carboxylate and a 1.0 wt% of $C_{19-23}$ IOS are simulated by UTCHEM with HLD-NAC model and compared with Hand's rule. Table 4-3 summarizes the core description and simulation parameters for the coreflood. This paper firstly simulated a coreflood with constant salinity, which 0.62 meq/ml for the given formulation. And another coreflood under salinity gradient was then simulated. The initial salinity in the core is 1.0 meq/ml, and the surfactant slug is at optimum salinity of 0.62 meq/ml followed by continuous water drive at 0.3 meq/ml. The initial salinity and injection scheme of these two cases are summarized in Table 4-4.

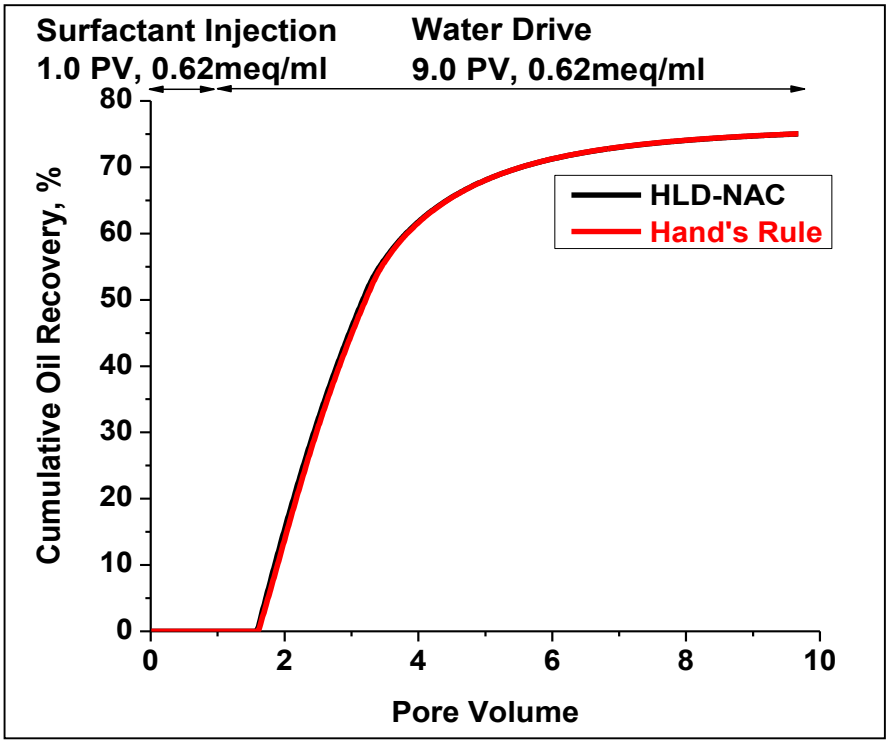


**Figure 4-5 Cumulative oil recovery of constant salinity injection (Case 1)**

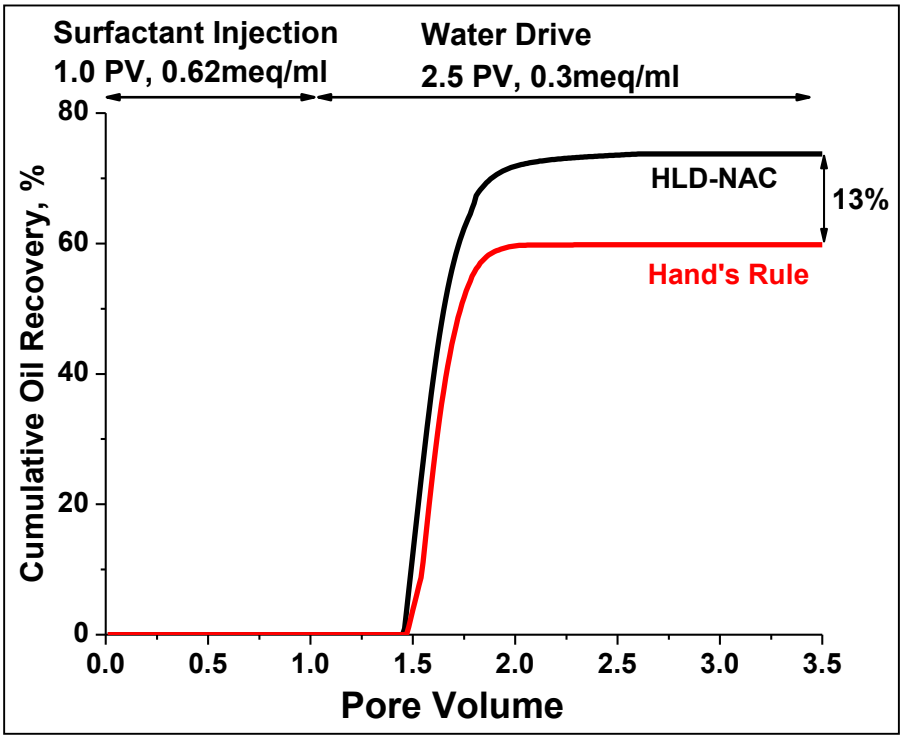


**Figure 4-6 Cumulative oil recovery of salinity gradient injection (Case 2)**

**Table 4-3 Summary of core description and simulation parameters**

| Term | Value | Term | Value |
|---|---|---|---|
| Core Dimensions, ft | 0.11×0.11×0.744 | $S_{1rw}$ | 0.3 |
| Porosity, fraction | 0.219 | $S_{2rw}$ | 0.33 |
| Absolute Brine Permeability, md | 72 | $S_{3rw}$ | 0.3 |
| Swi | 0.68 | $k^0_{r1w}$ | 0.3 |
| $\log(\sigma_{wo})$ | 1.3 | $k^0_{r2w}$ | 0.6 |
| $G_{11}$ | 13 | $k^0_{r3w}$ | 0.3 |
| $G_{12}$ | -14.8 | $e_{1w}$ | 2 |
| $G_{13}$ | 0.007 | $e_{2w}$ | 2 |
| $G_{21}$ | 13 | $e_{3w}$ | 2 |
| $G_{22}$ | -14.5 | $S_{1rc}$ | 0 |
| $G_{23}$ | 0.01 | $S_{2rc}$ | 0 |
| $T_{11}$ | 1865 | $S_{3rc}$ | 0 |
| $T_{12}$ | 59074 | $k^0_{r1c}$ | 1 |
| $T_{13}$ | 364.2 | $k^0_{r2c}$ | 1 |
| $\alpha_1$ | 1 | $k^0_{r3c}$ | 1 |
| $\alpha_2$ | 1 | $e_{1c}$ | 1 |
| $\alpha_3$ | 1 | $e_{2c}$ | 1 |
| $\alpha_4$ | 0.9 | $e_{3c}$ | 1 |
| $\alpha_5$ | 0.7 | $ad_{31}$ | 0 |
| $\mu_1$, mPa·s | 0.678 | $ad_{33}$ | 0 |
| $\mu_2$, mPa·s | 7 | $b_{3d}$ | 1000 |

**Table 4-4 Summary of injection scheme**

| Case | Type | Core salinity | Surfactant slug | Water drive |
|---|---|---|---|---|
| 1 | Constant salinity | 0.62 meq/ml | 1.0 PV at 0.62 meq/ml | 9.0 PV at 0.62 meq/ml |
| 2 | Salinity gradient | 1.0 meq/ml | 1.0 PV at 0.62 meq/ml | 2.5 PV at 0.3 meq/ml |

At optimum salinity, the water and oil solubilization ratios from both of HLD-NAC and Hand's rule are identical at 11.5. Figure 4-5 plots the cumulative oil recovery under constant salinity injection from both HLD-NAC model and Hand's rule. The two curves

are precisely overlapped, indicating the two models give the exactly same results. Figure 4-6 shows the cumulative oil recovery of case 2 with salinity gradient. The oil bank breakthrough times are identical from the two models. However the ultimate oil recovery predicted from the HLD-NAC model is 13% larger than that from the Hand's Rule model.

To detailed analysis the reason for the difference in ultimate oil recovery, salinity, surfactant and solubilization ratio profiles along the core at 0.6 PV and 1.6 PV are plotted as shown in Figures 4-7 and 4-8. The dimensionless of 1 is the inlet of the core, and 0 is the outlet. In these Figures, dots are results from simulation with Hand's rule, and the lines are from HLD-NAC model. At 0.6 PV, microemulsion is optimum Type III since the surfactants are in the region with salinity of 0.62 meq/ml, and the profiles from HLD-NAC model is consistent with Hand's rule. Therefore, it is not the surfactant front causes the differences in oil recovery. At 1.6 PV, the effective salinity and surfactant concentration profiles from both models are close to each other, but the oil solubilization ratio varies a lot. In the Type III portion, oil solubilization ratios from both models all gradually decrease. And oil solubilization ratio from the HLD-NAC model is larger than that from Hand's rule, which is due to the slightly higher effective salinity in the HLD-NAC model, so the microemulsion is more close to the optimum status. As the salinity is lower than 0.4 meq/ml which is the lower boundary of Type III window in the Hand's rule model, oil solubilization ratio from Hand's rule sharply turn to flat, however it from HLD-NAC model continuously slowly reduce. This trend is consistent with the modeled solubilization ratio curves in the phase behavior test.

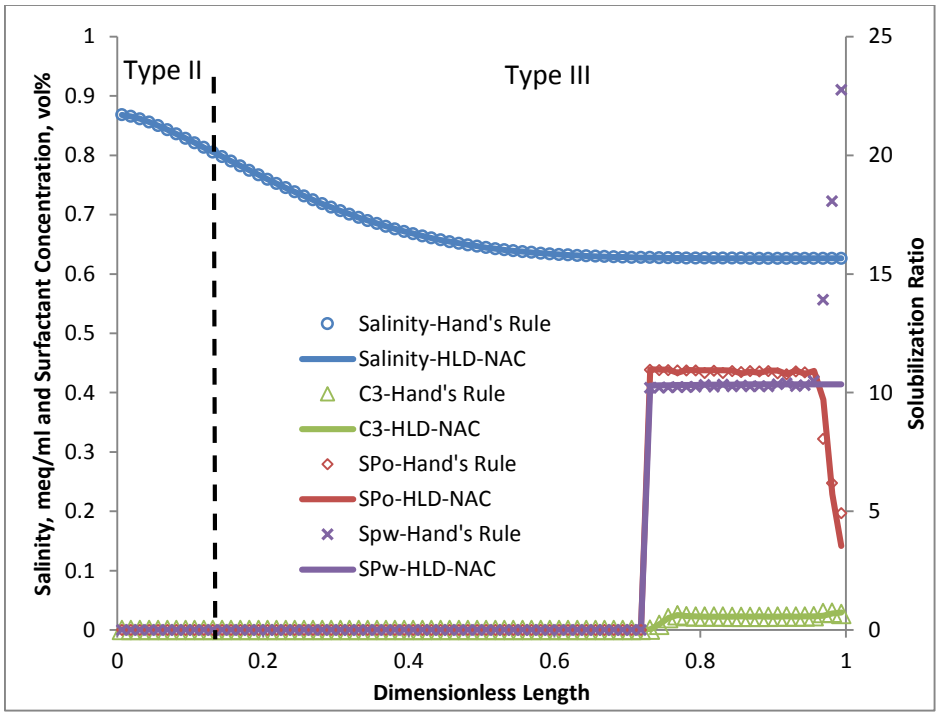


**Figure 4-7 Salinity, surfactant concentration and water solubilization ratio profiles of Case 2 at 0.6 PV**

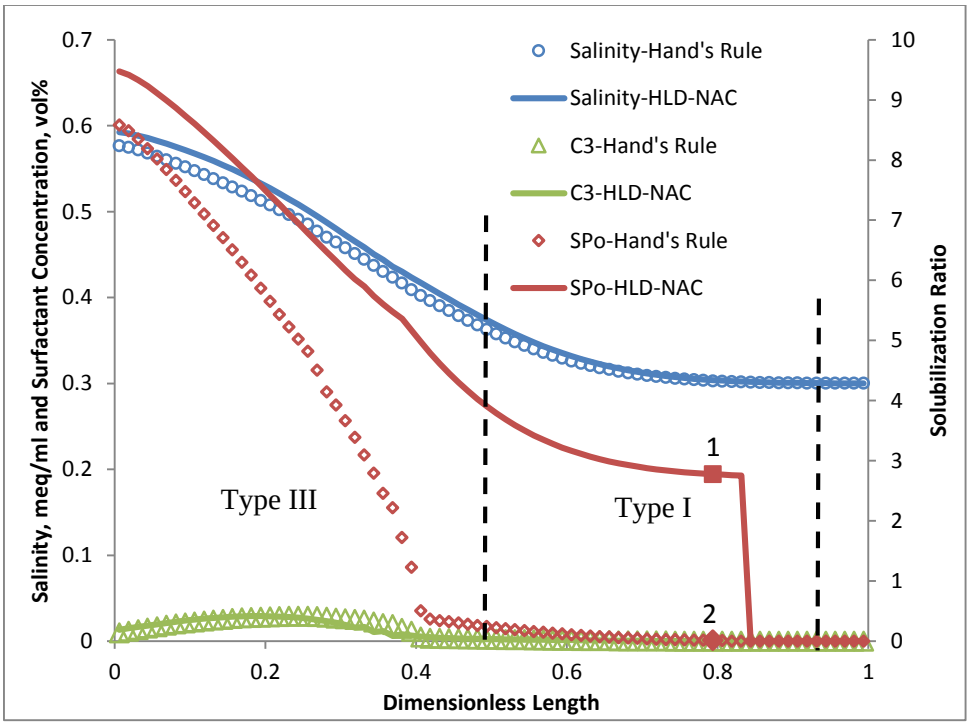


**Figure 4-8 Salinity, surfactant concentration and water solubilization ratio profiles of Case 2 at 1.6 PV**

At the portion with Type I microemulsion on Figure 4-8, oil solubilization ratio from the HLD-NAC model is much higher than the Hand's rule, which is contrary to the modeling results from phase behavior test. Oil solubilization ratio from the HLD-NAC model at point 1 on Figure 4-8 is 2.76 where the salinity is 0.3 meq/ml, which is the same as Figure 4-1. However, oil solubilization ratio from Hand's rule at point 2 is only 0.04 with the same salinity of 0.3 meq/ml, which is much smaller than 4.5 from modeling the phase behavior test. This can be explained by the differences on the ternary phase diagram as shown in Figure 4-9. The binodal curve from the HLD-NAC model is a triangle, while from Hand's rule is a curve. And the slope the line connecting the point on the binodal curve and the 100% water reflects the solubilization ratio. The smaller of the slope, the higher of the solubilization ratio. And comparing the two phase diagram, the binodal curves intersect at point e. Hence on the portion between the pure water point and point e, solubilization ratio from HLD-NAC model is higher, while on the other portion solubilization ratio from Hand's rule is higher. In phase behavior test, the overall composition at 0.3 meq/ml is on point a, and the microemulsion composition is on point b from HLD-NAC model and point c from Hand's rule. Correspondingly, the solubilization ratio from Hand's rule is higher as shown in Figure 4-1. However, during coreflood, the overall composition at point 1 and 2 of Figure 4-8 is on point d of Figure 4-9. The microemulsion composition is close to the left corner where the oil solubilization ratio from Hand's rule is much smaller. Therefore, the differences in the shape of the ternary diagrams from these two models lead to the inconsistency between solubilization ratios from phase behavior and coreflood simulation results at Type I region, and thereby cause the higher predicted cumulative oil recovery from the HLD-NAC model.

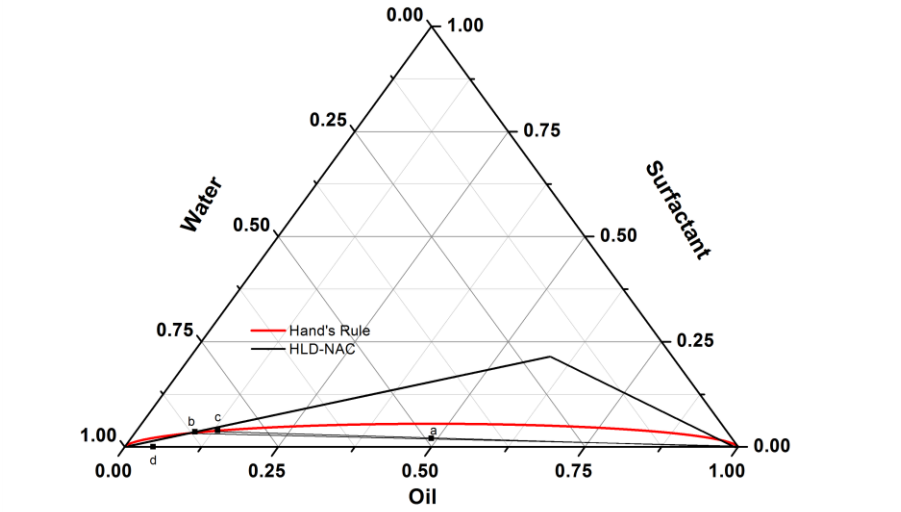


**Figure 4-9 Ternary phase diagrams plotted by HLD-NAC and Hand's Rule model of 1.0 wt% of C32-7PO-32EO-carboxylate and 1.0 wt% of C19-23-IOS for crude oil at 0.3 meq/ml**

## 4.4 Conclusions

1. This paper introduces the HLD-NAC model for compositional simulation of surfactant flooding. Comparing to the Hand's rule, the HLD-NAC model can well simulate microemulsion phase behavior with only one fitting parameter, L, which has been proved proportional to the surfactant carbon tail length.
2. An algorithm is developed to generate the ternary phase diagram with water, oil and surfactant as the pseudo components at various salinity conditions, and implemented into a chemical flooding simulator UTCHEM.
3. The HLD-NAC and Hand's rule models predict precisely same oil recovery for a surfactant coreflood under constant optimum salinity injection, indicating excellent compatibility of these two models.
4. Fore coreflood under salinity gradient, oil bank breakthrough times from both models are the same, but the HLD-NAC predicts higher ultimate oil recovery than

Hand's rule, which is due to the higher calculated solubilization ratio of Type I microemulsion from the HLD-NAC model at coreflood overall composition.

5. The HLD-NAC equation of state is a physics based model, that can improve the physical significance and thereby the predictability of surfactant flooding simulation, which can in turn shorten the surfactant screening process and help formulation design.

# Chapter 5 Analytical Solutions for Three Component, Two Phase Surfactant Flood Based on HLD-NAC Equation of State


## Abstract

Mechanisms and performances of surfactant floods are highly rely on the microemulsion phase behavior. To better understanding surfactant flood theories, analytical solutions and numerical simulators have been developed by coupling microemulsion phase behavior and multiphase displacement equations. Phase behavior models used in previous studies are either component partition models or empirical models. Such models lack of accuracy and have little predictive ability, which may lead to improper formulation design and unreliable recovery predictions.

In this work, we introduce a physics-based Hydrophilic–Lipophilic Difference (HLD) equation and the Net-Average Curvature (NAC) called thereafter HLD–NAC equation of state to model microemulsion phase behavior. And analytical solutions for two-phase three-component surfactant flooding based on this novel HLD-NAC EOS are developed by coupling the coherence theory. Composition routes, shocks as well as oil recovery are determined from the analytical method. Numerical simulation results are consistent with calculated analytical results, and numerical dispersion has little effect on simulated composition routes and recoveries. Surfactant adsorption reduces nontie-line path velocities, and retards oil bank front, surfactant front as well as solubilization front.

Using this novel HLD-NAC equation of state enables this analytical solution to systemically study the impacts of phase behavior dependent variables on surfactant flooding. And surfactant flooding performance under reservoir condition that differs from laboratory condition can be better evaluated. The influences of pressure and solution gas

on microemulsion phase behavior and surfactant flooding performance are taken as examples in this work to illustrate the advantages of the HLD-NAC EOS. Results found the combined effects of solution gas and pressure on microemulsion phase behavior will enhance or weaken surfactant flooding performance.

## 5.1 Introduction

The mechanisms of surfactant flooding include solubilization, oil swelling and low oil-water interfacial tension (IFT) and are depending on the microemulsion phase behavior (Healy and Reed 1976, 1977; Willhite et al. 1980; Nelson and Pope, 1978). Coupling the theories of microemulsion phase behavior and multicomponent multiphase flow in porous medium, mechanisms of surfactant flooding have been theoretically studied by both analytical and numerical methods (Pope and Nelson 1978; Larson 1979; Hirasaki 1981).

Mathematically describing microemulsion phase behavior is challenging because of involved complicated physics. Depending on the hydrophobicity of the environment, the addition of surfactant may form Type I microemulsion with excess oleic phase, Type II microemulsion with excess aqueous phase or Type III microemulsion that coexisting with both excess aqueous and oleic phases (Winsor 1954). Important factors in surfactant flooding that influence microemulsion phase behavior include brine salinity, oil properties, and temperature, surfactant and cosolvent properties (Salager et al. 1979a; Green and Willhite 1998).

In reported analytical solution or numerical simulators for surfactant flooding, there are two types of models were developed and utilized to simplify the microemulsion phase behavior: components partition model or empirical phase behavior model. Components partition model uses simple equations to describe the allocation of surfactant between the

aqueous and oleic phases (Liu et al. 2008). But it is constrained for two phase environment and cannot describe Type III microemulsion with middle phase, where oil-water IFT reaches minimum. Therefore, this model neglects important physics in surfactant flooding which may lead to incorrect results. A typical empirical phase behavior model is Hand's rule, which was invented to describe consolute liquid between immiscible liquids using empirical equations (Hand 1930). Pope and Nelson (1978) extended Hand's equations to represent tie-lines and binodal curves of microemulsion ternary diagram, and developed a 1D chemical flooding simulator based on Hand's equation. The functions of this 1D simulator were then well expanded and developed at The University of Texas at Austin to a state-of art compositional chemical flooding simulator, UTCHEM. However, Hand's rule needs five matching parameters to fit phase behavior experiments under salinity scan, and requires iterative calculations to solve phase compositions (UTCHEM Manual; Sheng 2010). Additional matching parameters are introduced to model other effects (Delshad et al. 1996). Moreover, Hand's rule cannot handle the effects of surfactant and oil properties, due to its empirical nature. Other microemulsion phase behavior models have been developed (Prouvost et al. 1984; Chou and Bae 1988), but are too complicated so have not been used in any surfactant flooding studies.

A Hydrophilic-Lipophilic Difference (HLD) Net Average Curvature (NAC) called thereafter HLD-NAC equation of state (EOS) for microemulsion phase behavior has attracted attentions in recent years, owing to its physical significance and simplicity. It was developed by Acosta et al. (2003) by using quantitatively characterized physical properties to determine microemulsion type, calculate solubilization ratio and oil water

interfacial tension (IFT) (Acosta et al. 2008a, 2008b, 2009, 2012). In this novel EOS, only the surfactant tail length $L$ is a matching parameter. Even though, $L$ is found proportional to the fully extended surfactant tail length. And correlations have been developed to predict its value (Acosta 2009; Tanford, 1980). Jin et al. (2015a, 2015b) applied the HLD-NAC model for surfactant/crude oil/brine system, and found the length parameter $L$ is independent of oil properties. Ghosh and Johns (2014 and 2015) modified and extended the HLD-NAC EOS to predict surfactant-oil-brine phase behavior for live oil and alkali-surfactant-oil-brine phase behavior, which advances the physical significance of the HLD-NAC EOS in modeling microemulsion for surfactant flooding. Jin et al. (2016) predicted microemulsion phase behavior for surfactant flooding by using the HLD-NAC model with experimentally measured surfactant parameters (Budhathoki, 2015). These researches well demonstrated the advantages of HLD-NAC EOS in modeling microemulsion phase behavior. But the significance of this novel HLD-NAC EOS in understanding surfactant flooding displacement efficiency has not been studied so far.

Larson (1979) applied the component partitioning model and studied the influence of phase behavior on surfactant flooding. Hirasaki (1981) utilized Hand's rule and multicomponent multiphase displacement theory to construct composition routes and study fronts propagation in surfactant flooding. These work shed light on the importance of microemulsion phase behavior in surfactant flooding. But the effects of surfactant properties, oil EACN and solution gas were not studied because of the constraints of these microemulsion phase behavior model. Therefore, the objective of this work is to develop an analytical solution based on the HLD-NAC EOS. Using this method the effects of

microemulsion phase behavior dependent properties on surfactant flooding efficiency can be easier evaluated.

## 5.2 Mathematical Model

### *5.2.1 Assumptions*

The theory and calculation procedures presented by Helfferich (1981) (called coherence theory) elucidate the prominent features of multicomponent, multiphase displacement in porous media. To formulate a system of mass-balance equations that can be solved by applying Helfferich's approach, the following standard assumptions are made:

1) The flow is 1D laminar and perpendicular to the gravitational field.
2) The porous media is homogeneous.
3) There are no dispersive phenomena such as diffusion, dispersion or capillary imbibition.
4) All phases are incompressible.
5) The phases are in local equilibrium.
6) Partial molar volumes of components are constant.
7) Isothermal flow.
8) There is no adsorption or dispersion unless explicitly stated.
9) The initial condition is at waterflood residual oil saturation and the boundary condition is a surfactant in water solution with constant concentration.

Additional assumptions are made in this paper for using the HLD-NAC equation of state.

10) Microemulsion could be represented as coexisting hypothetical spherical droplets of oil and water;
11) The concentration of the surfactant in monomer form is negligible;
12) Mole concentration of surfactant is calculated by assuming the surfactant density is 1 g/ml;
13) The surfactant head area is constant at various salinities;
14) Pseudocomponents are surfactant, brine, and oil;
15) Plait points are estimated as the intersection of solubilization capacity line and the catastrophic phase inversion line.

### *5.2.2 Material Balance Equation*

With the previous assumptions, flow is governed by the mass balance equations:

$$\frac{\partial C_i}{\partial t_D} + \frac{\partial F_i}{\partial x_D} = 0 \qquad i = 1, \dots, n_c - 1, \tag{1}$$

where $n_c$ is the number of components: 1, 2 and 3 corresponds to water, oil and surfactant, respectively.

$C_i$ is the overall volume fraction of component *i* and $F_i$ is the overall fractional flow of component *i*. $x_D$ is the dimensionless distance along the medium and $t_D$ is time measured in pore volumes injected (PVI). $C_i$, $F_i$, $S_i$ and $f_i$ are related by

$$C_i = \sum_{j=1}^{n_p} S_j c_{ij},\ F_i = \sum_{j=1}^{n_p} f_j c_{ij}, \tag{2}$$

where $n_p$ is the number of phase present, $c_{ij}$ is the volume fraction of component *i* in the *j*th phase, $S_j$ and $f_j$ are the saturation and fractional flow of the *j*th phase. In this paper, subscript $j$ equals 1, 2 and 3 represent aqueous, oleic and microemulsion phase, respectively.

By definition, the sum of $C_i$, $F_i$, $S_j$ and $f_j$, along with the equilibrium volume fractions $c_{ij}$ in each phase, is unity. Consequently, the overall concentration and fractional flow of the 3rd component can be easily calculated from those of component 1 and 2. Phase saturation $S_j$ and composition $c_{ij}$ are obtained from microemulsion equation of state, with given overall composition and phase behavior condition.

### *5.2.3 HLD-NAC EOS*

The first section of the algorithm is the HLD equation (Salager et al. 1979a, 1979b 1999) as:

$$HLD = ln(C_s) - K \times EACN - \alpha_T(T - 273.15) + Cc + f(A) - \beta(P - P_{ref}) \quad (3)$$

where,

$C_s$ = salinity (the electrolyte concentration, g/100 ml)

EACN = equivalent alkane carbon number of the oil

K = slope of the logarithm of optimum salinity as a function of ACN

f(A) = function of alcohol type and concentration

Cc = characteristic parameter of surfactant

$\alpha_T$ = temperature coefficient of optimum salinity expressed in units of ln S per °C

T = temperature, K

$\beta$ = pressure coefficient, $bar^{-1}$

P = pressure, bar

The NAC concept is that the net curvature is scaled to the HLD value by the surfactant length $L$:

$$H_n = \left|\frac{1}{R_o}\right| - \left|\frac{1}{R_w}\right| = \frac{-HLD}{L} \quad (4)$$

where $R_o$ and $R_w$ are the radii of coexisting hypothetical spherical aggregates of oil and water. $H_n$ is the curvature of surfactant film packed at the oil/water interface. A positive net curvature ($H_n > 0\ or$ HLD $< 0$) corresponds to Type I microemulsion ($R_w \gg R_o$), and negative values ($H_n < 0\ or$ HLD $> 0$) to Type II microemulsion ($R_o \gg R_w$).

The average curvature in Type III microemulsion is the reciprocal of the characteristic length $\xi^*$, and

$$H_a = \left|\frac{1}{R_o}\right| + \left|\frac{1}{R_w}\right| = \frac{1}{\xi^*} \quad (5)$$

$\xi^*$ corresponds to the maximum length scale at which any oil or water can be correlated to the surfactant membrane (De Gennes et al. 1982). This is the only parameter in the HLD-NAC model cannot be predicted, but can be calculated from the phase volumes in middle phase microemulsions:

$$\xi^* = \frac{6\varphi_o\varphi_w V_m}{A_s} \quad (6)$$

where $\varphi_o$ and $\varphi_w$ represent the water and oil volume fraction in the middle phase microemulsion, and $V_m$ is the volume of the middle phase. $A_s$ is the total surfactant interfacial area that can be obtained as (Acosta et al. 2003)

$$A_s = \sum_i V_w \times C_{surfi} \times 6.023 \times 10^{23} \times a_{3i} \quad (7)$$

where,

$V_w$ = the volume of water in the system;

$C_{surfi}$ = the concentration of the surfactant species *"i"* in the system, mol/L;

$a_{3i}$ = the surface area per molecule of the surfactant, Å$^2$.

The $1/H_a < \xi^*$ is a criterion in differentiating microemulsion types. Phase transition occures when the characteristic size ($1/H_a$) is larger than the characteristic length ($\xi^*$),

which means bicontinuous microemulsion system is formed coexisting with excess oil and water phases (Acosta et al., 2012).With the HLD-NAC model, $R_o$ and $R_w$ are obtained. Along with the total interfacial area, numbers of oil and water hypothetical droplets are calculated hence the phase composition and saturation. The NAC model also introduces the interfacial rigidity ($E_r$) to predict the interfacial tension in microemulsion systems,

$$\gamma_{om,wm} = \frac{E_r}{4\pi R_{o,w}^2} \tag{8}$$

where $\gamma$ is the interfacial tension.

To construct a composition space, this work estimates the plait point coordinates on ternary phase diagram by applying the catastrophic theory (personal communication with Acosta, 2015). As the internal phase volume fraction in the microemulsion increases to some point, the internal phase inverse to the external phase naming catastrophic phase inversion. The catastrophic phase inversion point is system dependent, a good assumption is that it occurs when internal phase volume fraction is over than 75% (personal communication with Acosta, 2015). Following equations are obtained by using this theory and related assumptions,

left plait point:

$$C_{1PL} = \frac{3V_{wm}}{4V_{wm}+3C_{33}}\,;\; C_{2PL} = \frac{V_{wm}}{4V_{wm}+3C_{33}}\,;\; C_{3PL} = \frac{3C_{3m}}{4V_{wm}+3C_{33}} \tag{9}$$

right plait point:

$$C_{1PR} = \frac{V_{om}}{4V_{om}+3C_{33}}\,;\; C_{2PR} = \frac{3V_{om}}{4V_{om}+3C_{33}};\; C_{3PR} = \frac{3C_{3m}}{4V_{om}+3C_{33}} \tag{10}$$

where subscripts *PL* stands for left plait point, and *PR* stands for right. $V_{wm}$ and $V_{om}$ are volume of water and oil in microemulsion that obtained from phase behavior test.

Consequently, equations for solving compositions in Type I microemulsion are,

$$\frac{C_{23}}{C_{33}} = \frac{C_{2PR}}{C_{3PR}}; \frac{C_{13}}{C_{33}} = \frac{C_1}{C_3} \tag{11}$$

and for Type II microemulsion are,

$$\frac{C_{13}}{C_{33}} = \frac{C_{1PL}}{C_{3PL}}; \frac{C_{23}}{C_{33}} = \frac{C_2}{C_3} \tag{12}$$

For Type III microemulsion, equations for solving left and right lobe are same as that for Type II and Type I microemulsion. And if the overall composition is in the three phases region,

$$C_{13} = \frac{V_{wm}}{V_{wm}+V_{om}+C_3}; C_{23} = \frac{V_{om}}{V_{wm}+V_{om}+C_3} \tag{13}$$

With the 11 assumption in this section that the concentration of the surfactant in monomer form is negligible, the excess phases are either pure water or oil.

### *5.2.4 Multiphase Flow*

A primary mechanism for surfactant flooding is the mobilization of trapped oil due to reduced interfacial tension (Healy and Reed 1979). Capillary number is the dimensionless number to represent viscous/capillary forces (Green and Willhite 1998),

$$N_c = \frac{v\mu}{\phi\gamma} \tag{14}$$

where

$v$ = the pore flow velocity of the displacing fluid (m/s);

$\mu$ = the viscosity of the displacing fluid (mPa·s);

$\phi$ = is the porosity in fraction.

In the absence of gravity and buoyance force, it was found that the residual saturations are a function of the capillary number (Morrow and Songkran 1981; Morrow et al. 1988). The relationship is expressed as (Delshad 1990; Pennell 1995),

$$S_{jr} = \min\left(S_j, S_{jr}^{high} + \frac{S_{jr}^{low} - S_{jr}^{high}}{1+T_{pj}N_c}\right) \qquad \text{for } j = 1,\ldots,n_p \tag{15}$$

We assume relative permeability is only a function of saturation and is modeled by Corey-type

$$k_{rj} = \begin{Bmatrix} 0 & S_j^* < 0 \\ k_{rj}^0 \left(S_j^*\right)^{n_j} & 0 < S_j^* < 1 \\ k_{rj}^0 & S_j^* > 1 \end{Bmatrix} \tag{16}$$

with

$$S_j^* = \frac{S_j - S_{jr}}{1 - \sum_{j=1}^{n_p} S_{jr}} \tag{17}$$

where $k_{rj}^0$ is the endpoint permeability of phase $j$, $S_{jr}$ is the residual saturation of phase $j$, $n_j$ is the exponent of relative permeability curve of phase $j$, and $S_j^*$ is the reduced saturation of phase $j$. The endpoints and exponents of the relative permeability curves change as the residual saturations change at high capillary numbers (Fulcher et al., 1985; Delshad et al., 1986). The endpoints and exponents in relative permeability functions are computed as a linear interpolation between the given input values at low and high capillary numbers ($k_{rj}^{0^{low}}, k_{rj}^{high}, n_j^{low}, n_j^{high}$):

$$k_{rj}^0 = k_{rj}^{0^{low}} + \frac{S_{jr}^{low} - S_{jr}}{S_{jr}^{low} - S_{jr}^{high}} \left(k_{rj}^{high} - k_{rj}^{0^{low}}\right) \quad \text{for } j = 1,\ldots,n_p \tag{18}$$

$$n_j = n_j^{low} + \frac{S_{jr}^{low} - S_{jr}}{S_{jr}^{low} - S_{jr}^{high}} \left(n_j^{high} - n_j^{low}\right) \quad \text{for } j = 1,\ldots,n_p \tag{19}$$

Viscosity of microemulsion phase is correlated to pure water and oil viscosities as well as the phase concentration in microemulsion,

$$\mu_3 = C_{13}\mu_w \exp[\alpha_1(C_{23} + C_{33})] + C_{23}\mu_o \exp[\alpha_2(C_{13} + C_{33})] + C_{33}\alpha_3 \exp[(\alpha_4 C_{13} + \alpha_5 C_{23})] \tag{20}$$

where the $\alpha$ parameters are determined by fitting laboratory microemulsion viscosity at several compositions.

The above correlations except the calculation of capillary number are the same as used in UTCHEM (UTCHEM Manual).

The fractional flow of each phase is defined by

$$f_j = \frac{\lambda_j}{\sum_{j=1}^{n_p} \lambda_j} \text{ and } \lambda_j = \frac{k_{rj}}{\mu_j} \tag{21}$$

where $\lambda_j$ is the mobility of phase *j*.

## 5.3 Analytical Solution

### *5.3.1 Composition path grid*

There are two independent variables for a three component, two phase system. The behavior of solutions to Eq. 1 is controlled by the properties of tie-lines, and hence it is convenient to let the slope of the tie-line, $\eta$, be one of the variables (Orr 2007). And let the water component concentration, $C_1$, be the other variable. The relationship between $\eta$ and $C_1$ is

$$C_3 = \eta C_1 \tag{22}$$

Consequently, Eq.1 can be reformulated as an eigenvalue problem,

$$\begin{pmatrix} \frac{\partial C_1}{\partial t_D} \\ \frac{\partial \eta}{\partial t_D} \end{pmatrix} + \begin{pmatrix} \frac{\partial F_1}{\partial C_1} & \frac{\partial F_1}{\partial \eta} \\ 0 & \frac{F_1}{C_1} \end{pmatrix} \begin{pmatrix} \frac{\partial C_1}{\partial x_D} \\ \frac{\partial \eta}{\partial x_D} \end{pmatrix} = 0 \tag{23}$$

The eigenvalue of this problem

$$\Lambda_t = \frac{\partial F_1}{\partial C_1}, \Lambda_{nt} = \frac{F_1}{C_1} \tag{24}$$

The corresponding eigenvector:

$$\overrightarrow{e_t} = \begin{pmatrix} 1 \\ 0 \end{pmatrix}, \overrightarrow{e_{nt}} = \begin{pmatrix} 1 \\ \frac{\Lambda_{nt} - \Lambda_t}{\frac{\partial F_1}{\partial \eta}} \end{pmatrix} \tag{25}$$

where the subscript *t* means tie-line and *nt* stands for nontie-line. The first entry in each eigenvector corresponds to change in $C_1$, and the second to changes in $\eta$. By integrating along the eigenvector directions, coordinates in composition space form curves known as composition paths, which represent composition variations that meet the coherence condition (Helfferich 1981).

Figure 5-1 is an example of for a Type I microemulsion system. The salient features of the composition paths have been well studied (Helfferich 1981; Orr 2007), and similar characteristics are also shown in this work:

1. There are no discrete composition directions in the single phase region, since $F_1 = C_1$ everywhere in this region.
2. In the sub-triangle representing the two phase region, there are tie-line paths and nontie-line paths.
3. The two phase envelope consisting of the solubilization capacity line and the last tie-line is a composition path with equivelocity, $\Lambda_{nt} = 1$.
4. Equivelocity curve along $\Lambda_{nt} = 1$ is also a composition path.
5. Nontie-line paths are tangent to the tie-line paths at two singular points, one on each side of the equivelocity curve.
6. The eigenvalues $\Lambda$ for the nontie-line paths are greater than unity on the side of the equivelocity curve where tie-lines are spaced widely and lower than unity on the other side.

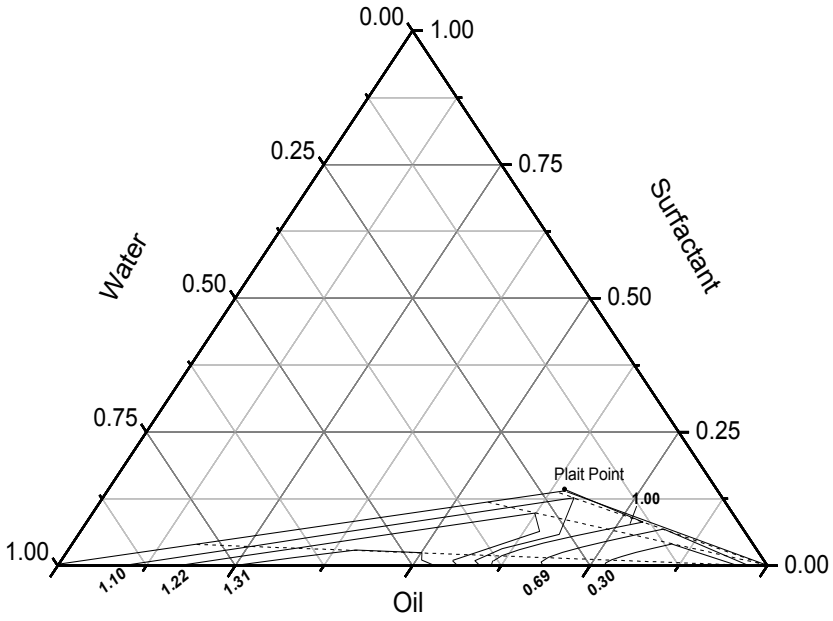


**Figure 5-1 Composition path grid, Type I microemulsion**

*5.3.2 Composition Routes and Shocks*

With given boundary and initial conditions, a composition route that is a curve in the composition space representing the sequence of compositions in a system can be determined. When the composition velocity upstream is slower than the downstream, compositions flow along the route as spreading wave. While shocks occur when upstream compositions flow faster than downstream composition to avoid multivalued solutions, which is also known as velocity condition (Laforce and Johns 2005). With the constraint of Rankine-Hugoniot (RH) condition, the velocity of any shock for three components is:

$$\frac{F_1^d - F_1^u}{C_1^d - C_1^u} = \frac{F_2^d - F_2^u}{C_2^d - C_2^u} = \frac{F_3^d - F_3^u}{C_3^d - C_3^u} = \Lambda \tag{26}$$

where $\Lambda$ is the shock velocity, superscript d denotes the downstream composition, u denotes upstream composition, and the subscripts is the component number as before.

Figure 5-2 is an example shows a composition route and compositions of shocks in surfactant flooding for Type I microemulsion. $C_i^I$ in is the injected composition (boundary condition) and point *d* is the water flood residual saturation (initial condition). To enter the two phase region from the injection condition, the composition route has been proved follow the tie-line path through that composition (Hirasaki 1981; Orr, 2007). Since the injected surfactant solution is undersaturated, the first front is named as solubilization front (Hirasaki, 1981) or miscible shock (Larson, 1979). Its velocity can be calculated using Eq. 26 with injection composition as the upstream condition, or a material balance of the composition step.

$$v_{SF} = \frac{dF_i}{dC_i} = \frac{F_i^a - F_i^I}{C_i^a - C_i^I} \tag{27}$$

Graphically, its solution is shown in Figure 5-3. The solid curves are overall fractional flow vs. overall concentration of oil and surfactant. There is a straight portion on oil fractional flow curve with slope of unity corresponding to single phase region. The slopes $dF_i/dC_i$ of these fractional flow curves are the velocities along the tie-line. Therefore, the slope of tangent line that pass through the injection composition is the velocity of solubilization front, and the tangent point corresponds to shock composition, which is also illustrated as point *a* on Figure 5-2.

Compositions flow down the tie-line as spreading waves. At the point *b* where the tie-line path is tangent to the nontie-line, the composition form surfactant front or microemulsion front. At point *b*, velocity on tie-line equals on nontie-line. Therefore, velocity and composition are solved by:

$$\Lambda_t = \Lambda_{nt} \tag{28}$$

Composition route then switch to the nontie-line path and changes as a step change to the oil bank, point *c*. Nontie-line velocity on point *c* is the same as point *b*, hence the composition of oil bank is obtained. The oil bank front propagates as a step change to the initial condition. As a results,

$$v_{OB} = \frac{F_2^c}{C_2^c - C_2^d} \tag{29}$$

The graphical solution for the oil bank front is shown in Figure 5-4. Each tie line corresponds to a fractional flow curve. On the fractional flow curve of surfactant flooding, it is able to find point *b* with the slope of its tangent line equals to the velocity of microemulsion front. The line connecting point *b* and initial condition point *d* intersects with the fractional flow curve of zero surfactant line at point *c*, representing the oil bank front. Slope of the line is the oil bank front propagation velocity.

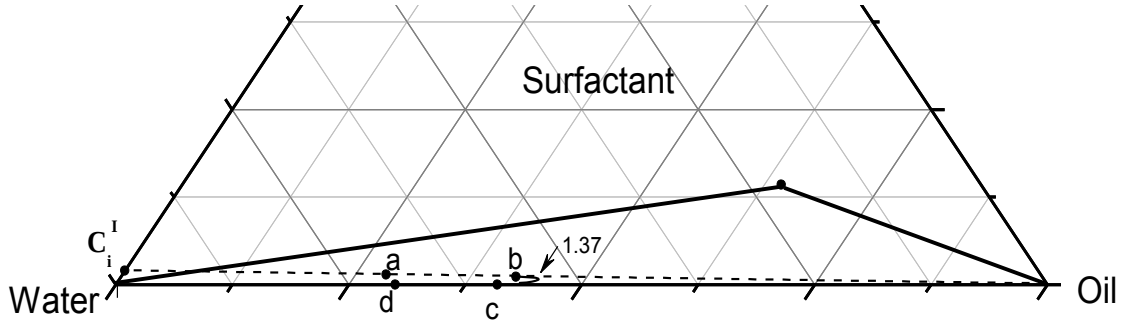


**Figure 5-2 Composition route for constant surfactant injection, Type I microemulsion**

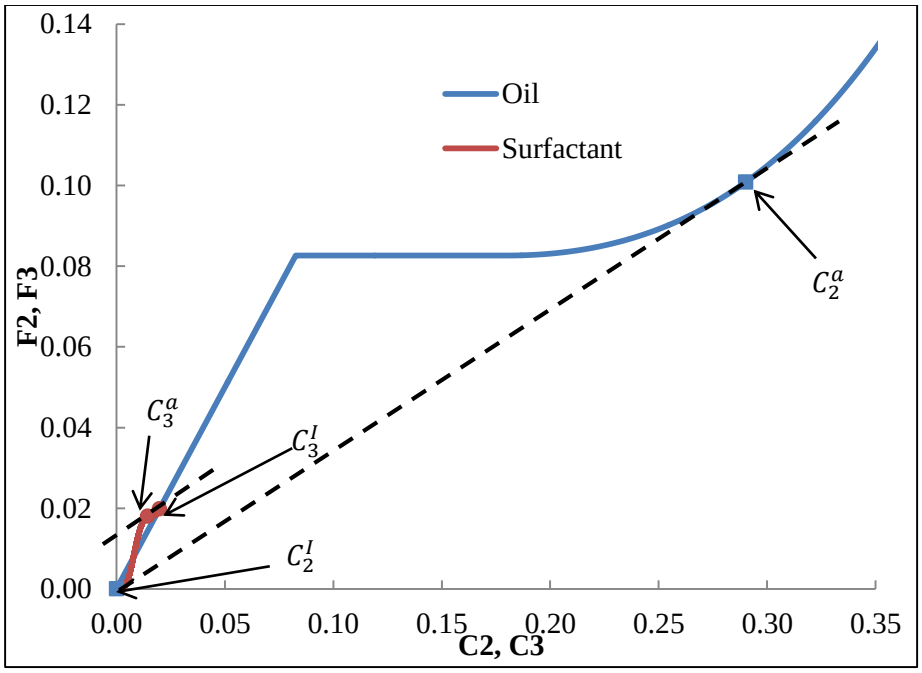


**Figure 5-3 Oil and surfactant overall fractional flow vs. overall concentration**

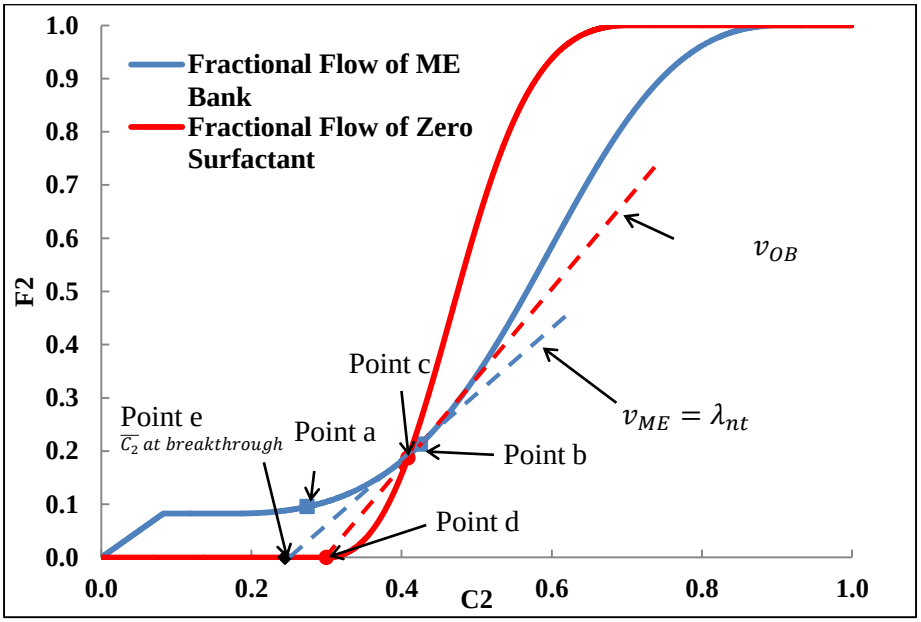


**Figure 5-4 Oil overall fractional flow vs. overall concentration**

*5.3.3 Oil Recovery*

There are two banks contain mobilized oil during surfactant flooding: oil bank with constant concentration and microemulsion bank with gradually reduced oil concentration

from downstream to upstream. Average oil concentration behind microemulsion bank front before its breakthrough is given by (Welge et al. 1961; Hirasaki 1981),

$$\overline{C_2} = C_2^{ME} - \frac{F_2^{ME}}{dF_2^{ME}/dC_2^{ME}}, \quad t_D < 1/v_{ME} \tag{30}$$

where the superscript ME denotes microemulsion bank front. Point *e* in Figure 5-4 represents the average saturation behind microemulsion bank front before breakthrough. After it breakthrough, $C_2$ and $F_2$ of microemulsion bank front in Eq. 30 becomes the fractional flow and concentration at the outlet. It is graphically interpreted as moving from point *b* to point *a* along the fractional flow curve of microemulsion bank. The wave propagate velocity $dF_2/dC_2$ correspondingly decreases, and the remaining average oil concentration reduces from point *e* to the original point in Figure 5-4. Oil recovery is hence determined.

### 5.4 Comparison with Numerical Simulation

The HLD-NAC equation of state is implemented into UTCHEM. Detailed description of the new simulator will be discussed in a companion paper. Generally, the new simulator retains most of the UTCHEM features, except replaced the Hand's rule phase behavior model by the HLD-NAC EOS (UTCHEM Manual). The simulator applies same multiphase flow models and numerically solves the same mass balance equations as the analytical methods. The simulations were run using 400 gridblocks for 1 foot long core. Input parameters are summarized in Table 5-1. Calculated HLD value from the input is -0.725, corresponding to a Type I microemulsion system. IFT between oil and microemulsion phase is 0.0288 mN/m, which is higher than traditional surfactant flooding that requires ultra-low IFT ($10^{-3}$ mN/m). Ultra-low IFT is usually reached at Type III microemulsion where three phases coexist. Analytically solving surfactant flooding of

Type III system needs to construct composition routes on a three phase composition space, which is more complicated and needed further investigation (Aanonsen 1989). Results from analytical solutions and numerical simulations for a constant surfactant and constant salinity surfactant flood are compared.

Figures 5-5 and 5-6 show comparisons of composition profiles at 0.3 and 0.5 PV of 5 wt% surfactant injection. Solid curves are obtained from simulated and dashed lines are from analytical determined. The analytical and simulated profiles are nearly identical, except for the microemulsion bank front where numerical dispersion is observed. Figure 5-7 plots cumulative oil recovery curves for 2 wt % and 5 wt% surfactant injection determined from both numerical and analytical solutions. The recovery curves are also almost overlapped with each other at different surfactant concentration. Injected surfactant concentration at either 2 wt% or 5 wt% is too high to be economical in real surfactant flooding case. It is used here just for better presenting the results. From Figure 5-7, reducing injected surfactant concentration delays oil bank breakthrough as well as solubilization front breakthrough, but enlarges the microemulsion bank and speeds up its propagation.

**Table 5-1 Summary of input parameters**

| Term | Value | Term | Value |
|---|---|---|---|
| **HLD Parameters, Type I micoemulsion** | | **Relative Permeability Parameters** | |
| Salinity, wt% | 1.76 | $S_{1rw}$ | 0.35 |
| Cc | 0.34 | $S_{2rw}$ | 0.35 |
| K | 0.17 | $S_{3rw}$ | 0.35 |
| EACN | 8.0 | $k^0_{r1w}$ | 0.3 |
| $\alpha_T$, $K^{-1}$ | 0.01 | $k^0_{r2w}$ | 0.6 |
| $T$, °C | 52 | $k^0_{r3w}$ | 0.3 |
| **NAC Parameters** | | $e_{1w}$ | 2 |
| Head area, $Å^2$ | 80 | $e_{2w}$ | 2 |

| | | | |
|---|---|---|---|
| L, Å | 65 | $e_{3w}$ | 2 |
| Molecular weight, g/mole | 524 | $S_{1rc}$ | 0 |
| $\xi^*$, Å | 347 | $S_{2rc}$ | 0 |
| $E_r$ | 6.4 | $S_{3rc}$ | 0 |
| **Capillary Desaturation Parameters** | | $k^0_{r1c}$ | 1 |
| $T_{11}$ | 1865 | $k^0_{r2c}$ | 1 |
| $T_{12}$ | 59074 | $k^0_{r3c}$ | 1 |
| $T_{13}$ | 364.2 | $e_{1c}$ | 1 |
| **Viscosity Parameters** | | $e_{2c}$ | 1 |
| $\alpha_1$ | 2 | $e_{3c}$ | 1 |
| $\alpha_2$ | 2 | | |
| $\alpha_3$ | 0 | | |
| $\alpha_4$ | 0.9 | | |
| $\alpha_5$ | 0.7 | | |
| $\mu_1$, mPa·s | 0.678 | | |
| $\mu_2$, mPa·s | 7 | | |

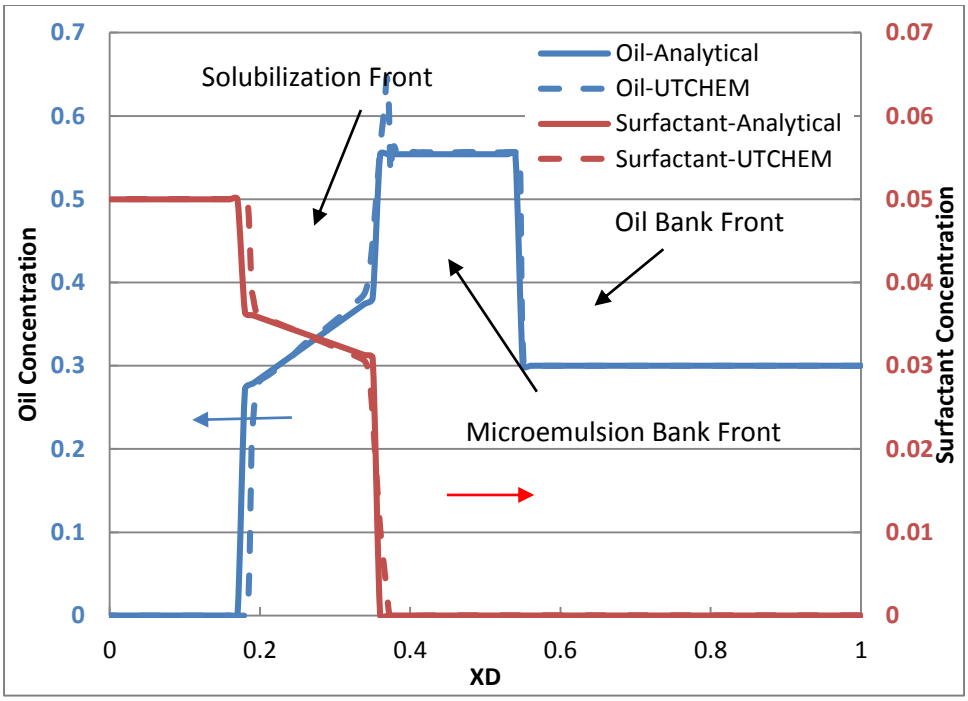


**Figure 5-5 Composition profile for continuous surfactant injection, 0.3 PV**

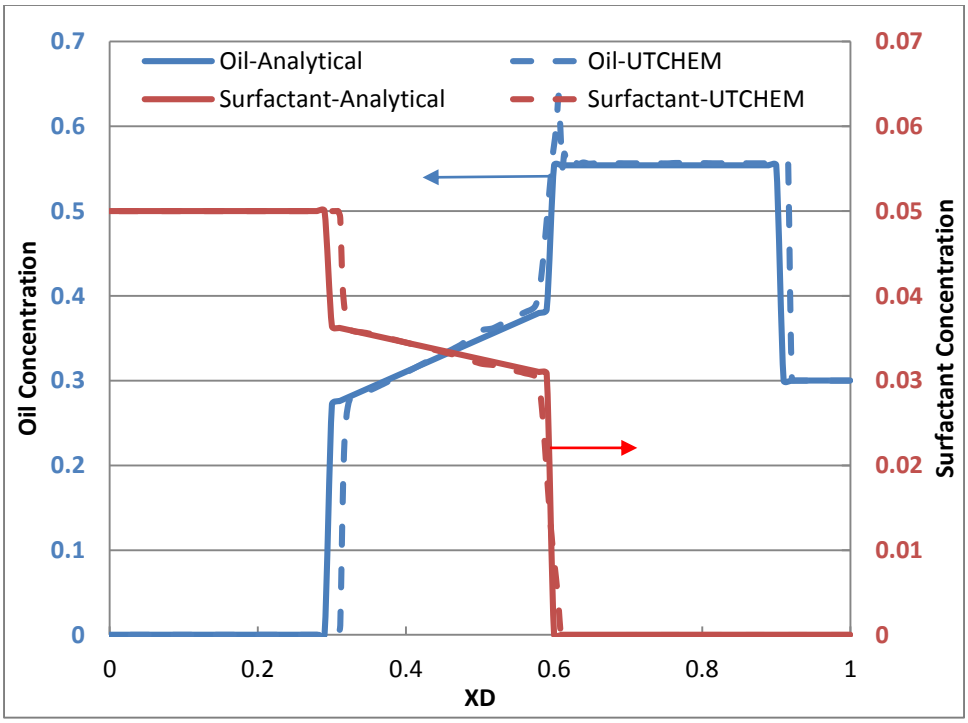


**Figure 5-6 Composition profile for continuous surfactant injection, 0.5 PV**

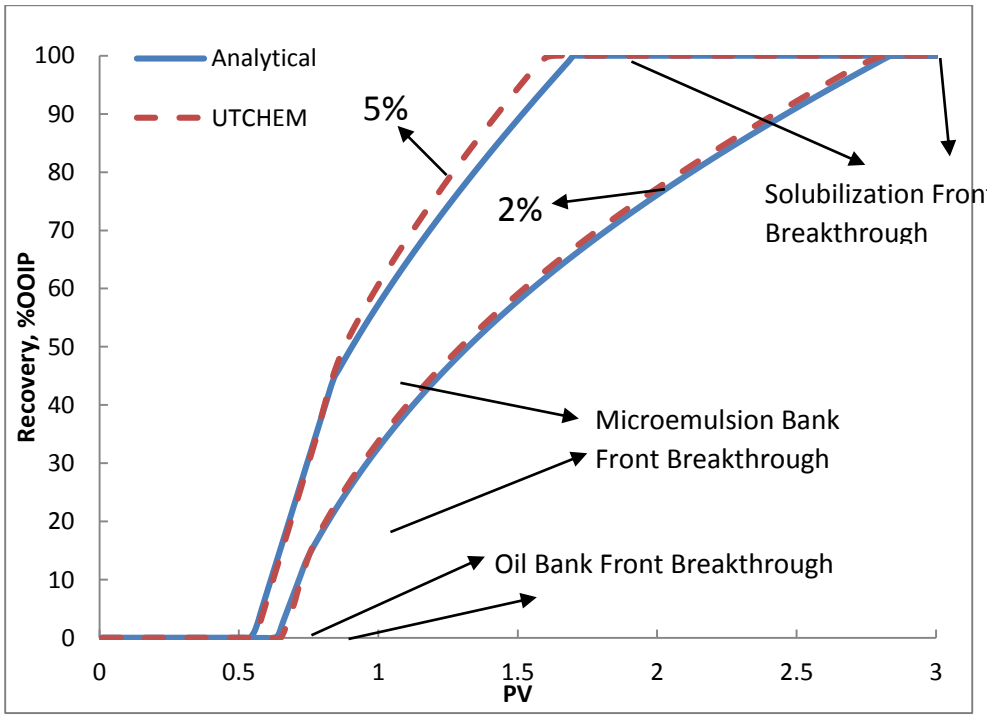


**Figure 5-7 Cumulative oil recovery for continuous surfactant injection**

## 5.5 Adsorption

Adsorption of surfactant on porous rocks is inevitable in surfactant flooding. Its impact on surfactant flooding performances has been both experimentally and theoretically investigated (Trogus et al. 1979; Pope 1980). Studies consistently show that surfactant adsorption retards the propagation of fronts (Green and Willhite, 1998). Similarly as other studies, we use Langmuir isotherm to describe the surfactant adsorption behavior in this work:

$$\hat{C}_3 = \frac{aC_3}{1+bC_3} \tag{31}$$

So the material balance equation of surfactant component becomes,

$$\frac{\partial(C_3+\hat{C}_3)}{\partial t_D} + \frac{\partial F_3}{\partial x_D} = 0 \tag{32}$$

As a result, the velocity of nontie-line path is retarded,

$$\Lambda_{nt} = \frac{F_1}{C_1(1+D_i)} \tag{33}$$

where $D_i$ is the retardation factor equals to $\hat{C}_3/C_3$. And all velocities are retarded to $1/(1+D_i)$, which is the same as Pope determined from fractional flow theory for three-component, two-phase displacements (Pope, 1980).

Figures 5-8 and 5-9 presents the comparison of composition profiles and cumulative oil recovery curves for surfactant flooding with and without adsorption. The results clearly show that the adsorption retards the velocities of fronts, reduces the oil concentration in oil bank, and shrinks the size of microemulsion bank. Results calculated from numerical simulation are also in good agreement with the analytical methods as shown in Figure 5-9.

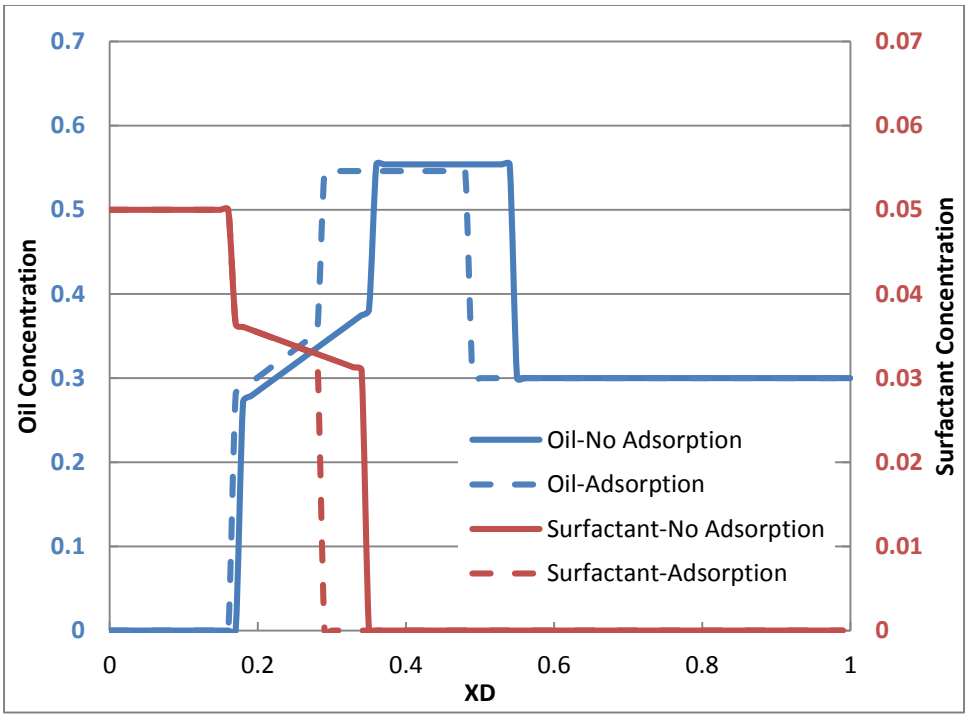


**Figure 5-8 Comparison of composition profile with and without adsorption, 0.3 PV**

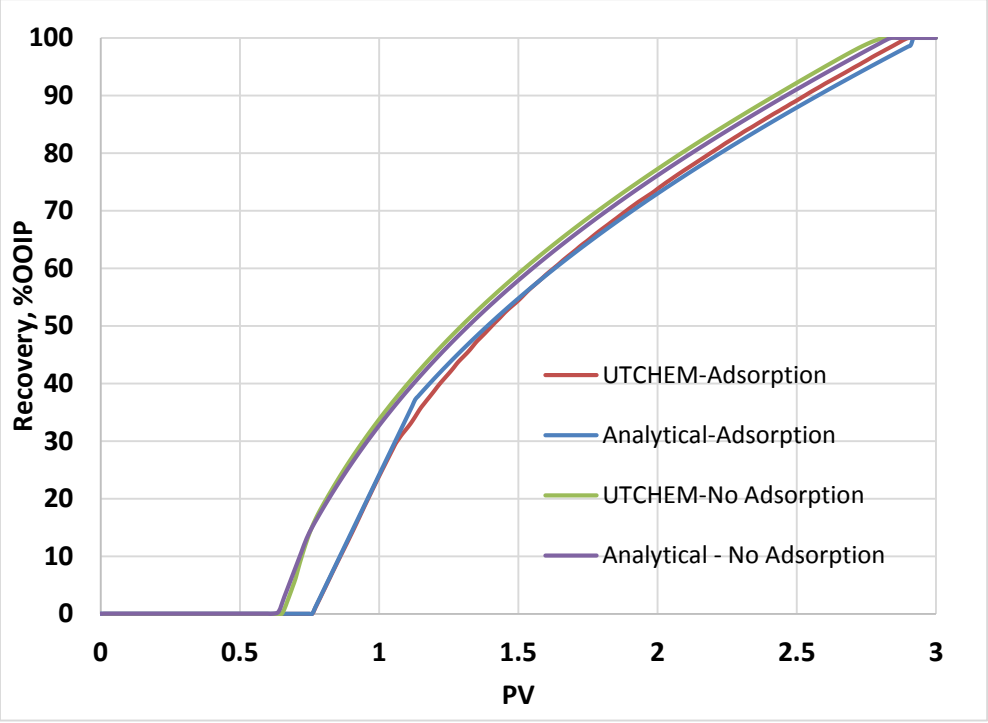


**Figure 5-9 Cumulative oil recovery for continuous surfactant injection**

## 5.6 Effects of phase behavior parameters

One of the most important features of the HLD-NAC EOS is that all input parameters have physical concept and can be experimentally characterized. Hence using this phase behavior model, the effects of microemulsion phase behavior dependent parameters on surfactant flooding performance are able to be systemically studied.

In the HLD-NAC model, the effects of phase behavior parameters on oil recovery can be studied from two aspects. First is the HLD value. When designing optimum formulation for a target reservoir, considered variables include brine salinity, oil and surfactant properties, as well as reservoir temperature. But at field scale, the solution gas would change oil EACN, injected cold water may cause a temperature gradient, chromatography separation of surfactant blends alternates the Cc value, and reservoir pressure will also shift the microemulsion phase behavior (Harwell 1982; Austad and Staurland, 1990; Austad et al. 1990; Skauge and Fotland 1990; Austad and Strand 1996; Roshanfekr and Johns 2011; Roshanfekr et al. 2012; Sandersen et al. 2012; Jang et al. 2014). All these parameters are reflected as changing the HLD value, and microemulsion phase behavior shifts accordingly.

Convention of the HLD value is defined as a negative or positive corresponds to Winsor Type I or Type II microemulsion respectively, and HLD value of zero suggests the optimum state with the highest solubilization ratio. As the HLD value increasing from negative to zero and to positive, solubilization ratio of the microemulsion firstly increase to optima and then decrease. Therefore, the smaller of the absolute HLD value, the higher of the solubilization ratio. Previous researches have proved that higher solubilization ratio of the microemulsion system corresponds to lower oil-water interfacial tension, and hence

higher oil recovery (Healy and Reed 1976 and 1977). Changing the HLD value can also be represented as the shift of optimum salinity, since

$$ln(C_s^*) = K \times EACN + \alpha_T(T - 273.15) - Cc - f(A) + \beta(P - P_{ref}) \quad (34)$$

Another aspect is the characteristic length, which is proportional to the optimum solubilization ratio (Jin et al. 2015). Ghosh and Johns (2016) proposed a correlation related the optimum solubilization ratio to the optimum salinity,

$$\frac{1}{\sigma^*} = B_1 lnC_s^* + B_2 \quad (35)$$

where the constants $B_1$ and $B_2$ are determined by fitting experimental data. From this equation, the increase of optimum salinity suppress the solubilization capability of the surfactant system.

Consequently, variations of phase behavior dependent parameters between field and laboratory conditions have a combined effect on the HLD value and optimum solubilization ratio. Therefore, whether the changed phase behavior conditions will enhance or weaken the surfactant flooding performance is case dependent, and should be studied individually. This work takes the effect of solution gas and pressure as an example to demonstrate this argument.

Roshanfekr et al. measured dead and live oil microemulsion phase behavior (2011, 2013). The formulation is a blend containing 1.5 wt% tridecyl propozylated alcohol sulfate and 0.5 wt% of $C_{13\text{-}18}$ internal olefin sulfonate along with isopropanol as a cosolvent. Ghosh and Johns (2016) determined HLD-NAC parameters for this system which are summarized in Table 5-2. It is noticed that the average head area is much higher than that from Jin et al. (2015) and head areas summarized in Rosen (2004). The first reason is that Ghosh and Johns (2016) used head area as the matching parameter, but

predicted the tail length by correlation (Tanford 1980), which is different from the approach that Acosta et al. developed (2003). Another is that the contribution of cosolvent on the interfacial area was not considered, leading to overestimated surfactant head area. Nevertheless, it does not affect the results since the microemulsion phase behavior was well reproduced.

Table 5-3 lists solution gas percentages and pressure for various scenarios. Conditions of scenarios 1 to 3 are the same as the experiments in Roshanfekr and Johns (2011, 2013). Methane is used to represent the solution gas and its EACN is considered to be unity. Mole fraction linear mixing was used to calculate the EACN of the mixture. The shifted optimum salinity and optimum solubilization ratio are determined by Eqs. 34 and 35. Scenario 1 is the base case for dead oil under atmosphere pressure. Scenario 2 is dead oil at high pressure of 68.95 bar (1000 psi), where optimum salinity increases and optimum solubilization ratio reduces due to the pressure effect, comparing to scenario 1. In scenario 3, 17% of methane is added on the basis of scenario 2. As a result the optimum salinity is reduced to 18,800 ppm, while the optimum solubilization ratio is greatly increased. Scenario 4 is a case with higher pressure but less solution gas compared to scenario 3. This combined effects lead to higher optimum salinity of 25,600 ppm and smaller optimum solubilization ratio. Figure 5-10 plots curves of solubilization ratio vs. salinity for different scenarios. Microemulsion phase behavior of live oil at reservoir condition is largely different from that observed at laboratory. A designed formulation forming Type III microemulsion in laboratory may shift to Type II because of the solution gas in reservoir or shift to Type I due to the high pressure. Consequently, ignoring these variable can lead to an improper surfactant flooding design.

**Table 5-2 HLD-NAC parameters of microemulsion system from Roshanfekr and Johns (2011, 2013)**

| Average MW, g/mol | Average head area, Å$^2$ | Average tail length, Å | K | EACN | $C_s^*$, ppm | $\beta$, bar$^{-1}$ | $B_1$ | $B_2$ |
|---|---|---|---|---|---|---|---|---|
| 232 | 167.33 | 35.96 | 0.18 | 9.9 | 23,000 | $7.71\times10^{-4}$ | 0.08 | 0.02 |

**Table 5-3 Phase behavior properties shift under effect of solution gas and pressure**

| Scenario | Methane | Pressure, bar | EACN | $C_s^*$, ppm | $\sigma^*$ | HLD of point a | σ of point a |
|---|---|---|---|---|---|---|---|
| 1 | 0 | 1 | 9.9 | 23,000 | 11.50 | -0.833 | 5.56 |
| 2 | 0 | 68.95 | 9.9 | 24,500 | 11.32 | -0.896 | 5.21 |
| 3 | 17% | 68.95 | 8.4 | 18,800 | 14.22 | -0.631 | 7.08 |
| 4 | 5% | 173.9 | 9.5 | 25,600 | 10.45 | -0.94 | 4.99 |

To further illustrate the concept, this work selects point *a* in scenario 1 to study the impacts of pressure and solution gas on shocks propagation. Salinity of point *a* is 10,000 ppm with a initial HLD value of -0.833. Its solubilization ratio and HLD value at various scenarios are summarized in Table 5-3, and its phase behavior shift is also plotted in Figure 5-10. It is found the HLD value of point *a* either increases or decreases depending on the reservoir conditions, so does its solubilization ratio. Figure 5-11 presents oil composition profiles of different scenarios at 0.3 and 0.5 PV. Scenario 3 has the largest oil bank and the fastest oil bank front and solubilization front velocity. And the oil concentration in scenario 3 is also slightly higher than other scenarios. The effect of other variables like temperature and surfactant ratio variation can be studied similarly.

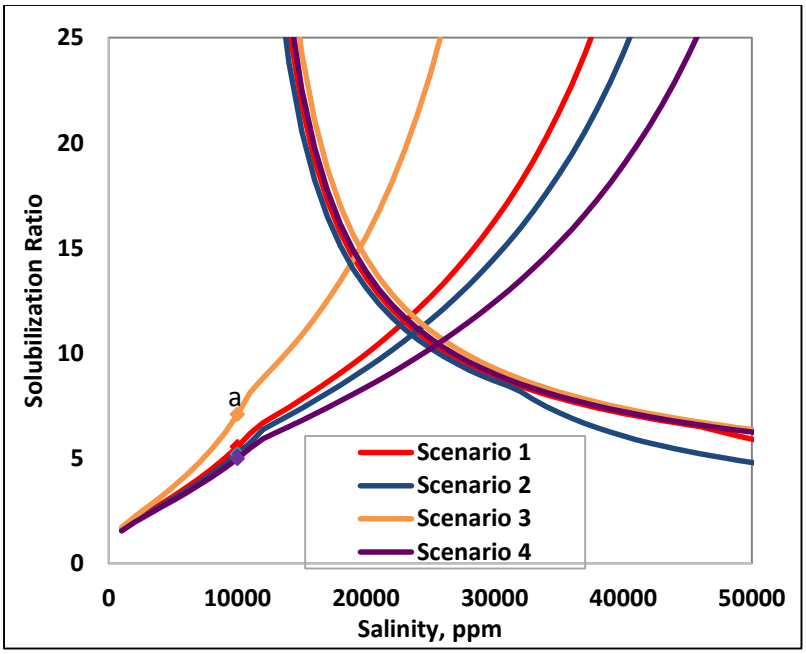


**Figure 5-10 Solubilization ratio vs. salinity of different scenarios**

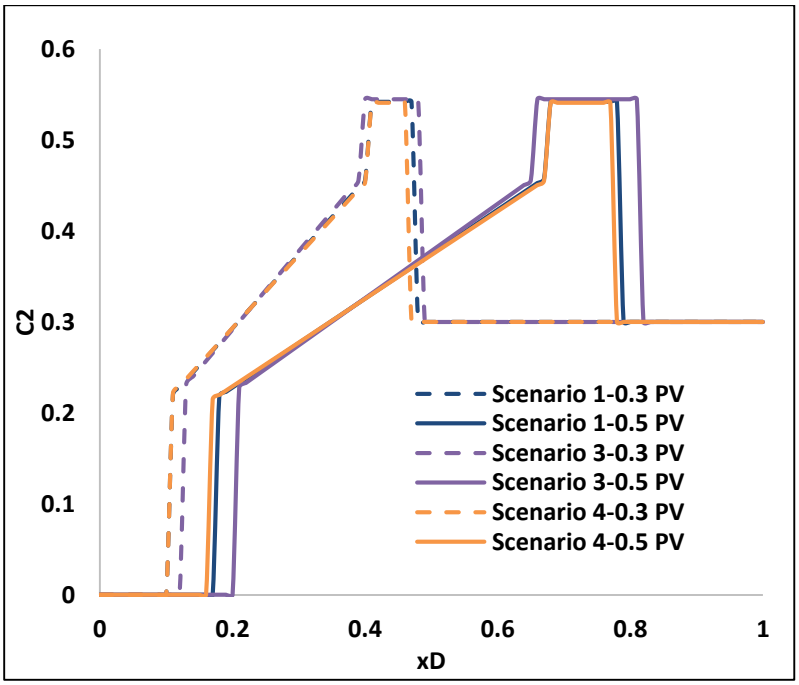


**Figure 5-11 Oil composition profiles at different scenarios**

## 5.7 Conclusions

1. This work constructs analytical solutions for two-phase three-component surfactant flooding by coupling the coherent theory and HLD-NAC equation of

state. Composition routes, shocks as well as oil recovery are determined from the analytical method.

2. Numerical simulation results are consistent with calculated analytical results, and numerical dispersion has little effect on simulated composition routes and recoveries.
3. Surfactant adsorption reduces nontie-line path velocities, and retards oil bank front, surfactant front as well as solubilization front.
4. Using the novel HLD-NAC equation of state, the impacts of phase behavior dependent variables on surfactant flooding can be systemically studied. And surfactant flooding performance under reservoir condition that differs from laboratory condition can be better evaluated.
5. The combined effects of solution gas and pressure on microemulsion phase behavior will enhance or weaken surfactant flooding performance.

## Nomenclature

*Roman*

$a_{3i}$ = *Surface area per molecule of the surfactant i (Å$^2$)*
$A_s$ = *Total interfacial area in microemulsion (Å$^2$)*
$B_1$ = *constant slot for $lnC_s^*$ vs. 1/ $\sigma^*$(dimensionless)*
$B2$ = *constant intercept for $lnC_s^*$ vs. 1/ $\sigma^*$(dimensionless)*
$c_{ij}$ = *volume fraction of component i in phase j*
$Cc$ = *characteristic curvature of surfactant (dimensionless)*
$C_{surfi}$ = *the concentration of surfactant species i in the system (mol/L)*
$C_i$ = *overall volume fraction of component i*
$C_s$ = *Salinity (g/100ml)*
$C_{si}$ = *the concentration of the surfactant species i in water (mol/L)*
$\hat{C}_3$ = *adsorbed concentration of surfactant ($L^3/L^3$ PV)*
$\overrightarrow{e_t}$ = *eigenvector of tie line path*
$\vec{e}_{nt}$ = *eigenvector of nontie line path*
$EACN$ = *equivalent alkane carbon number of the oil (EACN unit)*
$Er$ = *Interfacial rigidity ($m^2 \cdot kg \cdot s^{-2}$)*
$f(A)$ = *function of alcohol type and concentration (dimensionless)*

$F_i$ = *overall fractional flow of component i*
$f_j$ = *fractional flow of phase j*
*HLD* = *hydrophilic lipophilic difference (dimensionless)*
$H_a$ = *average curvature (Å$^{-1}$)*
$H_n$ = *net curvature (Å$^{-1}$)*
*K* = *slope of the logarithm of optimum salinity as a function of EACN (per EACN unit)*
$k_{rj}$ = *relative permeability of phase j*
$k_{rj}^{o}$ = *end point relative permeability of phase j*
*L* = *surfactant length parameter (Å)*
$N_c$ = *capillary number (dimensionless)*
$n_c$ = *number of components*
$n_j$ = *relative permeability exponent for phase j*
$n_p$ = *number of phases*
*P* = *pressure, bar*
$R_o$ = *radius of hypothetical oil droplet in microemulsion (Å)*
$R_w$ = *radius of hypothetical water droplet in microemulsion (Å)*
$S_j$ = *saturation of phase j*
$S_j^*$ = *reduced saturation*
*T* = *temperature (K)*
$T_{pj}$ = *trapping parameter for phase j*
$t_D$ = *dimensionless time (pore volumes)*
*v* = *the pore flow velocity of the displacing fluid (m/s);*
$V_i$ = *volume of component i in a phase (mL)*
*Vw* = *volume of water in a system (ml)*
$V_{om}$ = *volume of oil in microemulsion (mL)*
$V_{wm}$ = *volume of water in microemulsion (mL)*
$x_D$ = *dimensionless distance*
*IFT* = *Interfacial tension (dynes/cm)*

*Greek*

$\alpha_1, \ldots, \alpha_5$ = *microemulsion phase viscosity parameters*
$\alpha_T$ = *temperature coefficient of optimum salinity expressed in units of ln S (°C$^{-1}$ or K$^{-1}$)*
$\beta$ = *pressure coefficient, bar$^{-1}$*
$\varphi_i$ = *fraction of component i in the microemulsion (dimensionless)*
$\xi^*$ = *characteristic length of a microemulsion system (Å)*
$\gamma_{om}$ = *interfacial tension between oil and microemulsion*
$\gamma_{wm}$ = *interfacial tension between water and microemulsion*
$\mu_j$ = *the viscosity of phase j (mPa·s);*
$\phi$ = *is the porosity in fraction.*
$\lambda_j$ = *mobility of phase j*
$\eta$ = *slope of tie line*

*Subscripts*

| | |
|---|---|
| *i* | *= component in a phase* |
| *j* | *= phase j* |
| *m* | *= microemulsion* |
| *nt* | *= nontie line* |
| *o* | *= oil* |
| *om* | *= oil and microemulsion* |
| *OB* | *= oil bank* |
| *PL* | *= left plait point* |
| *r* | *= residual* |
| *RL* | *= right plait point* |
| *SF* | *= solubilization front* |
| *t* | *= tie line* |
| *w* | *= water* |
| *wm* | *= water and microemulsion* |
| *σ* | *= solubilization ratio* |

*Superscripts*

| | |
|---|---|
| *d* | *= downstream condition* |
| *high* | *= high capillary number* |
| *I* | *= injection condition* |
| *low* | *= low capillary number* |
| *ME* | *= microemulsion bank* |
| *u* | *= upstream condition* |
| * | *= optimum state unless mentioned otherwise* |

# Chapter 6 Conclusions and Recommendations

The objective of this section is to summarize the conclusion remarks in the individual chapters of this dissertation. Overall, this work focuses on advancing and extending the HLD-NAC equation of state in surfactant flooding, and addresses the problems stated in Chapter 1. The HLD-NAC model is a physics based equation of state and has distinctive advantages in shorten the formulation design process, predict microemulsion phase behavior, improve simulation accuracy, and easily study the effect of phase behavior dependent parameters on surfactant flooding performance.

In Chapter 2, solubilization ratio curves and phase volume fraction diagrams of single surfactant, surfactant mixture with and without alcohol for various crude oil are modeled using the HLD-NAC model. With only one fitting parameter, length constant $L$, the HLD-NAC model is capable of reproducing microemulsion phase behavior of various surfactant formulations. Even as a fitting parameter, the length constant is physically representing the surfactant tail length. The fitted parameter increases with the surfactant or surfactant mixture tail length in the formulation. Moreover, this work proved that the length parameter determined from one system can be readily applied to other oil, indicating the physical significance of the HLD-NAC model. The fitted length parameter for formulations with alcohol is underestimated because this paper assumes all alcohol partition on the interface leading to overestimated interfacial area. The effect of alcohol partitioning is subject to future studies. The HLD-NAC equation of state is proved to be a simple but robust tool for modeling phase behavior of surfactant/crude oil/brine systems. The HLD-NAC model can shorten the surfactant screening process hence help chemical EOR formulation design and optimization.

In Chapter 3, this work firstly predicts the optimum surfactant formulation for a target reservoir, by using HLD equation and measured parameters i.e. EACN, salinity, K value as well as surfactant Characteristic curvature (Cc). Comparing to experiment results, the HLD equation shows high accuracy in predicting optimum surfactant formulation for surfactant flooding, indicating its significance in shortening the surfactant screening process. In addition, this work predicts the microemulsion phase behavior of four surfactant binary mixtures by using the HLD-NAC equation of state. The predicted results are in good agreement with the measured equilibrium IFTs. This is the first time that the IFT behavior of surfactant-brine-crude oil system is predicted based on the quantitatively characterized surfactant hydrophobicity as well as surfactant structure properties, showing the physical significance of HLD-NAC equation of state in predicting microemulsion phase behavior. This paper then introduced a pseudo salinity concept that converts the IFT curves under surfactant scan into a salinity scan. Hence, empirical microemulsion phase behavior Hand's rule is able to model the IFT behavior. Five matching model parameters are required for each case. Comparing to Hand's rule, the HLD-NAC EOS is physics based and the characterized surfactant parameters can be used for different microemulsion system, indicating excellent predictability. Finally, two surfactant flooding sandpack tests are simulated using UTCHEM with the novel HLD-NAC equation of state. This work comprehensively demonstrated the capabilities of HLD-NAC equation of state in not only predicting optimum surfactant formulation but also microemulsion phase behavior based on the ambient conditions and surfactant structures, and its significance for surfactant flooding simulation as a predictive phase behavior model.

In Chapter 4, this work introduces the HLD-NAC model for compositional simulation of surfactant flooding. Comparing to the Hand's rule, the HLD-NAC model can well simulate microemulsion phase behavior with only one fitting parameter, L, which has been proved proportional to the surfactant carbon tail length. An algorithm is developed to generate the ternary phase diagram with water, oil and surfactant as the pseudo components at various salinity conditions, and implemented into a chemical flooding simulator UTCHEM. The HLD-NAC and Hand's rule models predict precisely same oil recovery for a surfactant coreflood under constant optimum salinity injection, indicating excellent compatibility of these two models. For coreflood under salinity gradient, oil bank breakthrough times from both models are the same, but the HLD-NAC predicts higher ultimate oil recovery than Hand's rule, which is due to the higher calculated solubilization ratio of Type I microemulsion from the HLD-NAC model at coreflood overall composition.

Chapter 5 constructs analytical solutions for two-phase three-component surfactant flooding by coupling the coherent theory and HLD-NAC equation of state. Composition routes, shocks as well as oil recovery are determined from the analytical method. Numerical simulation results are consistent with calculated analytical results, and numerical dispersion has little effect on simulated composition routes and recoveries. Surfactant adsorption reduces nontie-line path velocities, and retards oil bank front, surfactant front as well as solubilization front. Using the novel HLD-NAC equation of state, the impacts of phase behavior dependent variables on surfactant flooding can be systemically studied. And surfactant flooding performance under reservoir condition that differs from laboratory condition can be better evaluated. The combined effects of

solution gas and pressure on microemulsion phase behavior will enhance or weaken surfactant flooding performance.

Advantages of the HLD-NAC model in surfactant flooding is well demonstrated in this work. But there are still some uncertainties in this model. Its applications in modeling surfactant flooding have not been fully explored. Here I list some recommendations that needs to be further studied.

1. From the aspect of the HLD-NAC model
    a. Improve the HLD theory and develop new method to obtain the HLD parameters more quickly and precisely.
    b. Improve the surfactant mixing rule.
    c. Model microemulsion phase behavior considering the partition of alcohol between phases.
2. From the aspect of surfactant simulation
    a. Add the functions of modeling the effects of pressure and solution gas into UTCHEM.
    b. Use surfactant as single component to study the surfactant gradient concept.
    c. Analytically study surfactant chromatography by using HLD-NAC EOS and Trogus's adsorption model.

# References


Aanonsen, S. I., 1989. Application of Fractional-Flow Theory to 3-Phase, 1-Dimensional Surfactant Flooding. In ECMOR I-1st European Conference on the Mathematics of Oil Recovery.

Abrams, A., 1975. The influence of fluid viscosity, interfacial tension, and flow velocity on residual oil saturation left by waterflood. Society of Petroleum Engineers Journal, 15(05), pp.437-447.

Acosta, E., Szekeres, E., Sabatini, D. A., Harwell, J. H., 2003. Net-average curvature model for solubilization and supersolubilization in surfactant microemulsions. Langmuir, 19(1), 186-195.

Acosta, E. J., 2008a. The HLD–NAC equation of state for microemulsions formulated with nonionic alcohol ethoxylate and alkylphenol ethoxylate surfactants. Colloids and Surfaces A: Physicochemical and Engineering Aspects, 320(1), 193-204.

Acosta, E. J., Yuan, J. S., Bhakta, A. S., 2008b. The characteristic curvature of ionic surfactants. Journal of Surfactants and Detergents, 11(2), 145-158.

Acosta, E. J., Bhakta, A. S., 2009. The HLD-NAC model for mixtures of ionic and nonionic surfactants. Journal of surfactants and detergents, 12(1), 7-19.

Acosta, E. J., Kiran, S. K., Hammond, C. E., 2012. The HLD-NAC model for extended surfactant microemulsions. Journal of Surfactants and Detergents, 15(4), 495-504.

Adkins, S., Liyanage, P. J., Arachchilage, P., Gayani, W. P., Mudiyanselage, T., Weerasooriya, U., Pope, G. A., 2010. A New Process for Manufacturing and Stabilizing High-Performance EOR Surfactants at Low Cost for High-Temperature, High-Salinity Oil Reservoirs. In SPE Improved Oil Recovery Symposium. Society of Petroleum Engineers.

Adkins, S., Gayani, P. A., Solairaj, S., Lu, J.,Weerasooriya, U., Pope, G. A., 2012. Development of thermally and chemically stable large-hydrophobe alkoxy carboxylate surfactants. In SPE Improved Oil Recovery Symposium. Society of Petroleum Engineers.

Austad, T., & Staurland, G., 1990. Multiphase behavior of live oil using a one-component surfactant; Effects of temperature, pressure and salinity. In Situ; (USA), 14(4).

Austad, T., Hodne, H., & Staurland, G., 1990. Effects of pressure, temperature and salinity on the multiphase behavior of the surfactant/methane and n-

decane/NaCl brine system. In Surfactants and Macromolecules: Self-Assembly at Interfaces and in Bulk (pp. 296-310). Steinkopff.

Austad, T., & Strand, S., 1996. Chemical flooding of oil reservoirs 4. Effects of temperature and pressure on the middle phase solubilization parameters close to optimum flood conditions. Colloids and Surfaces A: Physicochemical and Engineering Aspects, 108(2), 243-252.

Bourrel, M., Verzaro, F., Chambu, C., 1987. Effect of Oil Type on Solubilization by Amphiphiles. SPE Reservoir Engineering, 2(01), 41-53.

Budhathoki, M., Hsu, T. P., Lohateeraparp, P., Roberts, B. L., Shiau, B. J., and Harwell, J. H., 2016. Design of an optimal middle phase microemulsion for ultra high saline brine using hydrophilic lipophilic deviation (HLD) method. Colloids and Surfaces A: Physicochemical and Engineering Aspects, 488, 36-45.

Camilleri, D., Fil, A., Pope, G. A., Rouse, B. A., and Sepehrnoori, K., 1987. Comparison of an improved compositional micellar/polymer simulator with laboratory corefloods. SPE Reservoir Engineering, 2(04), 441-451.

Cayias, J. L., Schechter, R. S., Wade, W. H., 1976. Modeling crude oils for low interfacial tension. Soc. Pet. Eng. J, 16(6), 351-357.

Chou, S. I., Bae, J. H., 1988. Phase-behavior correlation for high-salinity surfactant formulations. SPE reservoir engineering, 3(03), 778-790.

De Gennes, P. G., Taupin, C., 1982. Microemulsions and the flexibility of oil/water interfaces. The Journal of Physical Chemistry, 86(13), 2294-2304.

Delshad, M., Pope, G. A., Sepehrnoori, K., 1996. A compositional simulator for modeling surfactant enhanced aquifer remediation, 1 formulation. Journal of Contaminant Hydrology, 23(4), 303-327.

Delshad, M., 1990. Trapping of micellar fluids in Berea sandstone. Ph.D. Dissertation, The University of Texas at Austin, Austin, TX.

Delshad, M., Bhuyan, D., Pope, G. A., & Lake, L. W., 1986. Effect of capillary number on the residual saturation of a three-phase micellar solution. In SPE Enhanced Oil Recovery Symposium. Society of Petroleum Engineers.

Flaaten, A., Nguyen, Q. P., Zhang, J., Mohammadi, H., Pope, G. A., 2008, January. ASP chemical flooding without the need for soft water. In SPE Annual Technical Conference and Exhibition. Society of Petroleum Engineers.

Fulcher Jr, R. A., Ertekin, T., & Stahl, C. D., 1985. Effect of capillary number and its constituents on two-phase relative permeability curves. Journal of Petroleum Technology, 37(02), 249-260.

Foster, W.R., 1973. A low-tension waterflooding process. Journal of Petroleum Technology, 25(02), pp.205-210.

Ghosh, S., Johns, R. T., 2014. A New HLD-NAC Based EOS Approach to Predict Surfactant-Oil-Brine Phase Behavior for Live Oil at Reservoir Pressure and Temperature. In SPE Annual Technical Conference and Exhibition. Society of Petroleum Engineers.

Ghosh, S., and Johns, R. T., 2015. A Modified HLD-NAC Equation of State to Predict Alkali-Surfactant-Oil-Brine Phase Behavior. In SPE Annual Technical Conference and Exhibition. Society of Petroleum Engineers.

Ghosh, S., & Johns, R. T., 2016. An Equation-of-State Model to Predict Surfactant/Oil/Brine-Phase Behavior. SPE Journal.

Green, D. W., and G. P. Willhite., 1998. Enhanced Oil Recovery, Henry L. Doherty Memorial Fund of AIME, Society of Petroleum Engineer.

Griffin, W. C., 1949. Hydrophilic-lipophilic balance. Journal of the Society of Cosmetic Chemists, 1, 311-326.

Hammond, C. E., Acosta, E. J., 2012. On the characteristic curvature of alkyl-polypropylene oxide sulfate extended surfactants. Journal of Surfactants and Detergents, 15(2), 157-165.

Hand, D. B., 1939. The distribution of a consulate liquid between two immiscible liquids. J. Phys. Chem, 34, 1961-2000.

Harwell, J. H., Helfferich, F. G., & Schechter, R. S., 1982. Effect of micelle formation on chromatographic movement of surfactant mixtures. AIChE Journal, 28(3), 448-459.

Healy, R. N., Reed, R. L., & Stenmark, D. G., 1976. Multiphase microemulsion systems. Society of Petroleum Engineers Journal, 16(03), 147-160.

Healy, R. N., & Reed, R. L., 1977. Immiscible microemulsion flooding.Society Of Petroleum Engineers Journal, 17(02), 129-139.

Helfferich, F. G., 1981. Theory of multicomponent, multiphase displacement in porous media. Society of Petroleum Engineers Journal, 21(01), 51-62.

Hirasaki, G. J., 1981. Application of the theory of multicomponent, multiphase displacement to three-component, two-phase surfactant flooding.Society of Petroleum Engineers Journal, 21(02), 191-204.

Huh, C., 1979. Interfacial tensions and solubilizing ability of a microemulsion phase that coexists with oil and brine. Journal of Colloid and Interface Science, 71(2), 408-426.

Israelachvili, J. N., Mitchell, D. J., & Ninham, B. W., 1976. Thermodynamics of amphiphilic association structures. Journal of the Chemical Society, Faraday Transactions 2: Molecular and Chemical Physics, 72, 1525-1533.

Israelachvili, J. N., Mitchell, D. J., & Ninham, B. W., 1977. Theory of self-assembly of lipid bilayers and vesicles. Biochimica et Biophysica Acta (BBA)-Biomembranes, 470(2), 185-201.

Jackson, A. C., 2006. Experimental Study of the Benefits of Sodium Carbonate on Surfactants for Enhanced Oil Recovery. MS Thesis, The University of Texas at Austin, Austin TX.

Jang, S. H., Liyanage, P. J., Lu, J., Kim, D. H., Arachchilage, G. W., Britton, C., Pope, G. A., 2014. Microemulsion Phase Behavior Measurements Using Live Oils at High Temperature and Pressure. In SPE Improved Oil Recovery Symposium. Society of Petroleum Engineers.

Jin, L., Jamili, A., Li, Z., Lu, J., Luo, H., Shiau, B. B. and Harwell, J. H., 2015a. Physics based HLD–NAC phase behavior model for surfactant/crude oil/brine systems. Journal of Petroleum Science and Engineering, 136, 68-77.

Jin, L., Jamili, A., Harwell, J. H., Shiau, B. J., and Roller, C., 2015b. Modeling and Interpretation of Single Well Chemical Tracer Tests (SWCTT) for pre and post Chemical EOR in two High Salinity Reservoirs. In SPE Production and Operations Symposium. Society of Petroleum Engineers.

Jin, L., Mahesh Budhathoki, Ahmad Jamili, Zhitao Li, Haishan Luo, Mojdeh Delshad, Ben Shiau, SPE, Jeffrey H. Harwell, 2016. Predicting Microemulsion Phase Behavior for Surfactant Flooding, SPE Improved Oil Recovery Conference. Society of Petroleum Engineers.

Larson, R. G., 1979. The influence of phase behavior on surfactant flooding.Society of Petroleum Engineers Journal, 19(06), 411-422.

LaForce, T. C., & Johns, R. T., 2005. Composition routes for three-phase partially miscible flow in ternary systems. SPE Journal, 10(02), 161-174.

Levitt, D. B., Jackson, A. C., Heinson, C., Britton, L. N., Malik, T., Dwarakanath, V., and Pope, G. A., 2009. Identification and Evaluation of High Performance EOR Surfactants. SPE J. 12 (2): 243-253.

Liyanage, P.J., Lu, J., Arachchilage, G.W., Weerasooriya, U., and Pope, G.A., 2015: A Novel Class of Large-Hydrophobe Tristyrylphenol (TSP) Alkoxy Sulfate Surfactants for Chemical Enhanced Oil Recovery. Journal of Petroleum Science and Engineering, (in press).

Liu, S., Zhang, D., Yan, W., Puerto, M., Hirasaki, G. J., & Miller, C. A., 2008. Favorable attributes of alkaline-surfactant-polymer flooding. SPE Journal, 13(01), 5-16.

Lu, Jun, Upali P. Weerasooriya, and Gary A. Pope., 2014a. Investigation of gravity-stable surfactant floods. Fuel 124: 76-84.

Lu, Jun, Pathma Jith Liyanage, Sriram Solairaj, Stephanie Adkins, Gayani Pinnawala Arachchilage, Do Hoon Kim, Christopher Britton, Upali Weerasooriya, and Gary A. Pope., 2014b. New surfactant Developments for chemical enhanced oil recovery. Journal of Petroleum Science and Engineering.

Lu, J., Britton, C., Solairaj, S., Liyanage, P. J., Kim, D. H., Adkins, S., Pope, G. A. 2014c. Novel large-hydrophobe alkoxy carboxylate surfactants for enhanced oil recovery. SPE Journal, (Preprint).

Melrose, J.C., 1974. Role of capillary forces in detennining microscopic displacement efficiency for oil recovery by waterflooding. Journal of Canadian Petroleum Technology, 13(04).

Mitchell, D. J., Ninham, B. W., 1981. Micelles, vesicles and microemulsions. Journal of the Chemical Society, Faraday Transactions 2: Molecular and Chemical Physics, 77(4), 601-629.

Morrow, N.R., Songkran, B., 1981. Effect of viscous and buoyancy forces on nonwetting phase trapping in porous media. In: Shah, D.O. (Ed.), Surface Phenomena in Enhanced Oil Recovery. Plenum Press, pp. 387–411.

Morrow, N.R., Chatzis, I., Taber, J.J., 1988. Entrapment and mobilization of residual oil in bead packs. SPERE 3 (3), 927–934.

Nelson, R. C., & Pope, G. A., 1978. Phase relationships in chemical flooding. Society of Petroleum Engineers Journal, 18(05), 325-338.

Orr, F. M., 2007. Theory of gas injection processes. Tie-Line Publications.

Pennell, K. D., Pope, G. A., & Abriola, L. M., 1996. Influence of viscous and buoyancy forces on the mobilization of residual tetrachloroethylene during surfactant flushing. Environmental Science & Technology, 30(4), 1328-1335.

Pope, G. A., & Nelson, R. C., 1978. A chemical flooding compositional simulator. Society of Petroleum Engineers Journal, 18(05), 339-354.

Pope, G. A., 1980. The application of fractional flow theory to enhanced oil recovery. Society of Petroleum Engineers Journal, 20(03), 191-205.

Puerto, M. C., Reed, R. L., 1983. A three-parameter representation of surfactant/oil/brine interaction. Soc Petrol Eng J, 23, 669-683.

Puerto, M., Hirasaki, G. J., Miller, C. A., and Barnes, J. R., 2012. Surfactant systems for EOR in high-temperature, high-salinity environments. SPE Journal, 17(01), 11-19.

Puerto, M., Hirasaki, G., Miller, C. A., Reznik, C., Dubey, S. T., Barnes, J. R., and van Kuijk, S. R., 2015. Effects of Hardness and Cosurfactant on Phase Behavior of Alcohol-free Alkyl Propoxylated Sulfate Systems. SPE Journal.

Prouvost, L. P., Satoh, T., Sepehrnoori, K., Pope, G. A., 1984. A New Micellar Phase-Behavior Model for Simulating Systems With Up to Three Amphiphilic Species. paper SPE, 13031, 16-19.

Rosen, M.J., 1989. Surfactants and interfacial phenomena. 2nd ed.; John Wiley & Sons: New York.

Roshanfekr, M., & Johns, R. T., 2011. Prediction of optimum salinity and solubilization ratio for microemulsion phase behavior with live crude at reservoir pressure. Fluid Phase Equilibria, 304(1), 52-60.

Roshanfekr, M., Johns, R. T., Pope, G., Britton, L., Linnemeyer, H., Britton, C., & Vyssotski, A., 2012. Simulation of the effect of pressure and solution gas on oil recovery from surfactant/polymer floods. SPE Journal, 17(03), 705-716.

Roshanfekr, M., Johns, R. T., Pope, G., & Delshad, M., 2013. Modeling of Pressure and Solution Gas for Chemical Floods. SPE Journal, 18(03), 428-439.

Sandersen, S. B., Stenby, E. H., & von Solms, N., 2012. The effect of pressure on the phase behavior of surfactant systems: An experimental study. Colloids and Surfaces A: Physicochemical and Engineering Aspects,415, 159-166.Salager, J. L., Morgan, J. C., Schechter, R. S., Wade, W. H., Vasquez, E., 1979a. Optimum formulation of surfactant/water/oil systems for minimum interfacial tension or phase behavior. Soc. Pet. Eng. J, 19(2), 107-115.

Salager, J. L., Bourrel, M., Schechter, R. S., Wade, W. H., 1979b. Mixing rules for optimum phase-behavior formulations of surfactant/oil/water systems. Soc Petrol Eng J, 19(5), 271-278.

Salager, J.L., Antón R.E., 1999. In Handbook of Microemulsion Science and Technology; Kumar, P., Mittal, K.L., Eds.; Marcel Dekker: New York: 247-280.

Salager, J. L., Marquez, N., Graciaa, A., Lachaise, J., 2000. Partitioning of ethoxylated octylphenol surfactants in microemulsion-oil-water systems: influence of temperature and relation between partitioning coefficient and physicochemical formulation. Langmuir, 16(13), 5534-5539.

Sheng, J., 2010. Modern Chemical Enhanced Oil Recovery: Theory and Practice. Elsevier Science.

Skauge, A., & Fotland, P., 1990. Effect of pressure and temperature on the phase behavior of microemulsions. SPE Reservoir Engineering, 5(04), 601-608.

Solairaj, S., Britton, C., Lu, J., Kim, D. H., Weerasooriya, U., and Pope, G. A., 2012. New correlation to predict the optimum surfactant structure for EOR. In SPE Improved Oil Recovery Symposium. Society of Petroleum Engineers.

Stegemeier, G.L., 1977. Mechanisms of entrapment and mobilization of oil in porous media. Improved Oil Recovery by Surfactant and Polymer Flooding, pp.55-91.

Taber, J.J., 1969. Dynamic and static forces required to remove a discontinuous oil phase from porous media containing both oil and water. Society of Petroleum Engineers Journal, 9(01), pp.3-12.

Tanford, C., 1980. The Hydrophobic Effect: Formation of Micelles and Biological Membranes 2d Ed. J. Wiley.

Trahan, G., Nguyen, T., and Jakobs-Sauter, B. 2015. Applying the Hydrophilic – Lipophilic Deviation (HLD) Concept to Chemical EOR Formulations. 18th European Symposium on Improved Oil Recovery. Dresden, Germany.

Trogus, F. J., Schechter, R. S., & Wade, W. H., 1979. A new interpretation of adsorption maxima and minima. Journal of Colloid and Interface Science,70(2), 293-305.

UTCHEM-9.0., 2000. Technical Documentation for UTCHEM-9.0, A Three-Dimensional Chemical Flood Simulator, Austin.

Van-Quy, N., Simandoux, P., and Corteville, J., 1972. A numerical study of diphasic multicomponent flow. Society of Petroleum Engineers Journal, 12(02), 171-184.

Welge, H. J., Johnson, E. F., Ewing Jr, S. P., & Brinkman, F. H., 1961. The linear displacement of oil from porous media by enriched gas. Journal of Petroleum Technology, 13(08), 787-796.

Willhite, G. P., Green, D. W., Okoye, D. M., & Looney, M. D., 1980. A study of oil displacement by microemulsion systems mechanisms and phase behavior. Society of Petroleum Engineers Journal, 20(06), 459-472.

Winsor, P. A., 1948. Swollen microemulsion. Transactions of the Faraday Society, 44, 376-392.

Winsor, P. A., 1968. Binary and multicomponent solutions of amphiphilic compounds. Solubilization and the formation, structure, and theoretical significance of liquid crystalline solutions. Chemical reviews, 68(1), 1-40.

Witthayapanyanon, A., Phan, T. T., Heitmann, T. C., Harwell, J. H., and Sabatini, D. A., 2010. Interfacial properties of extended-surfactant-based microemulsions

and related macroemulsions. Journal of surfactants and detergents, 13(2), 127-134.

Zhao, P., Jackson, A., Britton, C., Kim, D. H., Britton, L. N., Levitt, D., Pope, G. A., 2008. Development of high-performance surfactants for difficult oils. In SPE Symposium on Improved Oil Recovery. Society of Petroleum Engineers.